"A STUDY OF THE LASER AND ITS APPLICATIONS IN THE PROCESS OF MATERIAL REMOVAL"

Thesis

Submitted to

Maharishi University of Information Technology

Lucknow U.P. 226013 India

For the degree of

Doctor of Philosophy

Physics

By

Krishna Kumar Shukla

Under the Supervision of

Prof. D.B. Singh

Professor and Chairman

Micro-Molecular & Biophysics Laboratory,

Dr. Shakuntala Misra National Rehabilitation University (Govt. of U.P.) Mohan Road,

Lucknow U.P.-226017, India

Under the CO-Supervision of

Prof. A.K. Mishra,

Professor and Head of Department

Jahangirabad Educational Trust Group of Institutions,

Barabanki U.P. – 225203, India

2021

Maharishi University of Information TechnologyLucknow U.P. 226013, India

CERTIFICATE

This is to certify that **Mr. Krishna Kumar Shukla** has completed the necessary academic term and the work presented by him is a faithful record of bonafide original work under the guidance and supervision of **Prof. D.B. Singh, Professor and Chairman Micro-Molecular & Biophysics Laboratory, Dr. Shakuntala Misra National Rehabilitation University (Govt. of U.P.) Mohan Road, Lucknow U.P.-226017, India**, **Prof. A.K. Mishra, Professor and Head of Department Jahangirabad Educational Trust Group of Institutions, Barabanki U.P.** **– 225203,India.** He is worked on "A STUDY OF THE LASER AND ITS APPLICATIONS IN THE PROCESS OFMATERIAL REMOVAL". No part of this thesis has been submitted by the candidate for the award of any other degree or diploma in this or any other University around the globe.

(Prof. A.K. Mishra)
Co-Supervisor
Professor & Head
Department of Applied Sciences & Humanities
Jahangirabad Educational Trust Group of Institutions,
Barabanki U.P.– 225203, India

(Prof. D.B. Singh)
Supervisor
Assistant Professor
Department of Physics
Dr. Shakuntala Misra National Rehabilitation University, Mohan Road,
Lucknow U.P.-226017, India

CANDIDATE'S DECLARATION

I hereby declare that the research work embodied in this thesis entitled **"A STUDY OF THE LASER AND ITS APPLICATIONS IN THE PROCESS OF MATERIAL REMOVAL"** carried out by me under the guidance and supervision of **Prof. D.B. Singh, Professor and Chairman Micro-Molecular & Biophysics Laboratory, Dr. Shakuntala Misra National Rehabilitation University (Govt. of U.P.) Mohan Road, Lucknow U.P.-226017, India**, **Prof. A.K. Mishra, Professor and Head of Department Jahangirabad Educational Trust Group of Institutions, Barabanki U.P. – 225203,India** is an original work does not contain part of any work, submitted for the award of the any degree either in this University or any other University around the globe.

Date:

(Krishna Kumar Shukla)

Place: Research Scholar

Maharishi University of Information Technology

Lucknow U.P. 226013, India

Date :…….

VIVA VOCE CERTIFICATE

This is to certify that this thesis entitled **"A STUDY OF THE LASER AND ITS APPLICATIONS IN THE PROCESS OF MATERIAL REMOVAL"** submitted to the **Maharishi University of Information Technology Lucknow U.P.226013 India,** in fulfilment of the requirement for the degree of doctor of Philosophy in Physics has been approved after an oral examination of the same in collaboration with an external examiner.

External Examiner

Date : ……

Place:

Dean Research

Maharishi University of Information Technology

Lucknow U.P.226013 India

Acknowledgements

The award of degree “Degree of Philosophy” is one of the hardest deserving achievements which are not easily found. During the entire research work some valuable people conceived their enormous positions in my heart. In this regard, I am grateful to the University and express my deep sense of gratitude to its Hon’ble Prof. (Dr.) Bhanu Pratap Singh Vice-chancellor for the delivering this great opportunity to me. I also want to convey Professor regards to the registrar Prof. (Dr.) Akhand Pratap Singh of MUIT, who has always motivated me for this work. I would like to express my special appreciation and thanks to my supervisor **Prof. D.B. Singh, Professor and Chairman Micro-Molecular & Biophysics Laboratory, Dr. Shakuntala Misra National Rehabilitation University (Govt. of U.P.) Mohan Road, Lucknow U.P.- 226017, India**, and **Prof. A.K. Mishra, Professor and Head of Department Jahangirabad Educational Trust Group of Institutions, Barabanki U.P. – 225203, India,** you have been a tremendous mentor for me. I would like to thank you for encouraging my research and for allowing me togrow as a research scientist. Your advice on both research as well as on my career have been priceless. I am heartily thankful to you for being a great mentor for greatly obliged cooperation, for having adequate belief in my abilities to help me incrementally in build up my understanding of the research area and for all your precious endeavour on behalf of me ,I also thanks to you for your invaluable suggestion, glorious supervision devoted encouragement, prosperous discussion, precious feedback and committed interest in the entire duration of my research work I would also like to thank my committee members Prof.Madhulika Singh (Former dean of School of Science and Dean Research), Dr. Neeraj Jain (Former Dean Research), Dr Sandhya Sinha Dean Research, Dr. Rama Kant Maurya Dean Maharishi School of Science, for serving as my committee members even at hardship. I also want to thank Mr. Girish Chhimwal Dy. Registrar MUIT Lucknow for encouraging me and helping in my research work. A specialthanks to my family and my friends for the valuable support. At the end I would like express appreciates to my beloved who spent sleepless nights with and was always my support in the moments when there was no one to answer my queries.

Krishna Kumar Shukla

Table of Contents

CHAPTER 1	**INTRODUCTION**	**1-11**
1.1	Introduction to Laser Materials Processing	
1.2	Methods of Processing-	
1.2.1	Welding Techniques	
1.2.2	Drilling Process	
1.2.3	Process of Cutting	
1.2.4	Laser Ablation	
1.2.5	Surface Modifications	
1.3	Transformations of the Material Medium During the Processing	
1.3.1	Melting of the substance	
1.3.2	Vaporization of the substance	
1.3.3	Phase shift	
1.3.4	Chemical transformations	
1.3.5	Thermal stress-induced changes	
1.3.6	Changes in the surface owing to sputtering	
1.3.7	Processing by laser shock (LSP)	
1.4	Processable Materials	
1.5	The Report's Structure	
CHAPTER 2	**REVIEW OF LITERATURE**	**12-22**
2.1	Survey of Literature	
2.2	The Work's Objective	
CHAPT ER 3	**ABOUT LASERS**	**23- 48**
3.1	Electromagnetic Spectrum and Electromagnetic Wave	
3.2	Laser Generation and Its Properties	
3.2.1	Mechanism of Laser beam generation	
3.2.1.1	Cavity of an Optical Resonator	
3.3	Gaussian Beam Optics	
3.3.1	Gaussian beam and geometrical optics	
3.4	Laser Beam Modes	

3.5	Laser Beam Profile	
3.5.1	Beam divergence	
3.5.2	Brightness	
3.5.3	Fluence	
3.5.4	Average power	
3.5.5	Power Density or irradiance	
3.5.6	Peak Power	
3.5.7	Pulse Energy	
3.5.8	Pulse Duration and Repetition Rate	
3.5.9	Beam diameter	
3.5.10	Spot Diameter	
3.6	Laser Types	
3.6.1	Gas lasers	
3.6.2	Solid-state lasers	
3.6.3	Semiconductor lasers	
3.6.3.1	GaInP (gallium indium phosphide) Semiconductor laser	
3.6.3.2	Vertical cavity surface-emitting lasers (VCSEL)	
CHAPTER 4	**LASER INTERACTION WITH MATERIALS**	**49-69**
4.1	Photon-Matter Interaction	
4.2	Matter's Absorption of Light	
4.2.1	Fresnel's theory of light absorption	
4.2.2	Lorentz model based on the classical theory of absorption	
4.2.3	The electromagnetic theory of light absorption	
4.3	Interaction of Laser and Materials: Effect of Technological Parameters	
4.4	Radiation Transmitted and Reflected	
4.5	Penetration Deepness	
4.6	Mechanism of Heat Transfer	

4.7	Laser Material Interaction Thermo Physical Process	
4.8	Rise in Temperature	
CHAPTER 5	**EXPERIMENTAL METHODS**	**70-85**
5.1	Experimentation with Laser Cutting	
5.2	Analytical Techniques Instruments	
5.2.1	Electron Scanning Microscopy	
5.2.2	Spectroscopy with EDX	
5.2.3	Profilometer for Stylus	
5.2.4	Microscope for Metal Working	
5.3	Sample Preparation and Material Processing with A Laser	
CHAPTER 6	**RESULTS AND CONVERSATION**	**86-115**
6.1	Cut Kerf	
6.2	Studies on Ta	
6.3	Rate of Material Removal	
6.4	Characteristics of The Surface	
6.4.1	Examinations of Surface Roughness	
6.4.2	SEM examinations of laser-cut surfaces	
6.4.2.1	Cracks at the laser cut surface	
6.4.2.2.	Irregularities on The Surface—Creation of Craters/Valleys	
6.4.3	White Layer on The Cut Surface	
6.4.4	EDXA Studies	
6.5	Studies on Microstructure and Grain Size	
6.6	Studies on Heat-Affected Zones	
6.7	Laser Etching of Metals	
CHAPTER 7	**PROCESS MODELING**	**116-141**
7.1	Basics of Neural Network Analysis	
7.2	Prediction of Kerf Width Using A Neural Network Model	
7.2.1	Algorithm for Back Propagation	
7.2.2	Method of Network Learning	
7.3	The Neural Network Model's Results for Kerf Width	
7.4	Basics of Multiple Regressions	
7.5	Kerfwidth Regression Model	
7.5.1	Regression Results	
7.6	Discussion of Results of The Model	

7.6.1 The Effect of Cutting Speed on The Width of The Kerf
7.6.2 Effect of Gas Pressure on Kerfwidth
7.6.3 Effect of Thickness on Kerf
7.6.4 The Effect of Laser Power on The Width of The Kerf
7.7 Model of A Neural Network for Surface Roughness
7.8 Results of The Model for Surface Roughness of Stainless-Steel Cut by Co_2 Laser
7.9 Fem Model to Study Temperature Distribution During Laser Cutting of Stainless Steel
7.9.1 Modelling Using Fem

CHAPTER 8 CONCLUSION 142-145
8.1 The Primary Results of Experiments with CO_2 Laser Cutting
8.2. Studies on Laser Etching with a Nd: YAG Laser
8.3 Studies in Modeling
8.4 The Work's Importance
8.5 Opportunities for Future Work

REFERERENCES

ANNEXURE

Appendix-I Published Research Paper
Plagiarism Report

LIST OF FIGURES

Figure Number	Figure Name	Page Number
Figure 1.1	Laser cutting is a procedure that involves the cutting of materials	5
Figure 1.2	with restricted ablation, laser shock processing is used	9
Figure 1.3	Process of laser shock ablation with direct ablation	10
Figure 3.1	Electromagnetic wave propagation	23
Figure 3.2	Diagrammatic representation of the energy levels involved in light emission	25
Figure 3.3	Stable resonator schematic diagrams	27
Figure 3.4	Diagrams schematics of unstable resonators	28
Figure 3.5	Gaussian beam optics illustrating the variation in the size of the spot and the beam divergence	30
Figure 3.6	Definition of Rayleigh range of a laser beam	30
Figure 3.7	Schematics of Laser Beam Focusing	32
Figure 3.8	Focussing of beam lens makers formula	32
Figure 3.9	within the gain profile, exciting laser modes	36
Figure 3.10	The intensity distribution of TEM modes in a laser cavity's center	37
Figure 3.11	Divergence of the beams with relation to the solid angle	38
Figure 3.12	Focusing of the incoming beam to determine the diameter of the spot	41
Figure 4.1	CO2 laser light absorption in steel with varying polarizations	62
Figure 4.2	At room temperature, the absorption of photons of various wavelengths by iron, aluminum, and copper	64
Figure 5.1	Assembling a laser cutting system schematically	71
Figure 5.2	Laser processing with beam delivery arrangement is built in an experimental configuration	72
Figure 5.3	Laser cutting machine Rofin Sinar CO2 (full view)	72
Figure 5.4	Rofin Sinar CO2 laser cutting machine's cutting head	73

Figure 5.5	Bystar 3015 CO2 laser cutting machine photograph	73
Figure 5.6	Schematic of the CO2 gas laser's cutting head	74
Figure 5.7	Sonic and supersonic nozzles for gas jet flow schematic	74
Figure 5.8	Laser marking machine using a 75-watt Nd-YAG laser for etching tasks	75
Figure 5.9	SEM image shows a Scanning Electron Microscope equipped with an Energy Dispersive Spectrometer and an Image Analyzer	78
Figure 5.10	Electron beam interaction with the specimen	78
Figure 5.11	A representative EDX spectrum	80
Figure 5.12	A shot of Mitutoyo's 211th surf test	81
Figure 5.13	System d'analyse d'images LECO 500	82
Figure 6.1	Laser cut kerf and key hole in 3 mm stainless steel using a 1500-watt laser and oxygen aid gas	86
Figure 6.2	Front view of the laser cut kerf and key hole in 3 mm stainless steel utilising an oxygen assist gas at a laser power of 1300 watts	87
Figure 6.3	Bottom view of the laser cut kerf and key hole in 3 mm stainless steel utilising Nitrogen as an assist gas	87
Figure 6.4	SEM image of a laser-cut hole demonstrating the alloy steel taper	89
Figure 6.5	Keyhole taper with laser power	90
Figure 6.6	MRR VS assist gas Pressure in cutting stainless steel	91
Figure 6.7	Variation of MRR with laser processing variables	92
Figure 6.8	Laser power vs Surface finish	94
Figure 6.9	MRR vs Surface roughness for Stainless Steel -304	95
Figure 6.10	Variation of Surface finish with cutting speed and work piece thickness	95
Figure 6.11	Surface variation Roughness as a function of cutting speed for a workpiece with a thickness of 2mm	96
Figure 6.12	SEM micrograph of the sliced surface of ss304 after it has been treated	96

with oxygen as an aid gas

Figure 6.13 When treated with oxygen as an aid gas, a SEM micrograph reveals fissures in the cut surface of 3mm ss-304 97

Figure 6.14 SEM micrograph of the cut surface of 3mm stainless steel after it has been treated with nitrogen as an assist gas 97

Figure 6.15 When alloy steel IS2062 is treated with nitrogen as an aid gas, SEM micrographs reveal fissures in the cut surface 98

Figure 6.16 SEM micrograph shows the cut surface of SS304 after processing using oxygen as an aid gas 99

Figure 6.17 SEM micrograph of the cut surface of 3mm SS304 with a laser power of 1200 watts, a cutting speed of 3000mm/min, and a gas pressure of 6 bar 99

Figure 6.18 SEM photograph indicating grains and peaks and valleys for stainless Steel -304 of 3 mm thickness 100

Figure 6.19 SEM micrograph showing damage of the cut surface of 5 mm stainless steel 101

Figure 6.20 SEM micrograph showing surface topography of laser cut surface of 5 mm Stainless steel -304 102

Figure 6.21 SEM micrograph showing enlarged view of surface topography of laser cut surface of 5mm Steel -304 102

Figure 6.22 SEM micrograph showing surface topography of CO_2 laser cut surface of 5mm Steel -304 103

Figure 6.23 SEM micrograph showing surface topography of CO_2 laser cut surface of 3mm Stainless Steel -304 103

Figure 6.24 SEM micrograph showing surface topography of CO_2 laser cut surface of 3mm Stainless Steel -304 104

Figure 6.25 SEM micrograph showing surface topography of CO_2 laser cut surface of 12mm alloy Steel IS2062 104

Figure 6.26 SEM micrograph of white layer in CO_2 laser cut surface of stainless Steel-304 105

Figure 6.27 SEM micrograph of white layer in CO_2 laser cut surface of stainless Steel-304 Enlarged view 106

Figure 6.28 EDXA image of base material Stainless Steel -304 107

Figure 6.29 EDXA image of CO_2 laser cut surface of SS-304 material with Oxygen cutting 108

Figure 6.30 EDXA image of CO_2 laser cut surface of SS-304 material with Nitrogen as assist gas 108

Figure 6.31 Microstructure of CO_2 laser cut SS-304 110

Figure 6.32 Enlarged view of microstructure of CO_2 laser cut SS-304 110

Figure 6.33 Microstructure of surface away from CO_2 laser cut surface of SS-304 111

Figure 6.34 Enlarged view of microstructure of surface away from CO_2 laser 111

cut surface of SS-304
Figure 6.35 SEM photograph of microstructure of Nd: YAG laser etched surface of stainless steel-304 112
Figure 6.36 SEM photograph of showing heat affected zone of CO_2 laser cut surface SS-304 113
Figure 6.37 SEM photo of etching of stainless steel by Nd: YAG laser beam 114
Figure 6.38 SEM photo of etching of stainless steel by Nd: YAG laser beam laser power =75 114
Figure 6.39 Enlarged view SEM photo of etching of stainless steel by Nd: YAG laser beam laser power =75 115
Figure 7.1 Multilayer Neural Network Model with 4-4-1 architecture 119
Figure 7.2 Weights of the different nodes forming the neural network model for laser cut stainless steel-304 119
Figure 7.3 Graph showing the error during training of the network 121
Figure 7.4 Response surface for kerfwidth with respect to cutting sped and laser power 122
Figure 7.5 Response surface for kerfwidth with respect to work piece thickness and laser power 123
Figure 7.6 Variation of kerfwidth with cutting speed for 304 grade 5mm thick stainless steel, assist gas pressure=6 bar, Laser power=2kW cutting speed=1500mm/min 123
Figure 7.7 Variation of kerf width with assist gas pressure for 304 grade 5mm thick stainless steel, Laser power= 2kwatts 124
Figure 7.8 Variation of kerf width with assist laser power for 304 grade 3mm thick stainless steel, Assist gas pressure= 6 bar (oxygen), cutting speed= 3000mm/ min 124
Figure 7.9 Results of evaluation of constants of regression model for Kerf analysis 129
Figure 7.10 Variation of kerf with cutting speed, Laser power for= 2000watts, assist gas pressure= 5 bar (oxygen) 130
Figure 7.11 Variation of kerf width with assist gas pressure. Cutting speed= 3000mm/ min, Laser power= 2000w, work piece thickness= 3mm 131
Figure 7.12 Variation of kerf with work piece thickness, laser power= 2000watts. Cutting speed= 3000mm/ min 131
Figure 7.13 Variation of kerf with laser power, gas pressure= 4 bar, work piece thickness= 3mm 132
Figure 7.14 Multilayer neural network Model with 4-7-1 architecture for optimizing surface 133

roughness of laser cut surface of SS-304
Figure 7.15 Information of Multilayer Neural network Model with 4-7-1 architecture for optimizing surface roughness of laser cut surface of SS-304 133
Figure 7.16 Weights of Multilayer Neural network Model with 4-7-1 architecture to optimize surface roughness in cutting stainless steel by CO_2 laser 134
Figure 7.17 Graph of network error during training of Multilayer Neural network Model with 4-7-1 architecture 135
Figure 7.18 Relative importance of process parameters in Neural network Model with 4-7-1 architecture 136
Figure 7.19 Results of roughness of neural network Model for surface roughness in cutting of stainless-steel CO_2 laser. T represents the test data. Q is the network output when a query is made with the trained network 137
Figure 7.20-Dimensional Model of work piece meshed Thermal solid 20 noded Brick element 139
Figure 7.21 Temperature distribution along the laser beam direction (nodal solution) in cutting stainless steel by CO_2 laser 139
Figure 7.22 Temperature distribution perpendicular to the laser beam direction (nodal solution) in cutting stainless steel by CO_2 laser 141
Figure 7.23 Temperature distribution along perpendicular direction to the laser beam direction. (Elemental solution) in cutting stainless steel by CO_2 laser 141

CHAPTER 1

INTRODUCTION

1.1 INTRODUCTION TO LASER MATERIALS PROCESSING:

Materials are processed in the engineering sector and Medical Sector using both conventional processes such as cutting, drilling, milling, and grinding and non-traditional processes such as EDM, EBM, abrasive water jet machining, and laser machining. Different processing processes are utilised depending on the industrial requirements. Conventional methods are employed when the cost of the initial investment, the speed with which the material is processed, the precision, precession, and other associated characteristics are acceptable. Otherwise, non-traditional procedures are employed. Among non-traditional approaches, laser material processing is gaining traction in the defence, aerospace, medical equipment, and other high-tech industries due to its abilityto give flexibility, efficient material utilisation, and a repeatable, regulatedprocess.

A laser is a concentrated form of electromagnetic radiation that is extremely monochromatic and coherent. This feature distinguishes it as a critical non-standard cutting tool in manufacturing engineering. The requirement for high productivity and quality has resulted in the development of laser-based material processing technologies. Lasers are used in manufacturing processes to apply a very high flux of energy to the surface of a work piece. Lasers offer a clear advantage over conventional heat sources such as flame cutters, gas cutters, arc cutting, and plasma jets in this regard.

A laser beam is an exceedingly clean stream of photons all travelling in the same way. Physics dictates, at a constant wavelength, that all photons have the same energy. When the wavelength of the beam is shorter, each photon has a larger energy. So, on an atomic scale, what happens if a surface absorbs that

stream of pure light or photons? The energy is generally turned into vibrations of the atoms that effectively heat the surface, although this may happen by an order of many thousandths of a millimeter, in other scenarios (or microns). Under exceedingly rare conditions, these photons can disrupt an atomic bond if their energy is adequate. Most laser operations, however, are thermal; they area result of accurately controlled melting and vaporisation processes. Most importantly, the laser is tunable geographically and temporally; that is to say,the heat can be accurately adjusted for the target. When an applications engineer creates a means to do a certain task it should guarantee that the laser's reliability and repeatability do not change the task.

Another way to understand laser processing is to focus just on the processes when a laser beam collides with a surface. A striking beam is either reflected, absorbed or transmitted to the surface. Just put, reflection + absorption + transmission is one. At least one of the three processes involve almost all practical situations. For processing applications, the absorption of the beam is crucial. This methodology can be applied for any laser processes and can helpus to understand a number of laser processing phenomena. If a large part of the beam is absorbed by the target, the average laser beam power, the intensity of the laser spot and the wavelength of the laser beam are the three main elements used in processing applications. Consequently, only a handful of the countless produced lasers are of industrial interest.

1.2 METHODS OF PROCESSING:

Industrial lasers are used for a variety of material processing operations, including laser cutting, laser welding, laser surface hardening, laser forming, laser fast manufacturing, laser cladding and alloying, and laser etching and engraving. The most often utilised industrial lasers in these material processing operations are the CO_2 laser, the Nd-YAG laser, the excimer laser, and the semiconductor laser. All laser material processing applications are based on the

local conversion of radiation to heat. Depending on the desired power density, the processes can be classified into three categories, namely

- Processes needing a laser power density of 10^4-10^5 w/cm^2
- Processes needing a laser power density of 10^5-10^7 w/cm^2

Example: Welding, cutting, marking etc.

- Processes involving vaporization that require a laser power density of10^7-10^{10} w/cm^2.

Example: Drilling, Cutting, etc.

- Additionally, laser material processing types can be divided according to the sort of movement used to treat the work piece. These are the Types.
- Processes in which the laser and the work piece move relative to one another
- For instance, cutting, grooving, and so forth.
- Processes that do not include any relative motion between the laser and the work item
- For instance, welding, drilling, and ablation

1.2.1 Welding Techniques:

To create a laser welding process, a laser beam can be used in two distinct ways: For low power densities (10^6 W/cm^2), the laser energy is deposited on the piece's surface and transferred to the interior via a heat conduction mechanism (conduction welding process). Increased power densities (>10^6 W/cm^2) result in the creation of a needle cavity on the metal surface that extends into the depth of the work piece. This cavity will be filled with ionised metals and gas vapours (referred to as a keyhole), which will allow the energy to penetrate deeply into the material (welding penetration process).

1.2.2 Drilling Process:

Through the use of focusing lenses or mirrors, the laser beam can be altered and focused into various shapes and geometries in order to get the holes of the desired shape; further, it may be addressed at previously unreachable concealed spots utilising work tools that function on contact. The increased ability of a laser beam to focus energy agrees to concentrate it in smaller places. This method, the temperature can be raised locally to the point of fusion and vaporisation of the material, allowing for the creation of holes or micro holes.

1.2.3 Process of Cutting:

Laser cutting of materials is the most prevalent and widely utilised use of laser systems. The energy absorbed from the material in the zone where the laser beam has focussed (power densities 10^5- 10^8 W/cm^2) is converted to heat during the cutting process. Localized heat causes a rapid increase in the piece's temperature; the fusion and/or evaporation of the interaction zone result in the creation of a hole. It could be a blind or transitory one.

In the first example, material is removed via aspiration of the particles, smoke, and vapours created. In the second, expulsion of the melted material is often aided by the action of a gas pressure termed cutting gas that impinges on the piece surface in conjunction with the laser beam. If the passing hole movesalong the piece while working, it causes the two cutting parts to separate.

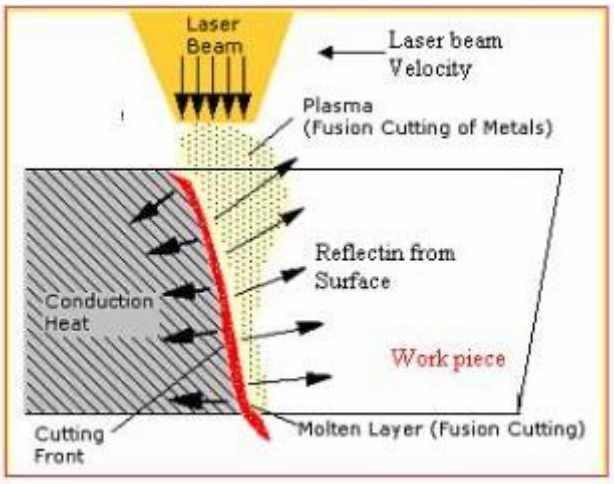

Figure 1.1 Laser cutting is a procedure that involves the cutting of materials.

1.2.4 LASER ABLATION:

Laser ablation is a procedure which involves the irradiation by a laser beam of a solid (or, in some situations, liquid) surface to remove material. At low laser flow the material is heated and the absorbed laser energy vaporises or sublimes. Typically, the material is converted into plasma at high laser flows. Laserablation typically involves removing material using a pulsed laser, although if laser intensity is sufficiently powerful, a continuous wave laser beam can be used to ablate the material. The depth at which laser energy is absorbed and the quantity of material removed by a single laser pulse depends on the material's optical and laser wavelength properties. Laser pulses can be precisely regulated over a wide variety of durations (milliseconds to femtoseconds) and fluxes. Asa result, laser ablation for industrial applications is particularly beneficial.

1.2.5 Surface Modifications:

Laser heat treatment uses include alloying, cladding, ringing, and material transformation hardening for surface modification. Unlike cuts and solding, most techniques of surface alteration use beam power levels between 103 and 104 W/cm2. At these intensities surface heating or superficial melting occurs.

Laser-assisted surface transformation hardening is often used to improve component wear and/or fatigue.

The laser surface treatment of the piece gives distinctive properties to thematerial which can be applied or used. The laser is particularly beneficial for surface treatments because it allows high energy levels and the rapid rise in skin temperatures in fractions of a second with low thermal change of the surrounding material (Bulk) and minor residual deformations to be achieved. A variety of surface effects can be achieved based on the energy density of the incident laser beam, its interaction, time, spatial distribution and wavelength of the beam and thermophysical properties of the material. Thus, the materials of interest generated by the passage of the laser beam can receive quick heatingand subsequent cooling as a photochemical process to remove thin surface layers of material, coating or other material induced by a molecular bond breakage.

1.3 TRANSFORMATIONS OF THE MATERIAL MEDIUM DURING THE PROCESSING:

A sufficient amount of thermal energy must be delivered to the work piece during material processing. This is accomplished by the use of the laser beam's heat. When a material is heated, some changes in the material medium are unavoidable. The following changes are significant from the standpoint of cutting, drilling, and welding processes:

1.3.1 Melting of the substance:

When a sufficient amount of heat energy is absorbed, the temperature of the work item increases. Melting occurs when a material reaches a specified temperature. If further heat is added, the temperature rises to the point offusion. At the fusion temperature, solid matter transforms into liquid. Different

processes like as cutting, welding, and drilling can be carried out in this condition either by removing the molten material or by fusing it into solid.

1.3.2 Vaporization of the substance:

When a liquid material is heated more, the temperature of the liquid melt increases. When a liquid reaches a threshold temperature known as the vaporisation point, it transforms into vapour. This procedure enables laser ablation.

1.3.3 Phase shift:

When the laser beam's energy is concentrated into a tiny volume, the heat absorbed by the material may be sufficient to change the material's metallurgical phase. Austenitic steel, for example, can be transformed to martensitic steel. These alterations have the potential to modify the surface properties of the laser-processed material.

1.3.4 Chemical transformations:

The laser's powerful and focussed beam will cause irreversible chemical reactions in the work item. The burning and subsequent removal of material from the work piece, as well as the exothermic reaction of the assist gas jetwith the work piece (as with steel and oxygen gas), may all have an effect on the strength of the processed material.

1.3.5 Thermal stress-induced changes:

Heat strains may be created when the focused laser beam causes a thermal gradient within the work item. The treated material may then expand, resulting in thermal fracture.

1.3.6 Changes in the surface owing to sputtering:

When a material vaporises, the kinetic energy of the heated vapour can be transferred to the molecules of the liquid in a limited location. By overcoming the surface tension forces between the liquid and the vapour interface, the liquid in such places can then be expelled from the heated zone. After the material solidifies, craters will form in certain places.

1.3.7 Processing by laser shock (LSP):

Shock processing with lasers Shock waves generated by a laser in a confined medium have been utilised to enhance the mechanical properties of a variety of metals, including aluminum, steel, and copper. LSP, in particular, might increase the target's fatigue life by inducing compressive residual stresses. The beam spot size is typically in the millimeter range, and the compressive stress can penetrate several millimeters into the target material. The technology has not been widely employed (Wenwu Zhang and Y. Lawrence Yao 2002), in part because a high power laser source is necessary to generate the high laserintensity required for a millimeter-sized beam. Additionally, it is seen as inefficient when a wide area of surface must be processed, as each laser pulse processes just a small region.

If the power density of a single laser pulse surpasses a particular threshold, shock waves can be generated. The shock wave is produced as a result of the ablation of material layers caused by the laser radiation's intense absorption. The surface of the material initiates a phase transition from solid to vapour.The plasma is a byproduct of the gas phase, which absorbs energy directly from the laser and from the material's surface reflection. By expanding, the plasma generates a shock wave. Shock waves can be generated in two distinct ways:

1. Confined ablation is a process that involves the addition of a water, glass, or quartz overlay (transparent for the wave length) to the specimen's surface, which reduces the specimen's expansion in the surrounding atmosphere and results in up to tenfold increased pressure on the material's surface, as illustrated in figure 1.2. Additionally, melting and material loss are decreased. The pressure generated by the laser-induced shock waves can induce residual stresses several millimeters deep, as local plastic deformation results in stretching of a tiny area that remains under pressure from the surrounding elastically formed material after the pressure is released.
2. As illustrated in figure 1.3, direct ablation occurs when the plasma expands undamaged in the surrounding atmosphere.

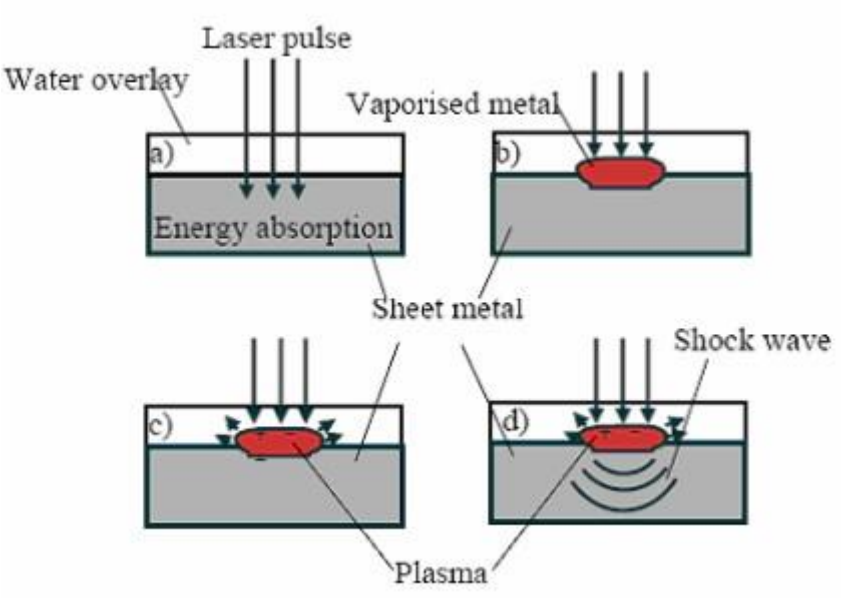

Figure 1.2 with restricted ablation, laser shock processing is used.

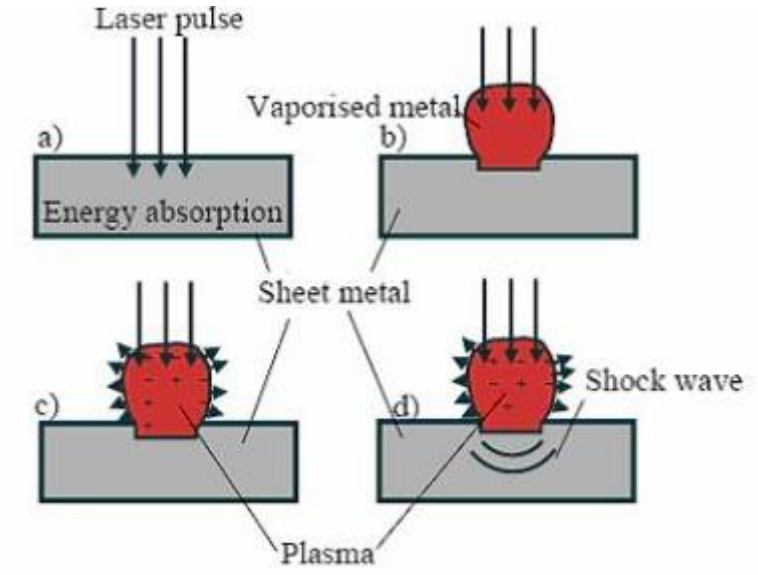

Figure 1.3 Process of laser shock ablation with direct ablation

1.4 PROCESSABLE MATERIALS:

Lasers can process a wide variety of materials, including metals, non-metals, textiles, polymers, wood, rock, and human tissue. The capacity to process them is dependent on the laser radiation being absorbed by the material, which in turn is dependent on the power, intensity, and wavelength of the laser being employed.

1.5 THE REPORT'S STRUCTURE:

The thesis begins with an introduction of laser material processing, outlining the various types of laser processes. It is followed by a review of the literature and a discussion of the purpose of this study. Following that, two chapters are devoted to the foundations of lasers and the interaction of lasers with matter. The following two chapters detail the experimentation, findings, and debate. It is then followed by process modelling investigations, and the thesis concludes with these findings. The chapter structure is as follows:

Chapter 2 is devoted to the review of the literature and the formulation of the problem.

Chapter 3 discusses the principles of laser beam creation and the many types of lasers, as well as the carbon dioxide laser and Nd-YAG laser that were utilised to conduct the work for this thesis.

Chapter 4 discusses the laser beam's interaction with materials, including heat transfer to the materials and laser absorption.

Chapter 5 details the experimental methodology and data gathering.

Chapter 6 is devoted to the conclusion and debate.

Chapter 7 is devoted to process modelling for the purpose of predicting and optimising process parameters.

Finally, Chapter 8 provides conclusions and recommendations for the future.

CHAPTER 2
REVIEW OF LITERATURE

2.1 SURVEY OF LITERATURE:

The literature survey on material processing with lasers places a premium on locating the work of various researchers in the field of laser material processing of stainless steel, with a particular emphasis on experimental data for material removal rates, kerf width analysis, and surface characterization using higher power lasers, as well as theoretical or analytical models to explain these results.

The kerf width determines the dimensional precision of a workpiece while laser cutting metals. In industrial manufacturing, the pace of material removal is critical. As a result, studies on the kerf width and material removal rate under various cutting conditions are crucial. The review of the literature reveals that there is a shortage of experimental data on these factors. There is a shortage of empirical data accessible in the literature addressing the material composition of the laser cut surface and the cut surface's surface properties. Furthermore, the literature previously published has scant data on the effects of process parameters such as laser power, gas pressure, speed and thickness of the material on the kernel width, removal rate and surface qualities of steel. For lasers with a capacity of fewer than 1000 watts, the majority of accessible data is.

During laser cutting, the material is removed by ejecting the molten material with the assistance of an assist gas. J Powell et al. [2000] published experimental data on the kerf width and material removal rate for stainless steel -304 thicknesses of 1.2, 1.9, 3.25, and 5.0 mm. Various oxygen assists gas pressures and cutting speeds using an 800-watt laser. They concluded that to cutsteel with a thickness of 5mm, a laser power of above 2000w is required due to the increased oxidation rate. Kai Chen et al. [2001] carried out and published models of mild steel experiments with a 1500-watt laser. In their analysis of the effect of assisting

gases on the laser cutting of mild steel, the shock structure of the impinging jet, which interacts with the workpiece, influences the material removal capabilities of the gas jet. According to one researcher, Gerald Davis [2001], must be modified to achieve a minimum of power, gas, and machinery, while cutting metals with a CO laser, the machining parameters such as feeding rate, focus location, power level, nozzle distance, gas pressure aid and so on. Toadjust the parameters, experiments are necessary as knowledge of these settings is a business secret. David Smith [2000] examined the effect of oxygen assist pure gas on carbon steel cutting. Their research shows that the purity of oxygen alone does not impact the cutting speed; laser strength and thickness of the material also play a role. Their study found that although there was no speed difference between 99.5% and 99.77% oxygen of purity, high purity oxygen resulted in a speed rise for thinner materials. The maximum speed neared that ofindustrial-grade oxygen with increasing thickness. Finally, due to the purity of oxygen, there is no evident advantage in terms of speed. Rajaram et al. [2003] examined 4130 steel kernel width utilizing CO_2 laser technology. The quality ofthe cut was determined by the breadth of the kerf, the heat zone affected by hot oxidation (HAZ) and the thermally treated area impacted at all locations on top and bottom of the cut. In addition, the kerf breadth and oxidation of HAZ in the laser beam velocity, power and oxygen gas pressures were examined. Theresults showed that the beam speed had the most significant impact on cuts quality among the variables evaluated. Thermocouples intrinsically positioned on the sample surface were used to determine the temperatures beside the cut. Temperatures were also monitored with an infrared sensor in and around the cutting zone. Technical variations and the quality of the amount had an impact on temperatures. However, there appear to be scarce data on kerf width, surface ruggedness and material removal rate.

Additionally, new lasers are being employed to research the effect of laser cutting settings on material processing. Wandera et al. [2006] conducted one such study.

They cut austenitic stainless steel using fibre and disc lasers, which are new laser types with a high beam quality. The performance of these novel lasers was compared to that of a CO_2 laser at a power level of 4 KW in terms of cutting speed, kerf breadth, kerf edge, and roughness. David L Carroll [1997] also investigated laser cutting of steel using a COIL laser. He compared O_2 aided cutting of plain carbon steel using a CO_2 laser to COIL laser cutting using existing data.

New lasers are also used to study the influence of laser cutting settings on material processing. This investigation was conducted out by Wandera et al. [2006]. They use fibre- and disc lasers to reduce austenitic stainless steel, whichare relatively new laser types with the excellent quality beam. The performance of these new lasers at a power level of four KW was compared to that of a CO_2 laser concerning cutting speed, kerf width, kerf edge and roughness. David L Carroll [1997] researched with a COIL laser on laser cutting of steel. He compared O_2 with a CO_2 laser cutting to COIL laser cutting using data available at the time.

Bruinsma, PLWM [1991] studied stainless n steel laser cutting. The results of cutting stainless steel of type AISI 304 at various thicknesses using a high-pressure nitrogen system is provided, together with other critical process parameters such as laser power and intensity, for laser powers less than 1 K.W.

The severance energy of any material indicates the amount of laser power required to cut a sheet of specified thickness at a desired speed. A.K. Nath [1998] published the severance energy values for several materials that their group got experimentally using a 5 KW CO_2 laser. Their values are as follows: mild steel: 7.0J/mm 2 (with O_2), stainless steel: 15J/mm 2 (with Ar), titanium: 15J/mm^2 (with Ar), zircaloy: 2J/mm^2 (with Ar), marble: 8.5J/mm^2 (with Ar), bakelite: 2.6J/mm^2 (with Ar), and wood: 0.5J/mm^2.

To completely understand the influence of process parameters on materials, research must be carried out, particularly in different cutting settings, and a laser

machining database must be created. According to J Dutta Majumdar and I Manna [2003], the method is characterized by an extraordinary fast temperature and cooling rate, extreme thermal gradient, and an extremely high resilience speed. These extreme processing conditions often lead to the generation of novel microstructures and compositions on the surface, which significantly increase solid solubility and generate metastable phases, if not amorphous.Thus, microstructure alteration, damage to the cutting surface and the development of intelligent cutting devices are currently at stake. This requires a considerable database interaction with the hardware. Therefore, continued efforts are needed to simulate the laser machining process to verify that the expected results are experimentally valid.

Rajendran N. [1991] produced two models to describe the AISI 1018 steel laser cutting process. A simple thermodynamic model and a two-dimensional model with finite elements both worked well in forecasting cutting quality. In addition, the models included the oxidation reaction and the oxygen gas jet convection cooling. The attempts to predict cut quality using simply the collected temperature data were quite successful.

The workpiece is not contaminated if the materials are processed with lasers due to the lack of a cutting tool. However, specific changes in the composition of the material will take place at least on the sliced surface due to another mechanism. Murali Manohar [2006] presents a technique to explain why residual elements are of more excellent quality. The research has shown that almost nil residual stress and a low quantity of residual compounds (Cu, Ni and Cr) are necessary to obtain clean piercings and consistent cutting quality in the use of traditional CO_2 laser cutting on thick (20 25 mm) sheets. However, more significant efforts are needed to have a deeper understanding of laser cutting.

During processing, many scientists have observed cracking of the surface of processed materials. Menson and Kotecki studied nitrogen's effect on austenitic

stainless-steel sod metal hot cracking in 1989 [Shankar v.2003]. Welded metal nitrogen may come from various sources, including pre-existing nitrogen in the base metal, intentional addition during the shielding gas process or unexpected absorption due to insufficient shielding during welding. Many studies have investigated nitrogen's influence on cracking in fully austenitic stainless steel. The findings, however, are controversial and show that nitrogen has a complex effect on soil solidification. Nitrogen absorbed during soldering promotes cracking significantly, minimizing the Ti or Nb to C or N ratio. However, with fully austenitic stainless steels, solidification cracking remains a concern, particularly when ferrite is controlled and no changes to the composition are allowed during welding. Several experiments have been undertaken on theeffect of impurity and alloying elements on cracking behaviour. Their research shows that the hot cracking in totally austenitic steel is carried out by pollutants such as Sulphur and phosphorous and small alloy elements such as boron, silicon, titanium, or niobium. Cracking is found to be based on theconcentrations of impurity elements in N-enhanced stainless steels. In heavily alloyed steels, cracking is more common than in leaner counterparts. For such hot cracking events, other methods of thermal material processing should be studied.

Numerous researchers have examined the effect of cutting settings on the roughness of the cut surface. Thirumala Rao and Nath [2002] demonstrated that changing the cutting speed impacts the cut surface roughness of low carbon steel and C45 material. Kai Chen et al. [2001] used a 1.5 KW CO_2 laser and discovered that the roughness of the cut surface varies with gas pressure for a given set of other cutting parameters when mild steel is 1.6mm thick. However, limited data is available on the surface texture of laser-cut stainless steel for various thicknesses and missing factors when utilizing oxygen support gas. Numerous researchers have documented the production of a white layer during conventional steel machining [Ranganath B J 1999] and electric discharge machining [Ranganath B J 1999]. (EDM). Lee H T and Tai T Y [2003]

investigated how surface cracks occur in tool steels by examining the white layer created during the EDM process. Cusanelli G et al. [2004] investigated the crystallographic and metallurgical properties of the white layer formed during the EDM process of cutting hard materials. According to Akcan.S, Shah S, and et al. [2002], the production of a white layer during machining has been linkedto the steel's surface being heated over the austenitizing temperature during the process rapidly self-quenching by the bulk of the material. Griffiths B J [1987] addressed how rapid heating and cooling, surface response, and plastic deformation of the fabric all contribute to creating the white layer on carbon and mild steel. According to Ranganath B J and Venkatesh V C [1980], whilecutting mild steel with a Titanium carbide tool, a white film forms on the tool material. C. P. S. Prakash and B. J. Ranganath [2006] described creating a whitecoating on the machined surface of a wire EDM. However, nothing is known about the white coating formed during laser cutting of stainless steel.

Laser material processing requires the laser to interact with the workpiece material. A study of this connection requires an understanding of the physical processes that occur throughout the encounter. These biological processes are inherently complex. Numerous researchers have investigated theoretical approaches to the problem of laser material contact. B.S. Yilbas and A.Z. Sahin (1993) established a theoretical framework based on physical factors to investigate the evolution of temperature profiles over time. They discovered that most evaporation occurs inside the region 1/e of the intensity distribution when liquid is ejected by radial flow due to a radially dependent pressure gradient on the surface. The highest temperature penetrates the material as the heating duration increases. This elevated temperature beneath the surface indicates a high nucleation rate or rapid vaporization due to the elevated temperature for material removal. Additionally, they predicted nucleation and critical point explosions in material removal mechanisms and explored previous theoretical approaches to laser-material interaction.

Experiments with laser processing are costly and time-consuming due to the method's reliance on material conditions and inherent practical challenges in controlling the process parameters, in addition to the equipment's high cost. To surmount these obstacles, Numerous researchers have conducted process modelling studies. Numerous academics have developed multiple mathematical models depending on the physical parameters of the material to be sliced. Schumacker D [1987] advocated Models for theoretically determining cutting speed, kerf width, peak temperature, and surface quality in his review study on laser cutting (e.g. carbon steels). Additionally, models can be pretty practical for predicting cutting performance and quality without experimental effort for altered or enhanced beam quality, new materials or dimensions. Schulz et al. [1987] constructed a model of the stationary cutting front for laser material processing and discovered that the cutting depth is highly dependent on the focus position.

Chen S L [1998] modelled the metal cutting process by treating the cutting front as an absorption surface to derive the function of production factors from the process's kinetics. Powell J et al. [2000] studied the influence of material thickness on cutting speed while using a laser with a power output of less than 1 K.W. Yilbas BS [2001] investigated the effects of two parameters on the kerf width, namely cutting speed and laser power, using a lumped parameter approach and discovered that increasing laser power increases kerf width.

J. Duan, H. C. Man and T. M. Yue [2001] have developed an energy balance mathematical model for cutting kerf geometry on a cutting front and have independently examined the effects of cutting speed on kerf width and the association between laser power and material thickening. This model is a variant of Kaplan [1996] and Petring et al. J Duan, H C Man, and T M Yue [2001] studied the effects on the cut kerf quality of material thickness and gas pressure using a mathematical model that had previously been constructed. Kovalev, O. B et al. [2004] introduces a front melting and destruction melted mathematical film model during gas-assisted laser metal cutting. They have reasoned that the

physical processes of melting, destroying and driving theliquid through the gas jet are comparable to spraying the metal in the incision. The modelling results are qualitatively compatible with the experimental data. Thus, the quality of laser cutting metals has been directly linked to the spraying properties of the liquid fusion and how it has been removed.

To examine the effect of assisting gas pressure on material removal rate, Farooq K and A Kar [2000] created a kerf width model based on Rosenthal modified solution. In their investigation on laser cutting and grooving applications, the effect of aiding gas pressure on the rate of material removal is studied. They found that if the bucket width of the order of the bucket width and careful cutting is assumed, the depth of the cut will remain constant beyond the critical pressure. The aid gas removes most of the molten material under pressures below this intense pressure. The model demonstrates that the cutting speed decreases when the assist gas pressure exceeds a critical point and the brace dimension is less than the pulse dimension. According to Xiufeng Wang et al. [2000], a significant vibration arises when material laser interactions with a thin specimen alter the experimental results. This component can also be taken into account while establishing an experimental model.

When machining materials using conventional or non-traditional techniques, microstructure analyses are crucial. There is, however, a lack of information on the microstructure of laser-machined steel. O. V. Akgun and O. T. Inal [1995] examined stainless steel type 304L microstructures melted and alloyed on the laser surface (molybdenum and tantalum). The primary solidification phase was revealed to be ferrite for these alloys. The chemical examination of laser-processed layers showed no change between received layers and laser-processed layers in the composition of the principal alloying components, chromium or nickel. Laser processing, however, reduced manganese concentration by 15 percent. In addition, TEM measurements demonstrated that laser processing increased the amorphous Mn-Si precipitation in the microstructure substantially.

The presence of nitrogen in the material being treated also influences the microstructure [Shankar v 2000].

While regression analysis is one of the methodologies that have been used to develop models to analyze the effect of process parameters on laser processing materials, few publications on laser steel processing in the literature, Rajendran, N[1991] conducted a study that identified the combined effects of power and feed rate on kerf width, surface roughness, striation frequency and thermos of the heat affected area by cutting samples of 4130 steel using carbon dioxide laser. The built regression model measures the effect of several process parameters on the quality of the laser cut.

Neural network modelling is another efficient technique to model the laser machining process. Basen I Yousef et al. [2003] developed a neural network model to forecast the pulse energy needed to produce the given depth and diameter of the dent in the Laser micromachining process. Their model shows how the nonlinear laser micromachining process may be examined using a multi-layered neural network to determine how much pulse energy is needed for the desired dental or crater depth and width. They impinge laser pulses with different energies on the surface of many test materials in their inquiry to assess the effect of pulse energy on the resulting crater geometry and the material volume. The obtained data are used to train and validate the performance of the neural network. Critical system inputs for the process model are the mean crater depth and diameter, whereas pulse energy, depth variance and diameter variance are system outputs. This study shows that the proposed approach in the neural network can accurately anticipate the material removal and surface roughness during laser machining.

The temperature distribution within the workpiece material can be estimated analytically or numerically. Numerous analytical models for studying heat conduction have been presented. However, their calculation is confounded by the

material's temperature-dependent characteristics. As a result, it is easy to determine the temperature distribution using a numerical computational model. However, the model would be material-dependent due to its temperature-dependent features. Yu L M (1997) created a model for laser cutting copper using the finite element approach. However, published results for FEM models for laser cutting generally and specifically for stainless steel are pretty restricted.

According to a literature review, less attention has been dedicated to developing a model from experimental data using statistical approaches in multivariate situations. Additionally, little emphasis has been dedicated to creating a model from experimental data suitable for real-time applications using a neural network or FEM. To optimize the cutting parameters in laser machining, a model based on an artificial neural network (ANN) is a valuable tool. This has not been documented in the literature for stainless steel-304. FEM is a usefulsoft computing technique for determining the temperature distribution inside the material during cutting and was not previously described for stainless steel. Additionally, no regression analysis model is provided in the literature for stainless steel -304 cutting settings to investigate the effect of process parameters on material removal rate, kerf width, and surface roughness.

2.2 THE WORK'S OBJECTIVE:

Laser processing of materials is gaining industrial interest as a cost-effective material processing method due to its enhanced flexibility, faster cycle time, fewer processing stages, and high-quality finished processed material. To accomplish these goals, laser processing must be carried out under ideal conditions for the process parameters. According to the literature review, most tests used a laser beam with a power of fewer than 1000 watts. However, there is very little recorded work using lasers with a power output greater than 1000 watts. Additionally, there is a shortage of data on material removal rate, surface texture, microstructure, an analytical model for laser cutting, cut surface flaws,

the material composition of the cut surface, and thermal analysis of alloy steels such as stainless-steel cut with a high-power laser. Additionally, experimental evidence in the literature indicates that the cut quality character changes as cutting parameters are changed.

Considering the available data in the literature and the requirement for further data to create intelligent systems [Manna 2003], studies on cutting stainless steel -304 with a high-power CO_2 laser was undertaken. The primary objective of this research is to create a database for cutting stainless steel -304 with a high-power laser and to experimentally investigate and understand the effect of cutting parameters on material removal rate (MRR), kerf width, and surface characteristics of stainless steel -304 laser-cut surfaces using a 2 KW CO_2 laser with oxygen and nitrogen as assist gases. Furthermore, using the findings of cutting experiments, a real-time domain process model will be created to investigate the effect of process parameters on kerf width, MRR, and surface roughness. For nonlinear systems such as laser machining, the developed model must be simple to use and rapid to process the data to determine the optimal value for the process parameters:

- Maximum MRR
- Minimum surface roughness
- Minimum cutting time
- Minimum surface and under surface deteriorations
- Minimum kerf width

This is advantageous since it automates the cutting process. The machine is applied optimally. The analysis may be utilized to implement an adaptive control strategy for the system to ensure its effectiveness.

CHAPTER 3

ABOUT LASERS

3.1 ELECTROMAGNETIC SPECTRUM AND ELECTROMAGNETIC WAVE:

Radiation is classified into two broad categories: electromagnetic radiation and particle radiation. The energy in one type is "packed" in microscopic units called photons or quanta. A photon or quantum of energy is devoid of substance. Due to the absence of matter, it has no mass or weight. Electromagnetic radiation is the name given to this sort of radiation. Within the electromagnetic radiation family, there are a variety of different forms of radiation that are utilized for a variety of various reasons. These include well- known radiations such as radio waves, light, infrared, ultraviolet, x-rays, and gamma rays. The designations are based on the energy contained within each photon.

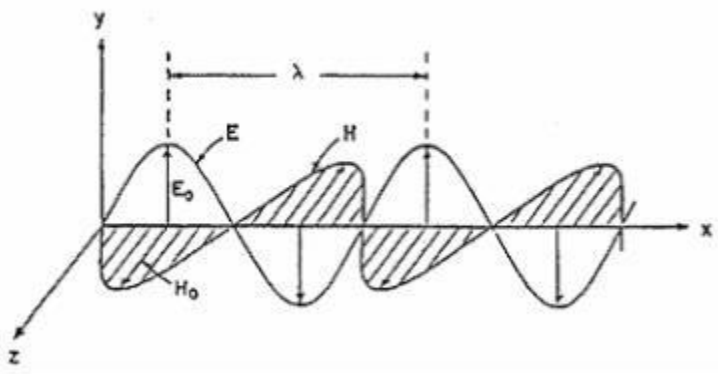

Figure 3.1 Electromagnetic wave propagation

A propagating electromagnetic wave comprises two components: the electric field E (measured in volts per meter) and the magnetic field B (measured in amps per meter). These components are perpendicular to one another, and the propagation direction of the wave is depicted in fig 3.1. The propagating wave in open space has a velocity C of approximately $3x10^8$ ms^{-1}, which is the most

incredible speed at which energy may flow. The frequency f and the wavelength of these waves are connected in the following way:

$$c = \lambda f \text{----------} (3.1)$$

Laser radiation is a component of the electromagnetic spectrum described in Table 3.1 and occurs between the wavelengths of 1 and 11 microns in the infrared, ultraviolet, and x-ray regions.

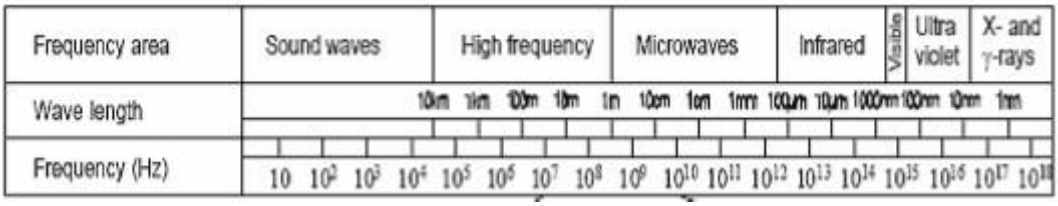

Table 3.1 Spectrum of Electromagnetic Energy

Thus, laser material processing is the technique of processing materials using electromagnetic energy in laser light in that frequency range. However, due to the absorption qualities of the materials being processed, only a limited frequency range of the laser is used for material processing.

3.2 LASER GENERATION AND ITS PROPERTIES:

A laser is a device that uses Light Amplification by Stimulated Emission of Radiation to generate coherent electromagnetic radiation. A laser is made of a gain medium for converting external energy to coherent light, pumping sources for transferring external power to the gain medium, and resonating the cavity to amplify the coherent light. The phenomenon of stimulated emission of radiation enables the emission of laser beams. For example, consider the well-known phenomenon of spontaneous emission. Atoms in an excited state E higherwould emit a quantum of radiation with frequency whenever they fall to a lowerenergy state E, as illustrated in figure3.2. Most laser sources use a medium (gas or solid) and external stimulation (electrical or optical) to generate light.

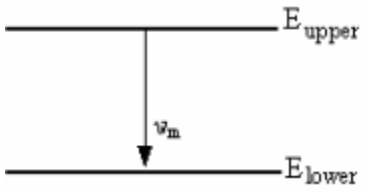

Figure 3.2 Diagrammatic representation of the energy levels involved in light emission

Laser output can be continuous, permanent (called CW or continuous wave), or pulsed using Q-switching, locking mode, or gain-switching processes. The laser beams are those with nominally constant output for seconds or longer. Pulsed lasers provide their energy at rapid power explosions and fire individual pulses or pulse sequences at regular intervals. In pulsed operation, peak power can be significantly enhanced. However, for industrial applications, the laser pulse width is also crucial. As a result, lasers of femtoseconds were used. In all conditions, the laser beam becomes extremely collimated, with a minimal discrepancy, but a perfectly collimated beam cannot form due to the influence of diffraction. However, a laser beam is substantially less widespread than an incoherent light beam. This is because the distance between the shaft and the square of its diameter is growing directly, but the angle with which the beam ultimately differs changes inversely with its diameter.

3.2.1 Mechanism of Laser beam generation:

A laser consists of an active laser medium or medium and a resonant optical cavity. The recovery medium is utilized to convert outside energy into laser energy. It is a pure, controlled, controlled, and controlled substance that amplifies the beam by the quantum mechanical process of the stimulated emission. An external source of energy energizes or pumps the medium of recovery. Electricity and light are examples of pump sources, such as a flashlight or other laser. The laser medium absorbs pump energy, leading to high-energy ("exciting") quantum states for some of its components. Population

reversal occurs when the number of particles in an excited state exceeds that of particles in a lower energy state. When an optical beam passes through a material, more stimulated emissions are created than stimulated absorption,amplifying the beam. Thus, an exciting laser medium can also serve as an amplifier. The light generated by the stimulated emission in terms of wavelength, phase, and polarisation is surprisingly equal to the input signal.This gives laser light a distinctive coherence and enables the consistent polarisation and monochromaticity of the optical cavity to be preserved.

3.2.1.1 Cavity of an Optical Resonator:

The optical cavity is a sort of cavity resonator. A coherent beam of light is enclosed between two reflective surfaces. Each photon is circulating through the recovery medium several times before sending out the output opening. As light cycles in the cavity, the gain medium passes. When the medium is larger than the resonator losses in gain (amplification), the power of the circulating lightcan increase exponentially. However, every stimulated emission event returns a particle to its ground condition reducing the medium's potential to amplify further. If this effect becomes considerable, the gain is deemed saturated. The balance of the pump power against saturation and cavity losses results in an equilibrium value for laser intracavity, which determines the point of operation of the laser. If the pump power selected is not adequate, the gain is insufficient to overcome the losses of the resonator, and the laser produces very little light. The lasing threshold is the minimum pump capacity necessary for laser action. The gain media increases all photons traveling around it, irrespective of orientation. But photons only pass through the medium more than once aligned with the cavity, leading to significant amplification. To achieve big improvements, we need a long, pumped road. One way is to reflect and fold the beam between two mirrors. This limits the beam into a resonant cavity, sometimes referred to as a Fabry-Perot resonator. Numerous resonator cavities

have been created and categorized as stable resonators. Figures 3.3 and 3.4 depict the form of the resonators.

If there is still an arbitrary beam in a laser resonator, it is considered stable. When a ray escapes after a significant number of reflections, it is called an unstable resonator. Unstable resonators require more retention media to sustain laser oscillation (Miloni and Eberly) and offer numerous advantages for some high-power lasers. Stable resonators face the problem of tiny needles, making them inappropriate for high-power resonators. As a result, a considerable percentage of the gain medium is not covered. Unstable resonators have a much broader mode volume and utilize the gain medium more widely and generate more power generation while operating in transverse low loss mode.

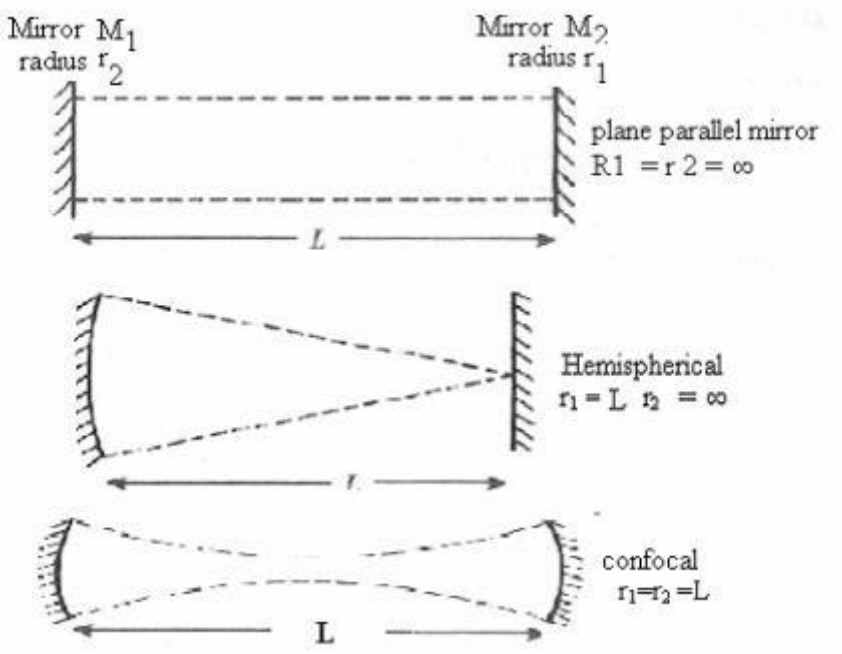

Figure 3.3 Stable resonator schematic diagrams

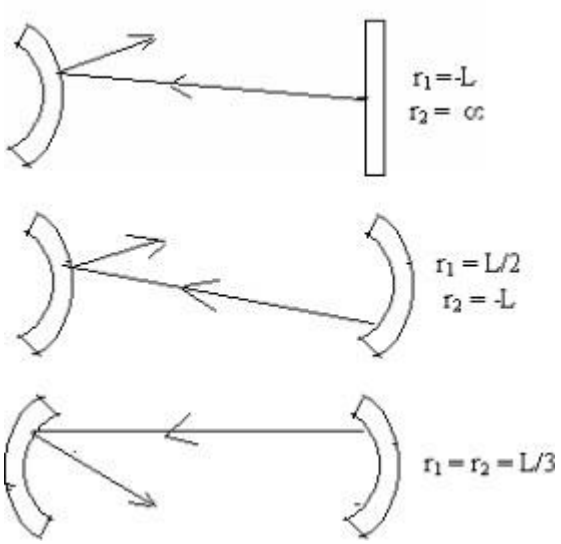

Figure 3.4 Diagrams schematics of unstable resonators

3.3 GAUSSIAN BEAM OPTICS:

Lasers should produce Gaussian beams, perfect for beam focus and high-intensity generation. The cavity beam and the laser output beam are found in space instead of waveguides (such as optical fiber laser); they are often Gaussian beams. If the shaft has no pure Gaussian shape, transverse modes of the beam can be analyzed as an overlay of Hermit or Laguerre. Although the beam can be collimated extensively, a fully collimated beam cannot be generated with minimal divergence due to the diffraction. But a laser beam is much less widespread than an incoherent beam. The shaft is collimated for a distance proportional to the square beam diameter before it is differentiated inan angle proportional to the beam diameter. Additional information is available elsewhere for accurate mathematical analysis of such beams (Milonni and Eberly 1988).

Laser beams exhibit an intensity profile similar to in a plane perpendicular to the spread direction (z) [3.1].

$$I(x, y, z) = |\varepsilon_0(r)|^2 e^{-2(x2+y2)/w2} \text{ ---------- } [3.1]$$

If the beam is shown on a screen, a spot with radius w is visible, and w isknown as the size of the Gaussian beam. Thus, the solution to (r) is available in the following format:

$$\varepsilon_0(r) = \frac{Ae^{-i\phi(z)}}{\sqrt{1+z^2/z_0^2}} e^{ik(x^2+y^2)/2R(z)} e^{-(x^2+y^2)/w^2(z)} e^{ikz} \text{ --------- } [3.2]$$

The spatial intensity distribution of the Gaussian beam is thus provided on any plane z = constant:

$$I(x,y) = I_0 e^{-\frac{2(x^2+y^2)}{w^2}} \text{ ----------[3.3]}$$

The point size(z) in some plane Z=0 has a minimum value of w and is increased according to the relationship [3.4]

$$w(z) = w_0\sqrt{1+z^2/z_0^2} \text{ ----------[3.4]}$$

Figure 3.5 illustrates this behavior. The spot size w(z) is defined as the radius at which the beam's intensity is 1/e 2 of its on-axis value. It is worth noting that even with a highly collimated beam, the beam size changes continuously alonga Gaussian beam's propagation path. There is a minimum diameter or beam waist somewhere along the shaft. This waist is often positioned inside the laser or at the output mirror for a Gaussian beam created by a laser. The plane with Z=0 is referred to as the beam waist. There is a zone about w where the beam remains relatively constant. The Rayleigh region encompasses that area. The

Rayleigh range is a metric for collimation. Z 0 is the Rayleigh range specifiedby

$$z_0 = \frac{\pi w_0^2}{\lambda} \quad \text{---------- [3.5]}$$

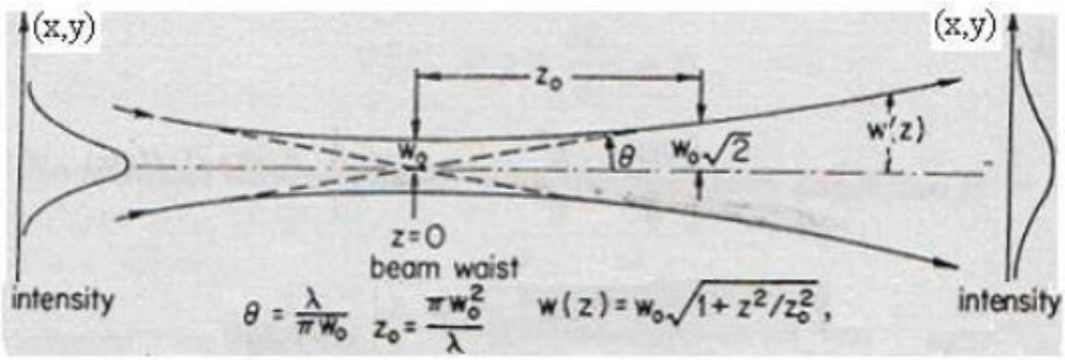

Figure 3.5 Gaussian beam optics illustrating the variation in the size of the spot and the beam divergence

The Rayleigh range, shown in Figure 3.6, is the smallest point area measure of the circumference of the waist region. The Rayleigh range is the distance from the beam's waist to the point where the beam expands by a factor of two. Thus, the smaller the point size W near the core of the shaft, the shorter the Rayleigh range, and the bigger the point size increases with Z further from the waist.

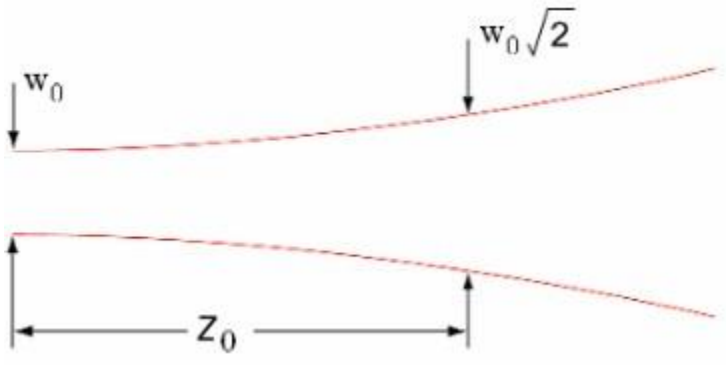

Figure 3.6 Definition of Rayleigh range of a laser beam

Diffraction dictates the minimum beam size, which results in the divergence angle. The Gaussian beam's divergence angle can be defined as

$$\theta \approx \frac{w(z)}{z} \approx \frac{w_0}{z_0} = \frac{\lambda}{\pi w_0} \quad z >> z_0 \qquad \text{---------- [3.6]}$$

The difference between the Gaussian beam and the flat wave diffraction can be compared to an opening with a diameterDw0 on the beam waist. As the beam gets more focused, it gets more divergent. As a result, the spot size w(z) will be vast distances from the beam waist.

$$w(z) = \frac{w_0 z}{z} = \frac{\lambda}{\pi w_0} \quad z >> z_0 \qquad \text{---------- [3.7]}$$

The spot size increases linearly with beam waist distance z. The light is focussed on the material surface using a lens for material processing applications. Since the lens is not planned, it will change the curvature of the beam.

The spot size increases linearly from the beam waist with the distance z. For applications in material processing, the light is focussed on the material surface by a lens. This will alter the beam curvature, as the lens will not affect the transverse intensity distribution of the beam laser. After a focal length f passes through a lens, the spot size at the waist of the new beam

$$w_0' = \frac{\lambda f}{\pi w_0} \frac{1}{\sqrt{1 + f^2 / z_0^2}} \qquad \text{----------[3.8]}$$

According to Equation 3.8, the Gaussian beam can be concentrated to a small spot, and so a Gaussian laser beam can be employed for material processing applications. This is seen in Figure 3.7

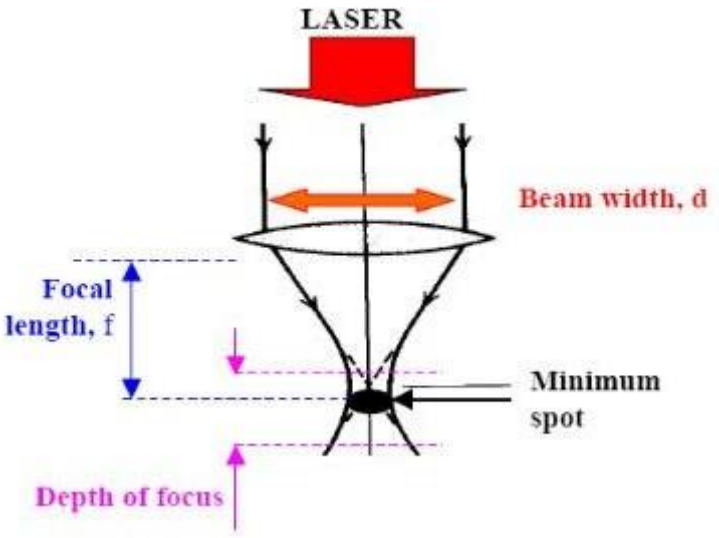

Figure 3.7 Schematics of Laser Beam Focusing

3.3.1 Gaussian beam and geometrical optics:

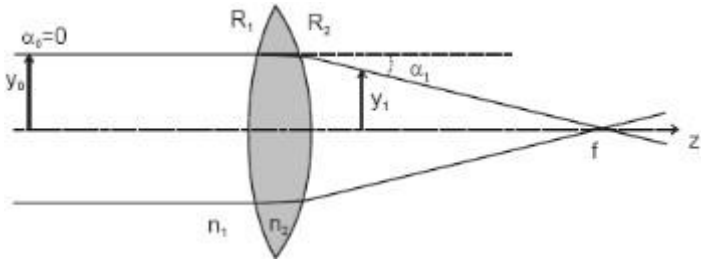

Figure 3.8 Focussing of beam lens makers formula

The lens manufacturers' equation [3.9] must be considered when examining the effect of a narrow lens on Gaussian beams. Concerning Figure 3.8, it is possible to demonstrate that the focal length, f, of a lens is defined by the refractive indices of the ambient and lens materials, n1 and n2, and the radius of curvature of the two lens surfaces, R1 and R2, respectively.

$$\frac{1}{f} = \frac{n_2 - n_1}{n_1}\left(\frac{1}{R_1} - \frac{1}{R_2}\right) \quad \text{---------- [3.9]}$$

What matters is that the approximation sin ( ) = holds, representing the angle formed by the beam with the optical axis. This condition is met by many regularly used optical systems, most notably those employing laser beams, where divergence angles are often relatively modest. Thus, the ABCD formalism can be used if the paraxial assumption is valid throughout the optical system. This statement indicates that the relationship between the distance from the optical axis, y, and the divergence angle of the ray, before and after a visual element, may be determined using equation [3.10].

$$\begin{bmatrix} y_1 \\ \alpha_1 \end{bmatrix} = \begin{bmatrix} A & B \\ C & D \end{bmatrix} \begin{bmatrix} y_0 \\ \alpha_0 \end{bmatrix} \quad \text{---------- [3.10]}$$

Given free space propagation of length z, the spot size equation [3.7] is equal to geometrical optics. The ABCD formalism for Gaussian beams can be used to study the transformation caused by a narrow lens of focal length, f. Consider the introduction of a complicated radius of curvature.

$$\frac{1}{q} = \frac{1}{R} + i\frac{\lambda}{\pi w^2} \quad \text{----------[3.11]}$$

The fundamental part of 1/q represents the reciprocal radius of curvature of the wave front, which is less than zero to the left of the beam waist, more significant than zero to the right of the beam waist, and equal to zero at the beam waist. The beam's dimensions are specified in the imaginary section of equation 3.11. Since the wave front may now be examined as it passes through optical devices,

$$q_f = \frac{Aq_i + B}{Cq_i + D} \quad \text{----------[3.12]}$$

Qr denotes the complex curvature after the optical element, and q represents the complex curvature preceding the optical element. The helpful fact is that the coefficients in eq. 3.12 are identical to those in Table 3.2 for geometrical optics.

Optical Element	$\begin{bmatrix} A & B \\ C & D \end{bmatrix}$
Propagation Length L	$\begin{bmatrix} 1 & L \\ 0 & 1 \end{bmatrix}$
Thin lens of focal length f	$\begin{bmatrix} 1 & 0 \\ -\frac{1}{f} & 1 \end{bmatrix}$
Combined optical system of propagation length followed by a thin lens of focal length f	$\begin{bmatrix} 1 & L \\ -\frac{1}{f} & 1-\frac{L}{f} \end{bmatrix}$
Refraction at a spherical surface, radius of curvature R, from refractive index n to n'. R = ∞ at flat interface	$\begin{bmatrix} 1 & 0 \\ \frac{n-n'}{Rn'} & \frac{n}{n'} \end{bmatrix}$
Spherical mirror, radius of curvature, R. Flat mirror : R = ∞	$\begin{bmatrix} 1 & 0 \\ \frac{2}{R} & 1 \end{bmatrix}$

Table 3.2 A ray is transformed by optical elements utilizing ABCD matrices.

3.4 LASER BEAM MODES:

We obtain a standing wave pattern of electric Field intensity in the resonant cavity generated by the mirrors that do not vary over time due to successive reflections of the mirrors. The term "mode of the resonator" refers to this steady-state spatial distribution of electric and magnetic fields. The criterion for obtaining such a wave pattern is

$$p\lambda/2 = L \text{ ----------[3.13]}$$

Where p is an integer and L is the cavity's optical path length. As a result, we have a series of frequencies denoted by

$$\nu_p = pc/2L \quad \text{----------[3.14]}$$

Where c is the speed of light, each p denotes the cavity's axial mode. As a result, the methods must be separated.

$$\delta\nu = c/2L \quad \text{----------[3.15]}$$

A 25cm cavity produces a mode separation of 600 MHz. Additionally, due to the mode separation and the structure of the gain medium, the potential frequencies are constrained. This means that only one or a few modes will be amplified sufficiently to lase, as illustrated in figure 3.9c. Only the modes below the dotted line's gain curve will have sufficient gain to lase. Only methods that fall under the gain profile's peak will be enhanced and sustained. Fig. 3.9 illustrates the combination of the gain profile and cavity modes that results in a succession of densely packed excited modes. Typically, the breadth of the mode peaks is expressed in terms of a Q factor.

$$Q = \frac{2\pi(\text{energyStored})}{(\text{Energy dissipated per cycle})} = \nu/\delta\nu \quad \text{----------[3.16]}$$

In general, a laser oscillates in a variety of transverse and longitudinal modes. Because a Gaussian laser beam always contains transverse electric methods, the so-called TEM's exist. The ways are denoted by the number of minima in the electric field strength observed when scanning up or across the cavity. As a result, we have TEM 00, TEM 01, and so forth. The most frequently used mode is the TEM mode, which automatically changes the mirror surfaces to be continuous phase surfaces. This mode radiates in a primary, angularly

symmetric pattern. Its fluctuation with radius is similar to that of numerous other functions seen in nature.

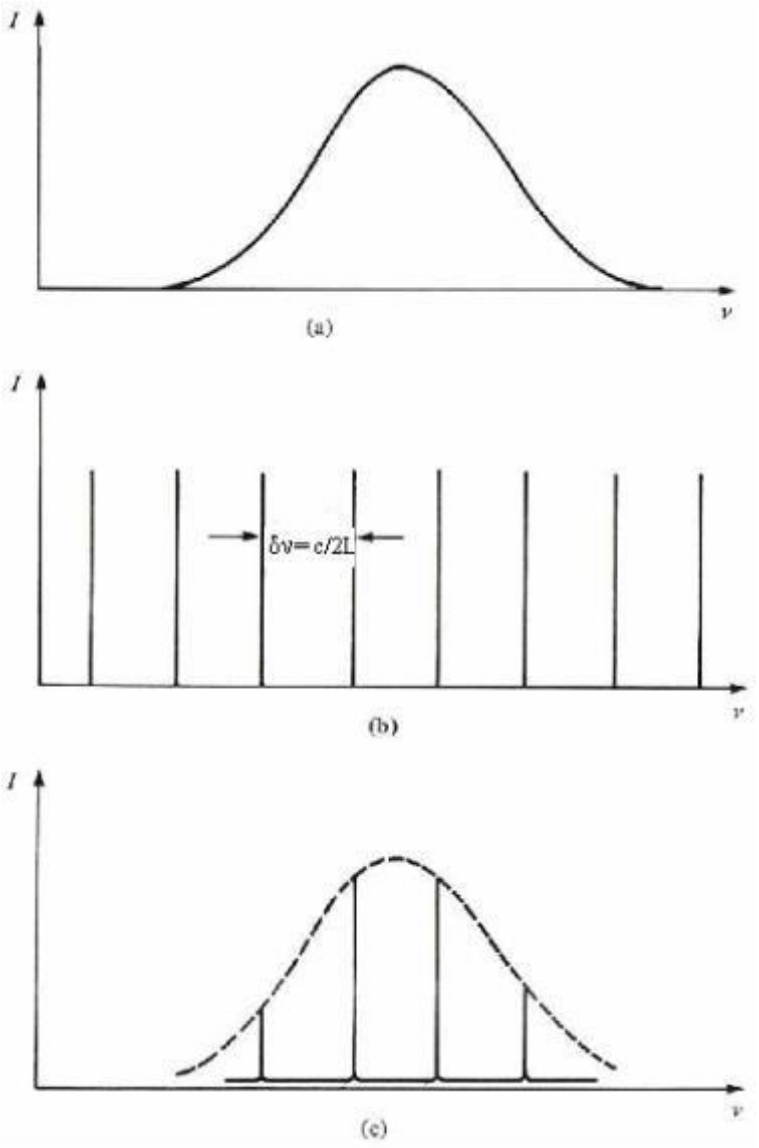

Figure 3.9 within the gain profile, exciting laser modes

An appropriate aperture in the cavity's center can pick out the TEM 00 mode, resulting in a so-called Uniphase mode. Specific lasers are multimode. Multimode lasing is obtained when the gain profile of the laser is broad compared to the mode separation or when the number of light roundtrips in the resonator is low, preventing the formation of a stable mode. The latter is true forhighly brief pulses of light. Diffraction effects are often less significant in

multimode lasers, although the beam quality is significantly better in single- mode lasers. The intensity distribution of TEM modes in the center of a laser cavity is depicted in Figure 3.10.

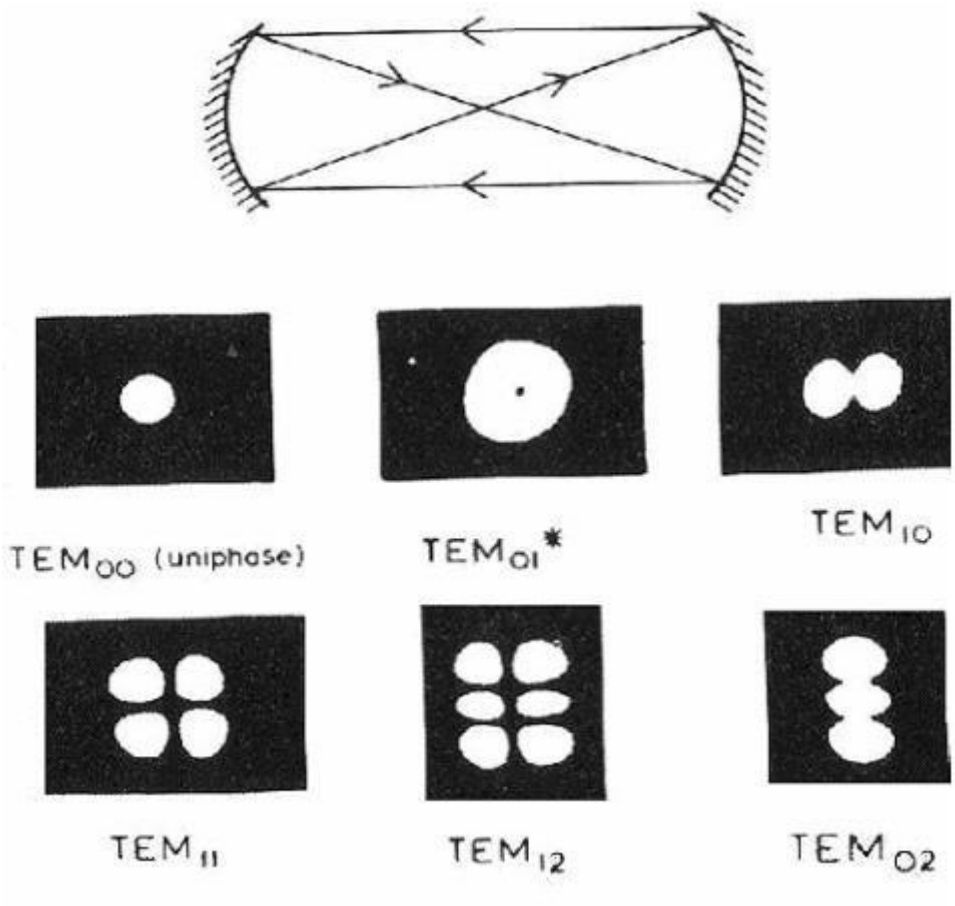

Figure 3.10 The intensity distribution of TEM modes in a laser cavity's center

3.5 LASER BEAM PROFILE:

The majority of laser material processes are energy density-dependent, as measured in Joules/cm 2. The energy profiles of laser beams can have a variety of effects on processes. A beam profile analysis comprises the measurement of a laser beam's power, beam divergence, brightness, spot size, and energy propagation parameters. Theoretically, a collimated intrinsic stigmatic beam with identical propagation parameters in the x and y transverse directions is ideal.

3.5.1 Beam divergence:

It is the beam's spreading angle, given in radians or milliradians. Figure 3.11 shows the divergence of the beam as a function of the diameter of the shaft. In small angles, when the beam divergence is about equal to the arc, the ratio of the cable length (beam diameter) to distance (range) from the laser aperture may be calculated quite accurately.

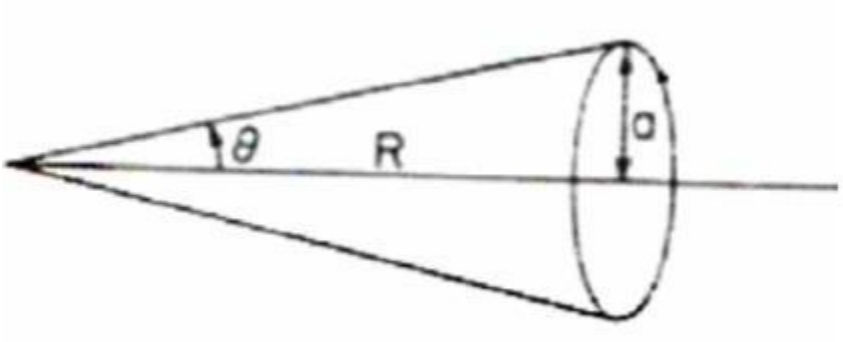

Figure 3.11 Divergence of the beams with relation to the solid angle

3.5.2 Brightness:

The emitted power per unit area per unit solid angle represents the visual sense of a light source's luminous intensity. This is advantageous when a laser needs to be focused by a lens to boost its intensity because the intensity obtained in the focal plane of a lens is proportional to the beam's brightness. The peak intensity at the beam's waist will be equal to the total power P conveyed by the shaft.

$$I_{max} = 2P/\pi w_0^2 \text{ ----------[3.17]}$$

The corresponding brightness will be

$$B = \frac{I_{max}}{\Omega} = \frac{2P}{\lambda^2} \quad \text{----------[3.18]}$$

where Ω is the associated with a divergence angle θ

3.5.3 Fluence:

The term "fluence" refers to the total energy applied per unit area.

Fluence = (power*time) /area ----------[3.19]

3.5.4 Average power:

By multiplying pulse energy by pulse repeat rate, the mean power of a pulsed beam is computed. The average intensity of a continuous wave (CW) beam is measured in watts per unit of time.

3.5.5 Power Density or irradiance:

The power density of material depends significantly on the number of laser photons. The power density is calculated by dividing pulse energy by spot in watts per centimeter squared. Even within one location, the power densityvaries substantially according to the quality of the laser beam. The maximum irradiance (power per unit area) I 0 is generally near the center of the beam design. All other values are usually compared with this maximum value.

3.5.6 Peak Power:

While the average power rating of a laser may be low, the maximum power of each pulse might be exceedingly high. For example, a standard 10-W laser can deliver a total capacity of up to 5 kW. This is possible because the laser beam is incredibly short in pulse duration. The pulse energy can be determined by dividing it by the pulse width. A 1 J pulse in 1 millisecond has a peak power of 1 kW. But since the predicted value is an average across the pulse period, the actual peak power can be higher because energy is not delivered uniformly over the pulse time.

3.5.7 Pulse Energy:

Most calculations start with the energy supplied in a single pulse. The point included in every pulse can be regulated for a particular delivery profile with the newest power generation, enabling a progressive ramp-up at the beginning and a gradual cooling down at the end of the pulse. Pulse shaping adds to improved process control.

3.5.8 Pulse Duration and Repetition Rate:

The pulse time is the laser energy pulse duration. The great majority of applications for laser processing are pulse-based. The pulse mode causes the laser to generate energy in the pulses of default duration and repeat rate. Continuous application wave or CW mode includes welding, cutting, welding, and heat treatment.

3.5.9 Beam diameter:

The distance in the cross-section of a circular beam between points opposed if the intensity is reduced by a factor of e=1(0.368) (for safety standards). The value is usually established at e=2(0.135) for production standards. The Beam

Radius is often defined as the radius at which the beam radiation amounts to 13.5% of the maximum radiation I0.

3.5.10 Spot Diameter:

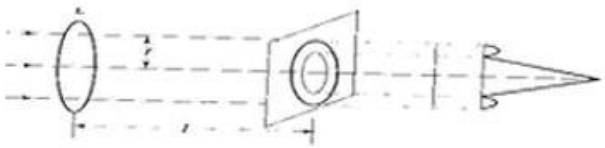

Figure 3.12 Focusing of the incoming beam to determine the diameter of the spot

By equation 3.20, the spot diameter is dependent on the focal length, wavelength, M^2, and beam diameter.

$$\text{Spot diameter} = 2f\lambda M^2 / D, \text{ ----------[3.20]}$$

Where f is focal length of the focusing lens, λ is the wavelength, M^2 is the beam quality metric, and D is the beam diameter. When a plane wave of wave length 'λ', falls on a lens of diameter 'D' in the focal plane of the lens, an intensity distribution occurs.

Most of the energy is confined to the region of diameter $2f\lambda / D$. If P is the power of the beam, equation 3.21 will give the intensity at the focussed region [Nambiar 2004].

$$I = \frac{PD^2}{4f^2\lambda^2\pi} \text{ ----------(3.21)}$$

Excimer lasers, however, create a poorly focused, quality beam. Instead, they flow through a mask to produce the required pattern and are often used to etch silicon chips. Except for the wavelength established after the laser type isselected, practically all other parameters are interdependent and carefully

adjusted. For example, by reducing the spot dimension with a shorter focal lens, boosting power density increases power density unless the overall capacity is decreased proportionally.

3.6 LASER TYPES:

To appreciate the limitations and the promise of laser processing, a fundamental understanding of the laser and its interaction with matter is necessary. While lasers may be handled in a wide range of materials, several essential characteristics and features make some materials more laser-friendly than others. Numerous materials have been discovered to have the attributes to form the laser gain medium needed to power the laser and result in the discovery of multiple kinds of lasers with different features suitable for other uses.

Lasers can be classified according to the laser material they use: gas Lasers, solid-state lasers, semiconductor lasers, and other lasers.

3.6.1 Gas lasers:

These lasers collect energy by employing a gas as the medium of gain. You can classify them as follows:

1) Atomic gas lasers – Eg:He-Ne laser
2) Ion lasers – Eg: Argon ion laser.
3) Molecular lasers - Eg :Carbon dioxide laser

The wavelengths of operation for a few gas lasers (Baruah GD2000) are listed in Table 3.3.

Gain medium of Laser	Operational wavelength(s) in μm
Helium-neon laser	0.6328, 0.5435, 0.5939, 0.6118, 1.1523, 1.52, 3.3913
Argon laser	0.4546, 0.488, 0.5145 0.351 , 0.4579 , 0.4658 , 0.4765 , 0.4727 , 0.5287
Krypton laser	0.416, 0.5309, 0.5682, 0.6471, 0.6764, 0.7525, 0.7993
Carbon dioxide laser	9.4 , 10.6
Nitrogen laser	0.337.1
Carbon monoxide laser	2.6 to 4, 4.8 to 8.3

Table 3.3 The operating wavelength of some gas lasers that are pumped electrically

3.6.2 Solid-state lasers:

Solid-state laser materials are often synthesized by doping a solid crystalline host with the right energy conditions. For example, the first working laser was aruby laser made of ruby or (chromium-doped sapphire). Another type consistsof the neodymium-doped yttrium aluminum grenade (YAG), known as Nd: YAG. Nd: YAG lasers have a high output power of 1064 nm in the infra red spectrum region. They are used for metal cutting, welding, marking, and laser spectroscopy, and pumping. If a visible (green) consistent source is needed, Nd: YAG lasers are often doubled to 532 nm.

Ytterbium, Holmium, Thulium, and Erbium are other frequent dopants in solid-state lasers. Ytterbium is used in crystals like Yb: YAG, Yb: KGW, Yb: KYW, Yb: SYS, Yb: BOYS, and Yb: CaF2, with a wavelength of around 1020-1050 nm. With Yb: YAG, exceptionally high intensities are feasible in ultrashort pulses. At 2097 nm, holmium-doped YAG crystals create and form an efficient wavelength laser, absorbed extensively by water-bearing tissues. The Ho-YAG

laser is usually utilized in a pulsed mode, passing through fiber-optical operating equipment to rebound joints, removing dental decay, spray malignancies, and pulverizing kidney and gallstone stones.

Ion	Host Material	Wave length μm
Nd^{3+}	$Y_3Al_5O_{12}$ (YAG)	1.06
Nd^{3+}	$CaWO_4$	0.9145, 1.0576 , 1.0633, 1.0641, 1.065, 1.066.
Nd^{3+}	$SrWO_4$	1.0574 ,1.0627, 1.0607
Nd^{3+}	$Y_3Ga_5O_{12}$ (YGaG)	1.0633
Nd^{3+}	CaF_2	1.0457
Nd^{3+}	BaF_2	1.060
Nd^{3+}	$PbMoO_4$	1.0586
Nd^{3+}	Glass	1.37 , 0.9180
Nd^{3+}	Borate Glass	0.918, 1.057, 1.401
Nd^{3+}	Silicate Glass	1.06
Nd^{3+}	Barium Crown Glass	1.061 to 1.062
Gd^{3+}	Silicate glass	0.3125
Yb^{3+}	Silicate glass	1.015
Er^{3+}	$CaWO_4$	1.612
Ho^{3+}	$CaWO_4$	2.046
Pr^{3+}	$CaWO_4$	1.0468
Tm^{3+}	$CaWO_4$	1.911, 0.916
Tm^{2+}	CaF_2	1.116, 1.189

Table 3.4 The wavelength at which specific rare-earth ion solid-state lasers operate

The unconverted pump energy that emerges as heat and phonon energy causes thermal restrictions in solid-state lasers. In combination with a high thermo-optical coefficient (dn/DT), thermal lensing can reduce quantum efficiency. Another unique, diode-pumped, solid-state laser, the thin disc laser, addresses

these difficulties. In this sort of laser, thermal limitations are circumvented using a laser medium geometry with a thickness much smaller than the pump beam diameter. This leads to a more even temperature gradient over the material. The thin disc lasers have been shown to generate up to kilowatts of power. The use of rare-earth ions in lasers [Baruah G D] has been extensively investigated. Table3.4 mentions the rare earth ions present in various host materials.

3.6.3 Semiconductor lasers:

The semiconductor lasers are based on semiconductor gain medium, commonly obtained via stimulated emissions under inversion conditions at inter band transition (i.e., a high carrier density in the conduction band). Much of the semi-conductive lasers are laser diodes pumped via the juncture of n-doped and p-doped semiconductor material by an electrical current. Optically pumped semiconductor lasers in which the absorbed pump light generates carriers are also available. The materials most often utilized in semiconductor lasers (including other optoelectronic devices) include

- InGaAs (indium gallium arsenide)
- InP (indium phosphide)

- GaAs (gallium arsenide)
- AlGaAs (aluminum gallium arsenide)
- GaP (gallium phosphide)
- InGaP (indium gallium phosphide)
- GaN (gallium nitride)

Semiconductor lasers, such as diodes and transistors, use pn-joints to force unidirectional current flow, rectifying alternating currents, to generate light through the combination of conducting electrons with so-called holes, locations

in an atom lacking in an electron and which are equivalent to free particles within a semiconductor. Because electron-hole pair formation demands some energy, recombining these particles provides power, preferably in light form. Because most basic semiconductors have a bandgap of less than 1 eV, this energy is generally emitted as visible or infrared light. The beam cross-section created by semiconductor lasers is relatively small, and therefore radiation diverges greatly depending on the product's beam parameter. Nonetheless, the output power of a single semiconductor device in continuous operation [Orazio svelto] is limited to a few Watts. Semiconductor laser light is between 0.4 and20 m wavelengths. The electric current is utilized for pumping the laser of the semiconductor. Table 3.5 lists the various types of diode lasers and their corresponding wavelengths.

Laser gain medium	Operation wavelength µm
GaN	0.4 µm
AlGaAs	0.63-0.9 µm
InGaAsP	1.0-2.1 µm
VCSEL	850 - 1500 nm,
Quantum cascade laser	Mid-infrared to far-infrared.
Hybrid silicon laser	Mid-infrared

Table 3.5 The operating wavelength of a few diode lasers

3.6.3.1 GaInP (gallium indium phosphide) Semiconductor laser:

Semiconductors with a direct bandgap, whereas semiconductors with indirect band gaps such as silicon do not produce photons in significant amounts. By selecting material compositions with different bandwidths, a range of emission wavelengths can be achieved. (The wavelength of emissions is often just above the wavelength of the bandgap.) Whereas most semiconducting lasers work in the near-infrared area, others (usually based on nitrides) generate blue or purple

light. In contrast, quantum cascade lasers emit light at wavelengths of more than 10 meters. Lead selenide (PbSe) is another often used material for mid-infrared adjustable emissions (lead salt lasers). Most semiconductor lasers generate continuous output. Due to their low capacity for energy storage (short upper stage life), they are not very useful for Q switching pulses. Still, they can beused for ultrashort pulse generation via mode-locking or gain switching. In general, the average output power of short pulses is restricted to several milliwatts, except optically pumped external-cavity semiconductor laser (VECSELs), which may reach an average multi-watt output power with multi- GHz repetition rates in picosecond pulses.

3.6.3.2 Vertical cavity surface-emitting lasers (VCSEL):

Semiconductor lasers, in particular, laser diodes with a monolithic laser cavity that emit light from the surface of the chip. Two semiconductor Bragg mirrors serve the laser cavity. Again, a zone between them generally contains several quantum wells and has only a few micrometers of the total thickness. The recovery medium is generally electrically pumped with a few tens of milliwatts and produces an output power of 0,5 to 5 milliwatts or more for multimode devices. The emission wavelength for VCSELs most commonly employed is about 850 nm, and the GaAs/AlGaAs system is used. However, methods based on indium phosphide can obtain wavelengths of up to 1.3 meters, 1.55 metres, or even more than 2 meters (as necessary for gas sensing, for example).

Only in tiny mode regions (diameters of few microns) can VCSELs create a high-quality beam and thus have limited output power. For wider mode regions, excitation in higher-order transverse modes cannot be avoided; this is due to only a few microns of the minimal cavity length. However, even in conjunction with some wavelength tunability, the short cavity allows a single-frequency operation. In addition, VCSELs may be operated in the gigahertz area with frequencies perfect for transmitting optical fiber communications. Multimode

VCSELs are used for short-range communications in conjunction with multimode fibers. More strange, but possibly more important, is the study of the threshold less laser. Beautiful in this field are vertical cavity surface lasers since they allow quantum phenomena related to cavity mode density modification. This approach has shown a threshold current of only 36 W. (Huffaker 1997).

CHAPTER 4

LASER INTERACTION WITH MATERIALS

The objective of this chapter is to outline in broad strokes how lasers are generated, how they interact with and are absorbed by materials, and how these interactions result in process heat generation. The distinctive properties of performance arising from laser and material interactions and What are the major influences of beam properties (radial mode, polarisation, full power of thebeam) and working part properties (thermal characteristics and dimension).

4.1 PHOTON-MATTER INTERACTION:

Laser material interactions are considered to be a highly complex thermophysical process involving the interaction of temperature, phase transition, and stress strain. It is relevant to laser, material, thermal, and dynamical physics, as well as a variety of other scientific domains. After the laser beam interacts with the material, thermal deformation and transformation deformation cooperate to deform the material. Radiation is the transfer of energy from one item, the source, to another object, the receiver. In general, radiation sources are composed of matter or equipment that convert various types of energy to radiation. In other circumstances, the object itself stores the energy to be converted. The sun and radioactive elements are two examples.

In some circumstances, the radiation source is merely an energy converter, and additional kinds of energy must be provided to generate radiation; examples include light bulbs, x-ray tubes, and laser gain media. The majority of kinds of radiation are capable of penetrating a certain quantity of materials. However, in the majority of cases, radiation energy is absorbed by the substance and transformed to another type of energy. Keeping in mind that photons are

discrete energy units, the passage of photon radiation through matter might result in the following interactions:

- It is capable of penetrating a portion of substance without interacting with it.
- By depositing its energy, it can interact with matter and be totally absorbed.
- It can interact with other particles and be scattered or diverted from its initial path, depositing some of its energy.

When a laser beam interacts with matter, energy absorption and subsequent deposition are critical from a material processing standpoint. The energy transfer interactions can be classified as follows:

- Interactions between photons
- Interactions between pair production
- The interactions of electrons

A photon transmits all of its energy to an electron situated in one of the atomic shells during the photoelectric contact. This energy causes the electron to be released from the atom and begin its journey through the surrounding materials. The electron rapidly loses energy and travels only a short distance from its starting point. As a result, the photon's energy is deposited in matter near the photoelectric contact site. The chance of photoelectric interactions occurring in a given material is strongly reliant on the photon's energy and its relationship to the electron's binding energy. The first stage is the photoelectric interaction, in which the photon transfers its energy to the electron. The second phase involves the electron depositing energy in the surrounding materials. This contact is conceivable only if the photon possesses sufficient energy to overcome the binding energy of the atom and remove the electron. The likelihood of photoelectric contacts is often believed to be inversely related to the cube of the

photon energy ($1/E^3$). This technique does not transmit enough heat to the material during laser material contact.

The photon interacts with the nucleus in such a way that its energy is transformed to matter in a pair-production interaction. The contact creates a pairof positively charged particles, an electron and a positron. These two particles have the same mass, which is equivalent to 0.51 MeV of rest mass energy. Pair creation is a photon-matter interaction that does not occur in laser beam interactions because it requires photons with energy greater than 1.02 MeV. Laser beam intensities are limited in the eV range.

The energy transmission from photons to matter occurs in two stages during electron interactions. The first stage is the one-shot interaction of the photon with an electron, during which all or a major portion of the photon's energy is transferred; the second stage is the energy transfer from the energetic electron as it passes through the material. This is accomplished through a succession of interactions, each of which involves the transmission of a negligible quantity of energy.

4.2 MATTER'S ABSORPTION OF LIGHT:

The amount of laser energy absorbed by a material is entirely dependent on its processing by lasers. Without a phase transition, the energy absorbed by the material in response to laser irradiation is completely transformed to a temperature increase. When a laser beam collides with a target material, a portion of the energy is reflected and the remainder is absorbed.

The amount of radiation absorbed by a material is primarily determined by the frequency of the radiation, the material's electrical conductivity, the angle of incidence and polarisation of the incident radiation material, and ultimately, the concentrated beam's intensity. All metals are excellent reflectors of light but poor absorbers. When the meting point is achieved, the absorptivity increases.

Laser radiation does not emit heat. Only when laser radiation is absorbed by a material can it be turned to heat. We claim that this process is resonant because materials exhibit variable absorption coefficients for lasers of different wavelengths; this absorption coefficient dependency on wavelength is determined by the material's microstructure and electromagnetic characteristics.

Radiation absorption by material can be categorised into three primary processes that include interaction between the material and the incident electromagnetic radiation: electronic absorption, lattice or phonon absorption, and free-carrier absorption. Electronic absorption occurs when incoming radiation interacts with the movements of electrons within the substance. Ifthere is an interaction link between the motions of thermally induced vibrations of the constituent atoms of the substrate crystal lattice and the incident radiation, lattice absorption occurs. However, the materials are constrained by limited absorption zones generated by atomic vibrations.

When incident radiations have frequencies that are in resonance with any of the lattice material's characteristics, they excite the atoms or electrons bytransferring their energy as thermal energy. To absorb incident radiation by a specific mode of vibration atom, a mechanism must exist to couple their vibrational motion to the electromagnetic radiation. When linked, the lattice vibration generates an oscillating dipole moment that can be driven by the radiation's oscillating electric field (E). To achieve total energy transfer, any mode of vibration must satisfy three conditions: energy conservation, momentum conservation, and the presence of a coupling mechanism between the material and the incident medium.

The coupling between the incident photon and the lattice phonon occurs as a result of a change in the crystal's electric dipole moment (M). When two equal and opposing charges are located relatively close together, a dipole moment occurs. It is the product of either of the charges and the distance between them. Thus, the energy collected from the radiation is transformed to atomic vibrations.

4.2.1 Fresnel's theory of light absorption:

The mechanism by which light is absorbed by the metal appears to be unresolved in the literature, and so numerous researchers have expressed their viewpoints. Schulz W et al. (1987) demonstrated that the classical mechanismof light absorption on a flat metallic surface, as stated in the Fresnel s formulae, is adequate to produce efficient absorption. For laser light in the infrared area, it is obvious that smooth metallic surfaces absorb only a few percent of theincident radiation at normal incidence. However, if the cutting front is tilted steeply, a significant portion of the incident light can be absorbed. As a result, a quick overview of Fresnel's absorption theory is provided below. The complete theory is available elsewhere [Stratton J A 1941].

The absorption of light is represented using a conventional Fresnel s formula, in which the light beam is considered to couple to a metal electron gas, which absorbs a portion of the intensity due to Joule heating. This technique results in an intensity-dependent absorption coefficient A that is essentially proportional to

(i) The laser beam's polarisation state

(ii) The angle of incidence of the laser beam as measured in relation to the surface normal

(iii) The quantity that is material dependent

$$\varepsilon^2 = \frac{2\varepsilon_2}{\varepsilon_1 + \sqrt{\varepsilon_1^2 + \Sigma^2}} \text{ ----------[4.1]}$$

This combines the real part of the dielectric constants ε_1 and ε_2 of the metal and the gas respectively, and the non dimensional conductivity

$$\Sigma = \frac{\sigma_{st}}{\omega \varepsilon_0} \text{----------[4.2]}$$

Here σ_{st} is the static conductivity of the metal at the laser frequency and ε_0 is the vacuum permeability. The absorption coefficient is then given by

$$A = 1 - \frac{2\cos^2\theta - 2\varepsilon\cos\theta + \varepsilon^2}{2\cos^2\theta + 2\varepsilon\cos\theta + \varepsilon^2} \text{ ----------[4.3]}$$

This holds true for both P-polarised light and the conductivities seen in metals. Its highest value of around 0.8 at glancing incidence is an order of magnitude more than its value at normal incidence. The substantial reliance of the Fresnel s absorption coefficient A on the incidence angle indicates that a steeper cutting front results in increased absorption.

4.2.2 Lorentz model based on the classical theory of absorption:

On the basis of the classical theory of absorption, a better understanding of the absorption of light as it interacts with the medium is based on the Lorentz electron oscillator model [Milonni P W 1988]. When no external forces act onan atom, the model assumes that each electron has a fixed equilibrium location. When an electromagnetic field is applied, the electron is subjected to the Lorentz force and is displaced from its equilibrium location. This displacement generates an elastic force that acts to return the electron to its original position. The Newton's equation can be used to describe the electron's velocity.

$$m\frac{d^2x}{dx^2} = e\,E(R,t) - k_s x \text{ ----------[4.4]}$$

Here, m denotes the reduced mass of the nucleus electron pair, R is the coordinate of its centre of mass, x denotes the relative coordinate, and k denotes

the spring constant associated with the hypothetical elastic force. If frictional force F is applied to the electron oscillators, equation [4.5] is changed to read

$$m\frac{d^2x}{dx^2} = e\,E(R,t) - k_s x + F \quad \text{----------[4.5]}$$

If we suppose that frictional force is compatible with the concept of frictional drag, then

$$F = -bv = -b\frac{dx}{dt} \quad \text{---------- [4.6]}$$

If we define $\sqrt{k_s/m} = \omega_0$ as the electrons natural frequency, and $\frac{b}{2m} = \beta$

[4.6] can be written as

$$\left(\frac{d^2x}{dt^2} + 2\beta\frac{dx}{dt}\omega_0^2 x\right) = \frac{e}{m}E(R,t) \quad \text{----------[4.7]}$$

E is also polarisation dependent on the material medium through which the field E propagates. This relationship can be expressed mathematically using Maxwell's fundamental electromagnetic field equation.

$$\nabla^2 E - \frac{1}{c^2}\frac{\partial^2 E}{\partial t^2} = \frac{1}{\varepsilon_0 c^2}\frac{\partial^2 P}{\partial t^2} \quad \text{----------} \quad [4.8]$$

Where c is the velocity of light in vacuum, ε_0 the electrical permittivity of free space, P is the electric dipole moment per unit volume of the medium. The solutions of equations 4.7 and 4.8 will provide the Lorentz model's prediction about the mutual interaction of light and matter. When there is monochromatic plane wave having linear polarisation, the electric field at the position of the atom has the form

$$E(z,t) = E_0\cos(\omega t - kz) \quad \text{----------[4.9]}$$

Where k is an arbitrarily chosen constant. E0 denotes the wave amplitude that is independent of time or position. If the wave propagates via a material medium,

then [4.9] is a solution to the linked Maxwell Newton's equation if the electric field drives the Newton's equation:

$$\frac{d^2x}{dt^2} + 2\beta\frac{dx}{dt}\omega_0^2 x = \frac{e}{m}E_0\cos(\omega t - kz) \quad \text{----------[4.10]}$$

Equation [4.10] gives a solution for the electron displacement x in the absence of frictional force.

$$x = \left(\frac{e E_0/m}{\omega_0^2 - \omega^2}\right)\cos(\omega t - k z) \quad \text{----------[4.11]}$$

If we define the atomic dipole moment as

$$p = ex = \alpha E \quad \text{----------[4.12]}$$

Where we define electronic polarisability

$$\alpha(\omega) = \frac{e^2/m}{\omega_0^2 - \omega^2} \quad \text{----------[4.13]}$$

As the ratio of the atom's induced dipole moment p to the electric field E that induces it. The density of dipole moments can thus be described as

$$P = Np = N\alpha(\omega)E = \left(\frac{Ne^2/m}{\omega_0^2 - \omega^2}\right)E_0\cos(\omega t - k z) \quad \text{---------- [4.14]}$$

Using this result for P in equation [4.8], we obtain the condition

$$k^2 = \frac{\omega^2}{c^2}n^2(\omega) \quad \text{----------} \quad [4.15]$$

where $$n^2(\omega) = 1 + \frac{N\alpha(\omega)}{\varepsilon_0} \quad \text{----------} \quad [4.16]$$

This identifies n(ω) as the refractive index of the medium for the light of frequency ω. In the presence of an frictional force, equation [4.10] can be solved easily by writing it in complex form

$$\frac{d^2x}{dt^2} + 2\beta\frac{dx}{dt} + \omega_0^2 x = \frac{e}{m}E_0 e^{-(\omega t - kz)} \qquad \text{----------[4.17]}$$

Here the physically meaningful part is the real part which should give solution for the electron displacement. Equation [4.17] can be solved by assuming the solution as

$$x(t) = a\,e^{-(\omega t - kz)} \qquad \text{---------- [4.18]}$$

Using equation [4.17] and [4.18] one can find physically relevant steady state solution as

$$x(t) = \mathrm{Re}\left(\frac{e/m\,E_0 e^{-(\omega t - kz)}}{\omega_0^2 - \omega^2 - 2i\beta\omega}\right) \qquad \text{----------[4.19]}$$

Here Re represents the real part of the solution. The polarisability of an atom will then become

$$\alpha(\omega) = \frac{e2/m}{\omega_0^2 - \omega^2 - 2i\beta\omega}$$

$$\alpha(\omega) = \frac{e^2}{m}\,\frac{\omega_0^2 - \omega^2 + 2i\beta\omega}{(\omega_0^2 - \omega^2)^2 + 4\beta^2\omega^2} \qquad \text{----------[4.20]}$$

The polarisation density P will then become complex and is given by

$$P = Np = N\alpha(\omega)E_0 e^{-(\omega t - kz)} \qquad \text{----------[4.21]}$$

Because of complex $\alpha(\omega)$ the refractive index $n(\omega)$ is also a complex number given by

$$n^2(\omega) = 1 + \frac{Ne^2}{m\varepsilon_0}\,\frac{\omega_0^2 - \omega^2 + 2i\beta\omega}{(\omega_0^2 - \omega^2)^2 + 4\beta^2\omega^2}$$

$$= \left[n_{R(\omega)} + i\,n_I(\omega)\right]^2 \qquad \text{---------- [4.22]}$$

The important consequence of equation [4.22] is that in a medium the electric field behaves differently from that of vacuum. The field strength decays with increasing distance of propagation due to $n_I(\omega)$. Since the intensity is proportional to the square of the electric field (real), the intensity shows exponential decay with distance z

$$I(z) = I_\omega(0)(e^{-[nI(\omega)]/c})^2 = I_0\,e^{-a(\omega)z} \qquad \text{-------[4.23]}$$

where 'a(ω)' as called absorption coefficient and is given by

$$a(\omega) = 2[n_I(\omega)]\omega/c \qquad \text{----------[4.24]}$$

$$\alpha(\omega) = \frac{2Ne^2}{\varepsilon_0 mc}\sum_j \frac{\beta_j\omega^2}{(\omega_j^2 - \omega^2)^2 + 4\beta_j^2\omega^2} \qquad \text{---------- [4.25]}$$

The propagation of laser radiation into a material medium is defined by Equation [4.23]. As can be seen from this equation, the amount of radiation absorbed decreases as the thickness of the work piece increases. As a result, laser radiation will not be absorbed by the material's interior since it will be attenuated by the medium.

4.2.1 The electromagnetic theory of light absorption:

Electromagnetic theory can be used to analytically analyse the propagation of light via a conducting medium (Hayt and Buck 2001). Currents are created in conductive materials by the travel of free electrons or holes under the influence of an electric field. The controlling relationship is

$$J = \sigma E \quad \text{----------[4.26]}$$

where σ is the material conductivity. With finite conductivity the wave loses power through resistive heating of the material. The wave propagation in an isotropic, homogeneous medium having permittivity ε and permeability μ is given by the Helmholtz equation

$$\nabla^2 E_s = -k^2 E_s \quad \text{----------[4.27]}$$

Where E denotes the electromagnetic wave's electric field component. K is the wave number that is material property dependent and is defined as

$$k = \omega\sqrt{\mu\varepsilon} = k_0\sqrt{\mu_R \varepsilon_R} \quad \text{----------[4.28]}$$

Equation [4.27]'s X component becomes

$$\nabla^2 E_{xs} = -k^2 E_{xs} \quad \text{----------[4.29]}$$

For a wave propagating in the Z direction, the electric component E_{xs} do not vary with x or y and [4.29] reduces to

$$\frac{d^2E_{xs}}{dz^2} = -kE_{xs} \qquad \text{----------[4.30]}$$

A critical property of wave propagation is that the dielectric constant k can have a complex value and is therefore referred to as the complex propagation constant. It is common practice to express the complex propagation constant in terms of real and imaginary portions as

$$jk = \alpha + j\beta \qquad \text{----------[4.31]}$$

A solution of [4.30] will be

$$E_{xs} = E_{x0}\, e^{-jkz} = E_{x0}\, e^{-\alpha z} E_{x0}\, e^{-j\beta z} \qquad \text{----------[4.32]}$$

Multiplying equation [4.32] by $e^{j\omega t}$ and taking real part

$$E_{xs} = E_{x0}\, e^{-\alpha z} \cos(\omega t - \beta z) \qquad \text{----------[4.33]}$$

E_{xs} is a homogeneous plane wave travelling in the forward z direction. As z increases, the amplitude of E xs decreases exponentially. If the constant has a positive value, it is referred to as the attenuation coefficient. Negative numbers indicate that the wave's amplitude increases with distance, and this is referred to as the gain coefficient, as in the case of laser amplifiers.

Physical processes occurring within a material have an effect on the waveelectric field. This can be explained by the form's complicated permittivity.

$$\varepsilon = \varepsilon' - j\varepsilon'' \qquad \text{----------[4.34]}$$

using [3.34] equation [3.28] can be written as

$$k = \omega\sqrt{\mu(\varepsilon' - j\varepsilon'')} = \omega\sqrt{\mu\varepsilon'}\sqrt{1 - j\frac{\varepsilon''}{\varepsilon'}} \qquad \text{----------[4.35]}$$

α and β are found by taking the real and imaginary parts of jk from [4.35].Hence

$$\alpha = \mathrm{Re}(jk) = \omega\sqrt{\frac{\mu\varepsilon'}{2}}\left[\sqrt{1 + \left(\frac{\varepsilon''}{\varepsilon'}\right)^2} - 1\right]^{1/2} \qquad \text{----------[4.36]}$$

$$\beta = \mathrm{Im}(jk) = \omega\sqrt{\frac{\mu\varepsilon'}{2}}\left[\sqrt{1 + \left(\frac{\varepsilon''}{\varepsilon'}\right)^2} + 1\right]^{1/2} \qquad \text{----------[4.37]}$$

With non-zero ε'' losses occur which are quantified through the attenuation coefficient α .The term $\frac{\varepsilon''}{\varepsilon'}$ is called loss tangent which will have a direct influence on the attenuation coefficient. In a conductive materials $\varepsilon''=\frac{\sigma}{\omega}$ and equation 4.35 becomes

$$jk = j\omega\sqrt{\mu\varepsilon'}\sqrt{1-j\frac{\sigma}{\omega\varepsilon'}} \quad \text{---------- [4.38]}$$

on simplification becomes

$$jk = j\sqrt{-j\omega\mu\sigma}$$

But $-j = 1\angle -90^0$

and $\sqrt{1\angle -90^0} = 1\angle -45^0 = \frac{1}{\sqrt{2}} - j\frac{1}{\sqrt{2}}$

Therefore

$$jk = j\left(\frac{1}{\sqrt{2}} - j\frac{1}{\sqrt{2}}\right)\sqrt{\omega\mu\sigma}$$

or $jk = (j1+1)\sqrt{\pi f\mu\sigma} = \alpha + j\beta$ ---------- [4.39]

Hence $\alpha = \beta = \sqrt{\pi f\mu\sigma}$ ---------- [4.40]

For a wave travelling in +z direction if we can associate only the E_x component , then

$$E_x = E_{x0}\, e^{-z\sqrt{\pi f\mu\sigma}}\left(\cos\omega t - z\sqrt{\pi f\mu\sigma}\right) \quad \text{----------[4.41]}$$

At any point within the conductor the conduction current density J is directly proportional to E:

$$J_x = \sigma E_x = \sigma E_{x0}\, e^{-z\sqrt{\pi f\mu\sigma}}\left(\cos\omega t - z\sqrt{\pi f\mu\sigma}\right) \quad \text{---------- [4.42]}$$

Equations 4.41and 4.42 contains wealth of information. At Z=0, the exponential factor is unity and decreases to 1/e when

$$z = \frac{1}{\sqrt{\pi f\mu\sigma}}$$

Equation 4.43 contains a critical parameter that describes how radiationinteracts with conductors. Any current density or electric field intensity created

at the conductor's surface rapidly decays as we move deeper into the conductor. Calculations of the penetration depth indicate that electromagnetic energy is not transported into the conductor's interior. At distances more than a few skin thicknesses from the surface, all fields in a good conductor such as copper are effectively zero.

4.3 INTERACTION OF LASER AND MATERIALS: EFFECT OF TECHNOLOGICAL PARAMETERS:

Laser material interaction is influenced by elements such as the laser output energy, the thickness of the work piece, and the material's composition peculiarities. Spatial coherence, collimation, and high intensity are all critical laser features in material processing. Spatial coherence and collimation are essential for high-power density focusing. For material removal applications, a high power density is necessary.

Xiufeng Wang et al., [2000], investigated these impacts. They reported that as laser power increases, the maximum temperature increases as well. This means that the amount of energy received by the work piece impacts its temperature value. Additionally, the maximum temperature position shifts to the lower side, suggesting an increase in the depth of heat transfer into the material's interior. They reported that when the same technological parameters are used, the material composition has a significant effect on the ultimate deformation of the work item. The influence of work piece thickness on heat transfer implies that the thinner the specimen, the more heat is transported inside the material,resulting in increased deformation and so affecting the experimental results.

4.3.1 Influence of wave polarisation on absorption of laser by material:

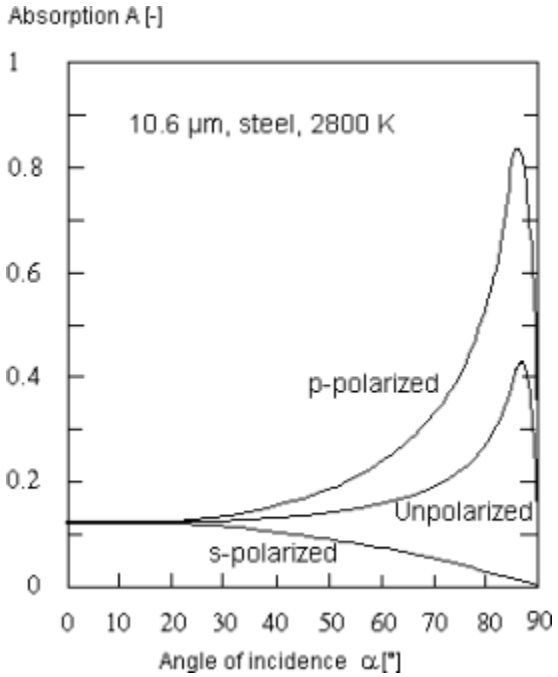

Figure 4.1 CO_2 laser light absorption in steel with varying polarizations

The angle of incidence and polarisation of the incident radiation material also affect the absorption of radiation, as illustrated in figure 4.1. Polarisation of a wave is defined as the orientation of its electric field vector as a function of time at a fixed point in space. If the electrical field strength of incident radiation is linearly polarised and perpendicular to the direction of propagation of a light wave, absorption remains constant and does not significantly change with increasing inclination of the laser beam relative to the absorbing surface until it reaches zero for striping incidence, at which point the wave does not enter the material at all. If the incoming wave is polarised in the opposite direction, the same absorption occurs as with perpendicular incidence, but with increasing inclination, current flows in the material become perpendicular to the surface as well. Because these current flows lose energy, they result in a greater absorption of radiation. Thus, as inclination increases, absorption increases. However,

because no component of the wave can enter the material at striping incidence, the absorption must likewise be zero. This means that maximal absorption occurs at a certain angle known as the Brewster angle. Due to this phenomenon, steel's initially modest absorption, around 10%, can increase to around 80%, although the Brewster angle is only slightly less than 90%, implying virtually perfect incidence of the wave.

The angle of incidence has a significant effect on material processing because most applications, such as laser cutting, produce a virtually perfect incidence of the beam to the material. No effect of the latter quantity on absorption has been found for intensities up to 1 MW/cm^2. Nonetheless, beyond this point, the work piece is heated to such a high temperature that evaporation occurs. Due to the vapour's high temperature, intense collisions between the vapour atoms occur, which can finally result in ionisation of the atoms, which means that electrons are deduced. The latter electrons can then be accelerated by the incoming light wave's electrical field, absorbing a tremendous amount of energy. Thus, when the intensity of the radiation exceeds a critical value of a few MW/cm^2, aplasma forms, resulting in a greatly accelerated absorption of the radiation that can reach nearly 100%, referred to as "abnormal absorption." Plasma creation has a good effect by increasing absorption, but it also results in the emission of UV radiation, which is harmful to the human body.

If the light wave's intensity is increased further, a large number of electrons are generated, resulting in a very high electron density, similar to that found in a metal. In this case, the previously mentioned reflecting properties of electrons may become significant, eventually leading to complete reflection of the laser beam by the plasma - a phenomenon known as 'plasma shielding'. Radiation absorption is also reliant on the material's properties, the wavelength of the radiation, and the temperature at which the absorption occurs. This is seen in figure 4.2 for a few metallic conductors.

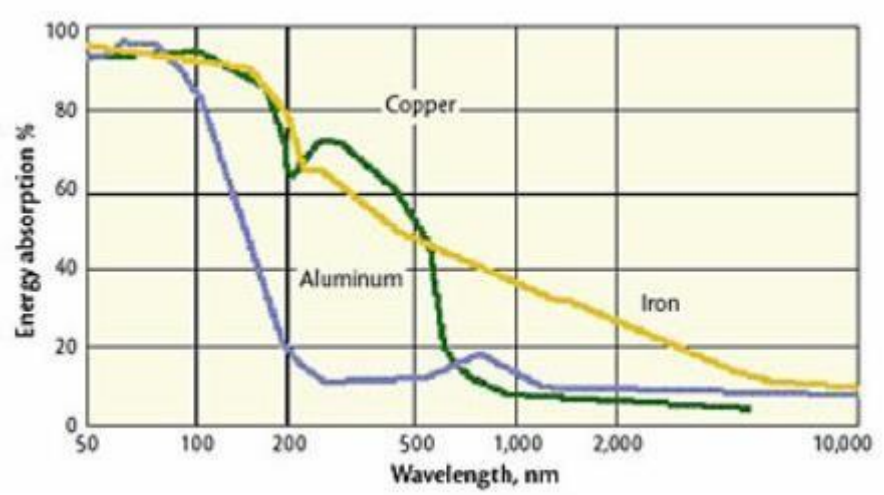

Figure 4.2 At room temperature, the absorption of photons of various wavelengths by iron, aluminum, and copper

4.4 RADIATION TRANSMITTED AND REFLECTED:

The transmission coefficient T is used to determine the amount of incident energy communicated into a material with a dielectric constant. It is defined as the ratio of energy transmitted to energy incident. The equation for calculating the transmission coefficient is as follows:

$$T = 2\sqrt{\frac{2\omega\varepsilon}{\sigma}} \qquad \text{----------[4.43]}$$

'σ ' the electrical conductivity of the medium can be found out using the relation

$$\sigma = \frac{Ne^2}{m(1-i\omega)} \qquad \text{----------[4.44]}$$

Where N is the number of atoms per cubic metre and l denotes the damping constant. Equations 4.43 and 4.44 show how laser absorption is dependent on the incident frequency and electrical property of the material. Copper, for

example, has a 2 percent absorptivity in 10.6-micron CO_2 lasers but a substantially higher absorptivity in UV lasers (about 60 percent).

4.5 PENETRATION DEEPNESS:

Equation 4.45 can be used to calculate the Depth of Heat Penetration for a given laser pulse.

$$D = \sqrt{4\alpha \, dT} \quad \text{----------[4.45]}$$

Where D is the depth of heat penetration, α is the diffusivity of materials, dT is the pulse duration. Conversely, one can estimate the minimum pulse duration needed to penetrate a certain depth. Then we have:

$$dT = \frac{D^2}{4\alpha} \quad \text{----------[4.46]}$$

From equation 4.46, an important component explaining the behaviour of conductors in electromagnetic fields is specified as the skin depth or penetration depth of the electromagnetic wave.

$$\delta = \frac{1}{\sqrt{\pi \, f \mu \sigma}} \quad \text{----------[4.47]}$$

Because the value of is relatively tiny for the conductor, the electric fieldcreated on the surface of the conductor decays rapidly as the wave penetrates into the conductor medium. As a result, the electromagnetic energy is nottransported into the conductor's interior. Due to the skin effect, when the conductivity of the material is very high, the fields attenuate fast toward the interior of the sample. The magnetic characteristics of the material play a role inthe skin effect. A combination of the magnetic field and the current produces a force that pushes conducting electrons outward into a restricted area next to the

border when a substantial current flow inside the sample due to high conductivity. The depth of the skin varies from a few millimeters to a few metres. Table 4.1 shows the penetration depth or skin depth of several industriallasers in various materials. When the skin depth is greater than the sample dimension, the effect may be overlooked. Energy penetration will be limited in this circumstance, making uniform heating impossible. The penetration depth computed using equation [4.47] for a laser beam of wavelength 10.6 microns propagating inside stainless steel with =0.11x10 7 and = is roughly 90-100 nm.

Type of Laser	Wavelength	Penetration depth δ		
		Stainless steel	Aluminium	Copper
CO_2 laser	10600nm	90nm	33nm	12.5nm
COIL	1315nm	32nm	5.4nm	4.4nm
Nd: YAG laser	1060 nm	29 nm	4.9 nm	3.9nm
VCSEL	850nm	25.5nm	4.35nm	3.5nm
Diode laser – GaN	400nm	17.5nm	2.9nm	2.4nm
Excimer laser-KrF	248nm	13.8nm	2.35nm	1.9nm

Table 4.1 At certain wavelengths, the penetration depth of various conductors is measured

4.6 MECHANISM OF HEAT TRANSFER:

The electromagnetic energy interacts with the surface of the material to be processed during laser material processing. A portion of the incident energy is absorbed by the material at its surface, where it is transformed to heat. The molecule charges in the medium vibrate about their mean position when infrared electromagnetic waves penetrate into the material media due to interaction with the incident wave's oscillatory electric field [Matveev, 1998].

Additional velocity and current results are acquired by the electrons in the medium. These electrons collide with the material's ions and are dispersed. An electron loses energy every time it collides with an ion. This energy is passed on to the ion, which vibrates at a higher frequency. The energy released by billions of electron collisions is distributed across all atoms, causing the material to heat up. This is referred to as Joule heating. In laser material processing, the laser beam normally heats up and melts the work piece, and occasionally evaporatesit in a limited zone defined primarily by the focal spot. With increasing specific heat and density, the temperature reached for a given heat input per unit volume drops. As a result, the temperature finally achieved on the work piece's surface and inside along the processed track is primarily determined by the processing speed, the work piece's thermal characteristics, and its thickness [George Chryssolouris, 1997]. Obviously, the highest temperature is obtained when the laser strikes the work piece, and it gradually decreases in lateral direction in a co-ordinate system travelling with the beam with respect to the work piece. The laser beam hits regions that were not previously heated in the direction of relative movement between beam and work piece, causing high heat conduction and a large temperature differential in the depth of cut.

4.7 LASER MATERIAL INTERACTION THERMO PHYSICAL PROCESS:

When considering what happens to the heat, it is possible that it is transmitted, radiated, or convected away from the location. Many mathematical models suggest that convection and radiation play a little role in most practical settings. As a result, conduction is the most important step. When the rate of heat input to the target zone exceeds the rate of heat conduction out from the target zone, the temperature rises locally, resulting in melting, vaporisation, or a mix of the two, however some scientists will point out the potential of sublimation. As a result, when a laser beam is irradiated on the specimen surface, the temperature

on the upper surface in the heated zone rapidly rises until it reaches its melting point. Large temperature gradients will occur along the specimen's thickness direction. The heated material region causes material to collect and compressive plastic deformation, causing the specimen to deform away from the laser beam. The deformation decreases as the heat penetrates into the lower surface. The lower layer grows continuously as the cooling phase progresses, reducing specimen deformation away from the laser. The martensic transformation can produce volume expansion, increasing deformation away from the laser beam, as long as the material possesses the phase transition feature. The experimental results of Xiufeng wang et al. [2000] reveal that the thermophysical process of laser material interaction is divided into two phases: heating and cooling.

When the laser beam is irradiated on the specimen surface during the heating phase, the temperature on the upper surface in the heated zone rapidly rises (not exceeding the Melting point of that material). The material heated region creates complete plastic deformation and causes material to collect due to considerable thermal expansion and low yield stress on the upper surface at a high temperature. As a result, the material begins to deform away from the laser beam. The deformation grows larger and larger when the pulse duration is extended. However, heat conductance causes the heat energy that conducts into the lower surface to be reflected into the specimen, improving the interior of thespecimen. As a result, the distortion is reduced. When the laser beam is turned off during the cooling phase, the upper surface temperature drops rapidly. The material contracts, allowing some of the accumulative material to be recovered and the compressive stress to be reduced. The lower layer of the specimen expands continuously as the chilling process progresses due to heat conductivity, causing it to elongate. The martensitic transformation can generatevolume expansion, increasing the deformation away from the laser beam, as long as the material exhibits phase transformation property. As a result, the

angle of deformation is the result of a combination of thermal and transformation deformation.

4.8 RISE IN TEMPERATURE:

As a result of the absorbed heat transfer (Q), the target temperature rises as specified by

$$T=[Q\ A\ t]/MCp \quad \text{----------[4.48]}$$

where T denotes the product, temperature rise in Kelvins (K), and A denotes the target area (cm^2) M is the target mass (kg), and Cp is the target specific heat (W-s/kg-K), and t is the heating dwell time. The time t necessary for the surface of the material being treated to reach the melting temperature can be estimatedif the heat fluxes H remain constant (Cohen M I,1972) utilising the phrase

$$t_m = \frac{\pi}{\alpha}\left[\frac{[\theta_{mk}]}{2H}\right]^2 \quad \text{---------- [4.49]}$$

The material's thermal conductivity is measured in K. The period t will be exceedingly short, allowing for high-speed laser processing of materials.

The surface temperature of the laser radiation absorbing surface has been studied using a theoretical model created by Yilbas BS and Sahin AS[2003]. They discovered that as the heating time is extended, the temperature rises. The maximum temperature progresses into the material medium as the heating time increases. The surface temperature time dependence could be approximated (Grabowski 2006) using the one-dimensional heat conduction equation with the condition that no phase transition occurs.

$$T(t) = T_0 + (I_0 A/k\alpha)\left[2\alpha\sqrt{\frac{\kappa t}{\pi}} + \exp(\alpha^2\kappa t)\operatorname{erfc}(\alpha\sqrt{\kappa t}) - 1\right] \text{------[4.50]}$$

This distance denoted by δ is termed the depth of penetration or the skin depth

$$\delta = \frac{1}{\sqrt{\pi f \mu \sigma}} = \frac{1}{\alpha} = \frac{1}{\beta} \quad \text{----------[4.43]}$$

CHAPTER 5

EXPERIMENTAL METHODS

Because this thesis is primarily experimental in nature, it strongly relies on a variety of instruments. The three laser processing systems serve as the principal instrument for this endeavour. Apart from these, a variety of additional supporting instruments were used in the current experiment. This chapter provides background information on all of the instruments utilised and details the author's experimental findings.

5.1 EXPERIMENTATION WITH LASER CUTTING:

Experiments with laser cutting were conducted using two CO_2 laser cutting systems operating in continuous wave mode. Rofin Sinar of Germany and the Bystronic Company supplied the systems. The laser beam's power density distribution was (TEM) 00 mode. The CO_2 laser system, supplied by Germany's Rofin Sinar, is linked with Balliu's CNC automated cutting system, which includes a cutting table, cooling system, and automation. The system's maximum laser output power is 2000 watts. The beam focussing system consists of a 190 mm focal length Zinc Selenide focussing lens. The system's cutting range was 3000 mm X 1500m. To remove the melt, either oxygen or nitrogen gas is used to help the cutting. The amount of gas consumed was determined by the cutting material.

By securing the work piece over the cutting platform, the system enabled the laser head to scan the cutting area. The x-parameter was assigned to the stationary cutting table, while the y & z parameter was assigned to the cutting head. The entire laser cutting procedure is managed by a CAD programme that designs the laser beam's path for cutting and the cutting parameters are modified in the manufacturer-supplied software. To perform the actual operations, the profile of the work piece to be cut must be structured using CAD software and

then uploaded to the laser PC for manufacturing. Figure 5.1 depicts a schematic of the laser cutting system.

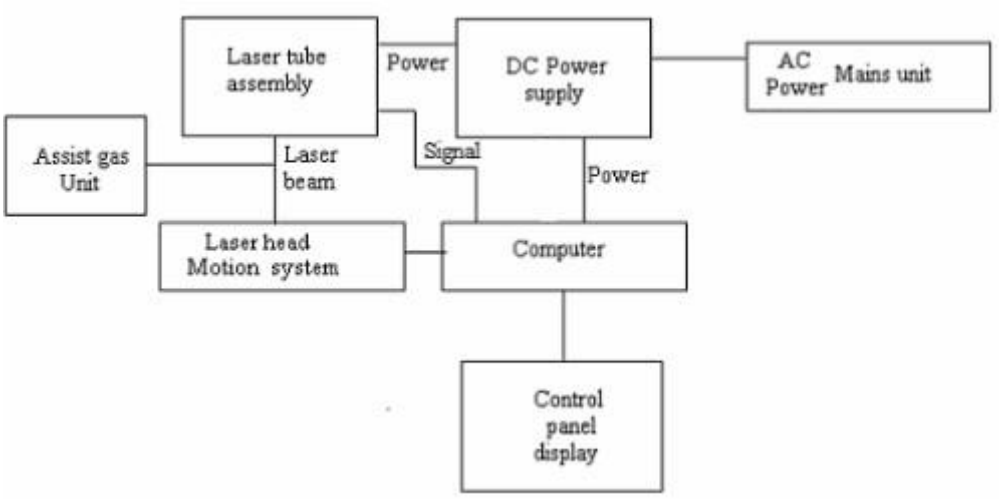

Figure 5.1 Assembling a laser cutting system schematically

Prior to usage, the laser cutter must be focused. This is accomplished using the plastic focus tool and the laser cutter's Z settings. A laser beam delivery system comprised of a mirror telescope, beam-bending mirrors, and a phase shifter directs the beam to the laser cutting head in the most efficient manner possible. Once the beam is directed to the laser head, a focusing lens accurately centres the point on the work area. In CO_2 lasers, lenses consisting of materials with strong far infrared transitivity, such as zinc selenide, gallium arsenide, and germanium, are favoured. A meniscus lens reduces the diameter of the beam, hence minimising spherical aberration and beam waste while precision cuttingor marking. Additionally, the lens features a reduced spot size, which produces the same amount of light in a smaller area. To obtain the lowest possible spot size, the concave side of the lens is angled downward toward the material being cut. Meniscus lenses provide a more precise cut, boosting cutting speed by up to5%. The experimental setup for laser material processing is depicted in Figure 5.2.

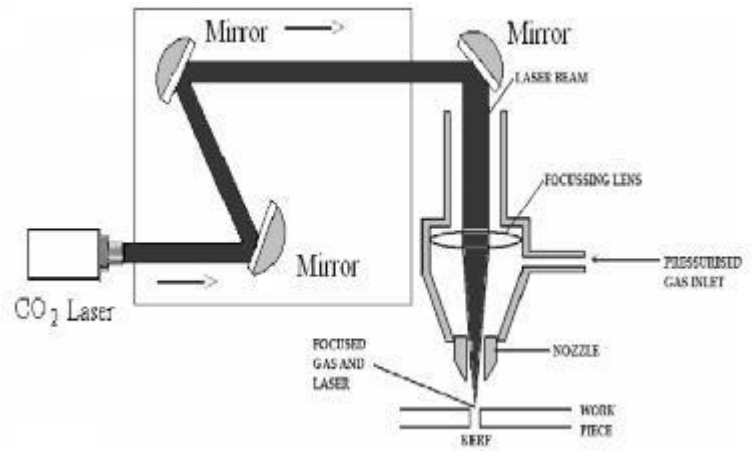

Figure 5.2 Laser processing with beam delivery arrangement is built in an experimental configuration

With oxygen as an assist gas, the Rofin-Sinar laser system was employed totreat materials. You may see Rofin Sinar's genuine laser cutting machine in figures 5.3 and 5.4. For this technique, the laser system of Bystar was used. Thissystem, Bystar-3015, was capable of maximum laser output of 3000 watts and was integrated into the system for processing of the materials as well as the cooling system and automation system. Manual control unit (LCU) was used to regulate the cutting system and the Keyboard used to monitor it. In the plane of the cutting platform, the cutting range is 1.5m x 3m.

Figure 5.3 Laser cutting machine Rofin Sinar CO_2 (full view)

Figure 5.4 Rofin Sinar CO_2 laser cutting machine's cutting head

Metallic mirrors are utilised in the beam delivery system of the laser system used in this work due of their high reflectivity. The laser beam is delivered, manipulated, divided, and focused using external mirrors. In CO_2 laser systems, water-cooled polished copper mirrors are used. Figure 5.5 depicts an image of the Bystar laser cutting machine.

Figure 5.5 Bystar 3015 CO_2 laser cutting machine photograph

As test material, commercially available 304 grade stainless steel plates of various thicknesses were used. The laser beam was focused on the top surface

of the work piece using a 190 mm focal length Zinc Selenide lens. The diameter of the nozzle was 1.2 mm, with a standoff distance of 1 mm. Varying thicknesses of stainless-steel material were cut using oxygen as an assist gas to accommodate different cutting conditions. Laser power, cutting speed, and assist gas pressure were all used as processing factors. Additionally, plates of 3mm thick stainless steel and 12mm thick IS2062 alloy steel were cut at a speedof 1500/min using a 3-kilowatt BYSTAR 3015 laser. The schematic diagram of the laser's cutting head is shown in Figure 5.6.

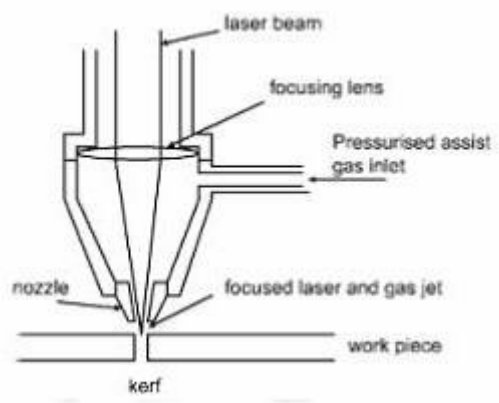

Figure 5.6 Schematic of the CO_2 gas laser's cutting head

Nozzles for gas jet flow exhibit considerable differences in terms of gas dynamics. The supersonic minimum length nozzle is arguably the most investigated form, since it offers the best trade-off between shock-free flow, nozzle length, and manufacturing ease. However, as illustrated in Figure 5.7, sonic nozzles are the industry standard for industrial laser cutting.

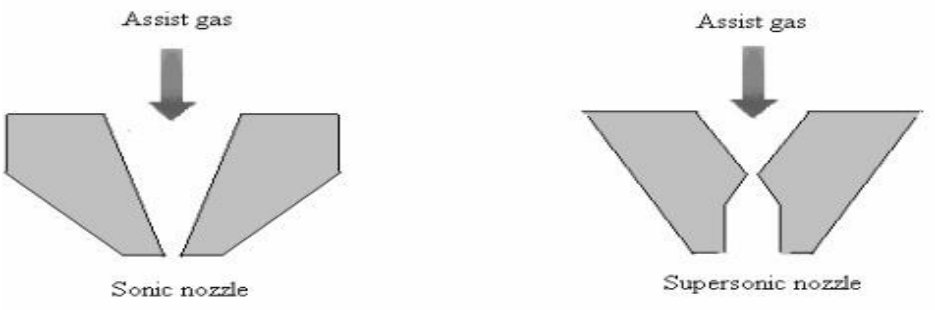

Figure 5.7 Sonic and supersonic nozzles for gas jet flow schematic

Experiments with laser etching were conducted utilising a 75-watt Nd: YAG laser Q -switching marking equipment from France's Laser Chavel. It is a Q-switched laser capable of operating in both pulsed and continuous modes and generating light with a wavelength of 1.064 m. The machine features a 160mm × 160mm X-Y feed and is capable of etching 240 characters per second. While the laser beam moves, the material is etched while remaining attached to the processing platform. Figure 5.8 depicts the machine.

Figure 5.8 Laser marking machine using a 75-watt Nd-YAG laser for etching tasks

LENS software is simple and user-friendly and is utilised in laser marking systems. It includes a graphical editor for creating and running marking programmes. LENS is used to make simple geometric shapes, straight andcircular text, 1D and 2D barcodes, and to import bitmap and vector pictures. LENS objects are associated with a set of laser parameters. These are adjustedto get

the desired effect (depth, aspect, and quality) for the particular type ofpart being engraved. LENS has a plethora of applications. The LENS automation functionalities, which are accessed via the built-in Script editor, expand the capabilities of LENS. When coupled to the optional axis system, LENS can be utilised to automate axial functions such as programmed focus correction, component movement on an X-Y table, and labelling on cylindrical parts.

5.2 ANALYTICAL TECHNIQUES INSTRUMENTS:

While laser cutting machines were the primary instruments used in this study, other instruments such as a scanning electron microscope, an Energy Dispersive X-ray spectrometer, an optical microscope, a metallurgical microscope, and a stylus profiler were used in supporting roles for the analysis of the processed for cut sample characterization. SEM analysis is used to confirm the presence of a hard-white etching layer on the cut surface and to characterise the surface structure. The material composition was determined using Energy Dispersive X-ray Analysis. The cut surface material composition was then compared to the bulk material composition. Mitutoyo surf test-211 was used to determine the roughness of the laser cut surface. SEM was used to investigate the microstructure of the laser cut surface. A brief summary of the other instruments is provided to acquaint the reader with them.

5.2.1 ELECTRON SCANNING MICROSCOPY:

A Scanning Electron Microscope (SEM) is essentially a high magnification microscope that generates images of the sample using a focused scanned electron beam. The microscope is composed of an illuminating system and a top-mounted electron gun. A series of electromagnetic lenses are installed beneath the electron gun to compress and focus the electron beam on thesample. A pair of coils deflect the beam to scan the sample. An electron detectorwill detect the signals produced by the electron beam's contact with the sample surface and will provide an image

of the sample being scanned. The primary electron beam interacts with the material in a number of critical ways to form that image: -

- Primary electrons produce low-energy secondary electrons, which tend to emphasise the specimen's topography.
- Backscattered primary electrons provide images with a high degree of atomic number (Z) contrast.

When an electron in the beam collides with a nucleus in the sample, Coulomb attraction causes the electron's path to be deflected. This phenomenon is referred to as Rutherford elastic scattering. Several of these electrons will be entirely backscattered and reemerge from the sample's incident surface. Due to the substantial dependence of the scattering angle on the atomic number of the nucleus involved, the primary electrons arriving at a given detector point can be used to generate pictures including both topological and compositional information. The incident electrons may also interact with the sample's weakly bound conduction band electrons. Due to the modest amount of energy impartedon these secondary electrons by the interactions, they have a very limited range throughout the sample (a few nm). As a result, only those secondary electrons created within a relatively small radius of the sample's surface are able to escape. As a result of the high-resolution topographical images produced by this detection mode, it is the most extensively employed of the SEM modalities. Hence Electron Microscopy is enabled by the interaction of a specimen with an electron. The snapshot of the SEM with EDX attachment is shown in Figure 5.9.

Figure 5.9 SEM image shows a Scanning Electron Microscope equipped with an Energy Dispersive Spectrometer and an Image Analyzer

The use of electrons to test the surface properties enables extremely high magnifications, which are typically limited by the aberrations of the lenses utilised, rather than the de-Broglie wavelength of the electron. It is feasible to focus the beam to a spot size of 10 nm or better using the electron as a probe. Another critical aspect of electron microscopes is their depth of focus, which is determined by the Rayleigh length, equation 3.5. The reader is referred to Reimer L for a full examination (1985).

5.2.2 Spectroscopy with EDX:

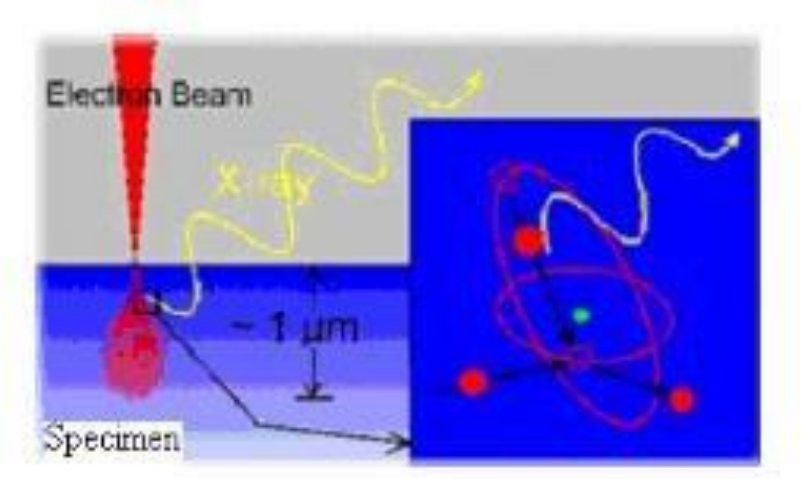

Figure 5.10 Electron beam interaction with the specimen

An energy-dispersive x-ray analyzer (EDX) is a typical accessory that enhances the scanning electron microscopes (SEM) capability for elemental analysis and characterising the studied volume's elemental composition. The interaction of an electron beam with a specimen is depicted in Figure 5.10. To generate X-rays, an electron beam with an energy of typically between 5,000 and 20,000 electron volts (eV) is generated to interact with the object to be studied in a scanning electron microscope (SEM). The energy required to retain electrons in atoms (the binding energy) varies between a few eV and many kilovolts. When an electron beam from the SEM interacts with (rather than merely passing through or transmitting unmodified) the atoms in a sample, the incident electrons suffer two forms of scattering: elastic and inelastic.

Only the trajectory is altered in the former, while the kinetic energy and velocity stay constant. Inelastic scattering occurs when some incident electrons collide with and displace electrons from their orbits (shells) around the nuclei of atoms on the sample's surface. When this interaction removes an electron from a specimen's atom, the vacancy is frequently filled by an electron from an outer shell (or orbital). When an outer electron fills a vacancy, it must sacrifice a certain amount of energy in order to enter the nearby shell. To balance the energy difference between the two electrons, an x-ray is released. The x-ray emitted will have the energy of the parent atom. By coupling an appropriate X- ray detector to a collection of electrical components (amplifiers, counters, and analog-to-digital converters) and a computer, one can detect and analyse X-rays released by a sample that has been illuminated with electrons. The x-ray detector is used to determine the number of emitted x-rays in relation to their energy. The x-energy ray's is a property of the element from which it was emitted. A spectrum of the energy versus relative counts of the detected x-raysis obtained and analysed to determine the elements present in the sampled volume on a qualitative and quantitative basis. The X-rays emitted are indicative of the components present in the sample's upper few metres. The resulting X-ray spectrum can be viewed in

energy-dispersive mode (Energy Dispersive X-ray Spectroscopy - EDS). Figure 5.11 illustrates a typical EDX spectrum produced by the analyzer.

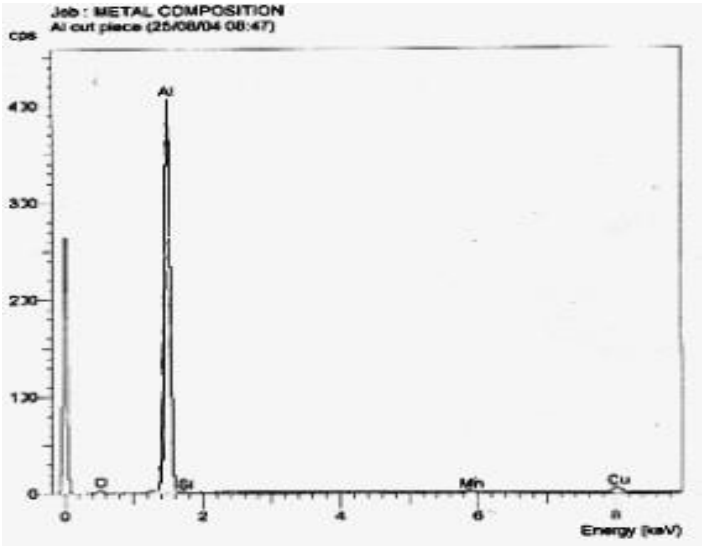

Figure 5.11 A representative EDX spectrum

The peaks of the specimen are particularly distinctive. These peaks contain peak-specific elements. X-rays generated from a sample subjected to electron bombardment are collected and evaluated by a solid-state detector based on their energy. Typically, the EDS computer programmes present a real-timehistogram of the quantity of X-rays detected per channel versus the energy indicated in KeV. (thousand electron volts). In practice, EDS is most frequently used for qualitative elemental analysis, determining the presence and relative abundance of elements. The constituent parts of the specimen can be determined by collecting and evaluating the energy of these x-rays.

5.2.3 PROFILOMETER FOR STYLUS:

It is the simplest instrument for characterising surfaces. In its simplest form, it is simply a pickup—for example, a diamond pyramid—that is dragged along the

surface. Transduction, e.g., a magnet rotating in a coil, converts the vertical movements of the stylus into electrical signals. A two-dimensional map of the surface can be built by recording the distance traversed on the abscissa and the height measured on the ordinate. Additionally, the device can be calibrated to read the recorded data in digital mode automatically. Accurate surface roughness (average values Ra) assessment of machined work parts is critical, especially in the precision engineering and manufacturing industries. Mitutoyo surf test-211 stylus instrument was employed in this study. It is totally automated, and the surface profile data is displayed numerically.

Figure 5.12 A shot of Mitutoyo's 211th surf test.

The illustration 5.12 depicts a portable surface roughness tester Mitutoyo surf test211. It is a modern surface texture measuring tool that electronically records the stylus movement along the evaluation length and generates output values with a high level of detail. The roughness of a manufactured surface is generally determined by the manufacturing process, not by the machining process, if any.

The portable surface roughness tester is used to determine the average roughness Ra, which is defined as the area between the roughness profile and itsmean line,

or the integral of the roughness profile height in absolute value over the evaluation length. This is the parameter that has been universally used for a long period of time. The method of detection was skid measurement. It includeda diamond-tipped stylus with a 90o/ 5 mR angle. It had a 2.5cm cutoff length and a 2.5mm sample length. The instrument employed has a measurement rangeof 12.5mm and an x-axis drive unit. It displays the roughness value on a digital display. As a result, the values can be directly read.

5.2.4 MICROSCOPE FOR METAL WORKING:

Micro-examination is performed on cut-to-size samples for a variety of objectives, the most obvious of which is to determine the material's structure. Additionally, metallurgical anomalies such as third phase precipitates, excessive grain development, and so on are frequently examined. Numerous routine tests, such as phase counting and grain size estimation, are conducted concurrently with micro inspections.

The grain size of a material is critical because it impacts its mechanical properties. In most materials, a refined grain structure results in increased toughness, and alloying elements are introduced purposefully during the steel manufacturing process to aid in grain refining. ASTM E112 illustrates charts with outline grain structures at various dimensions to define a scale for grain size. This has resulted in a widely accepted standard for grain sizes rangingfrom 1 (very coarse) to 10. (very fine). Figure 5.13 depicts an image of the LECO -500 microscope.

Figure 5.13 System d'analyse d'images LECO 500

5.3 SAMPLE PREPARATION AND MATERIAL PROCESSING WITH A LASER:

Stainless steel -304 is used in various thicknesses for CO 2 laser processing, alloy steel is used in thicknesses of 5mm and 12mm, and stainless steel -304 is used in thicknesses of 2 mm for Nd-YAG laser marking. The parameters examined are as follows:

- Kerf width is dependent on a variety of process conditions.
- During the procedure, a taper is formed.
- Rates of material removal
- The sliced surface's surface properties, notably
- Analyses of the microstructure and grain structure
- Modeling investigations of processes

The sample's surface is cleaned to remove any dust or corrosion. Clamps are used to secure the cleaned work piece to the work bench. With a standoff distance of 1.0mm, the laser cutting head is aligned with the work piece so that the beam and assist gas nozzle are perpendicular to the work piece's surface and the gas flow direction is perpendicular to the work piece's surface. The nozzle selected has a diameter of 1.2mm. Keyhole method is used to treat the material.

To drill a hole, the laser was set to P mode and operated for 0.5 seconds with a pulse time of 3 milliseconds. Following that, the work piece was sliced utilising continuous wave. The processing material was stainless steel (SS-304) plate in a variety of thicknesses. Four processing variables were chosen for parametric optimization: cutting speed, gas pressure, laser power, and sample thickness. The stainless-steel plates were cut utilising oxygen as an assist gas for various values of the indicated process parameters. The work piece is stainless steel plates with a thickness of 2mm, 3mm, or 5mm. The Rofin Sinar laser has a maximum power of 2000watts. The assist gas utilised is 99.96 percent pure oxygen. At gas pressures ranging from 1000 bar to 8000 bar, the cutting speed varied between

1000mm/min and 7000mm/min. Different laser powers are usedto process the workpiece. Stainless steel plates with a thickness of 3mm are processed at a cutting speed of 1500mm/min at a power of 2700watts utilising nitrogen at a pressure of 14 bar using a Bystar laser with a maximum output of 3000watts. 5mm and 12mm thick alloy steel (IS 2062) plates are cut using nitrogen as an assist gas at an 8-bar pressure. The laser power is 1600 watts at a cutting speed of 3000 mm/min and an operating pressure of 8 bars for 5mm thick plates. The cutting speed for 12mm plate is 1500mm/min at a laser power of 2500watts and a gas pressure of 14 bars. For nitrogen gas processing, the focal point was maintained in the centre of the plate to be processed.

With a maximum power of 75 watts for the Nd-YAG laser marking machine, 304 grade stainless steel plate is marked with a laser power of 52 watts, a speed of 12mm/sec, and a pulse length of 300 microseconds and a frequency of 10khz. With a 75-watt laser, the material was marked once more with a Q-switched pulse of frequency 3 kHz and duration two microseconds travelling at a speedof 100mm/sec. The marking machine's x-y feed is 10 x 160 mm, with a maximum character rate of 240 characters per second.

To investigate the kerf width, material removal rates, and taper created when the sample is cut, an optical microscope is employed. To investigate the surface characteristics SEM, a cut surface analysis was performed utilising the LEICA 440i. Mitutoyo surf test 211 is used to determine the roughness of the laser cut surface. The LECO 500 microscope is used to conduct microstructure and grain analysis research. Elemental analysis of the sliced surface is performed using the EDXA attachment for the LEICA 440i scanning electron microscope.

To examine the microstructure and grain size, the samples are polished to a fine finish using one-micron diamond paste and then etched in an appropriate chemical solution before being examined under a metallurgical microscope. Oxalic acid in water was employed as the etching chemical solution (10 ml oxalic acid, 100 ml

H_2 O) was etched for 5 to 20 seconds at 6V using a platinum or stainless-steel c a t h o d e. The distance between electrodes is 3/4 to 1 inch. This approach is effective for distinguishing between sigma phase and carbides in austenitic stainless steels. The grain size of a polished and etched sample is assessed using optical microscopy at a magnification of 100X. Carbides are attacked first, followed by etched phase. Ferrite and austenite are attacked on a minor scale.

CHAPTER-6
RESULTS AND CONVERSATION

6.1 CUT KERF:

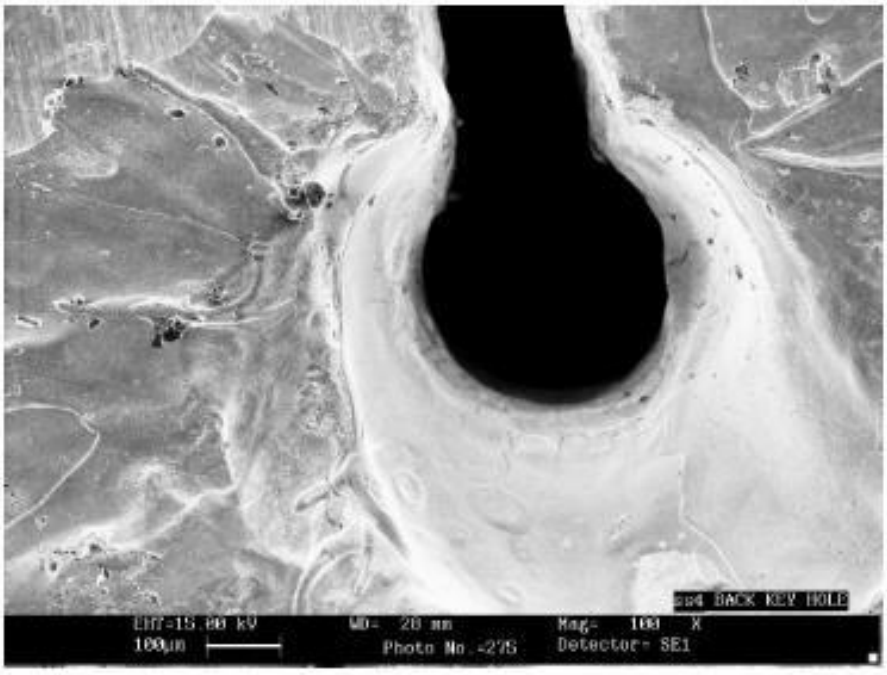

Figure 6.1 Laser cut kerf and key hole in 3 mm stainless steel using a 1500-watt laser and oxygen aid gas

Laser cutting creates a kerf that penetrates the entire work piece because to the relative velocity between the work piece and the impinging laser beam. Figures 6.1 and 6.2 illustrate the key hole and kerfwidth used in laser cutting stainless steel. Additionally, the hole's opening and the flow of material at the crater, as well as the dross sticking to either side of the hole, can be seen.

The kerfwidth produced by both reactive gas and inert gas cutting of the work piece is seen to be narrow. This kerfwidth is discovered to be parameter dependent. As illustrated in Figures 6.2 and 6.3, selecting the proper help gas makes a significant difference in the amount of dross produced.

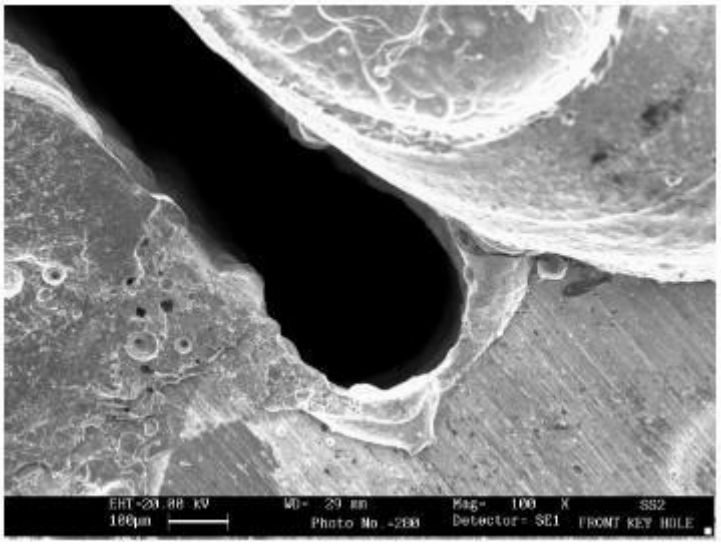

Figure 6.2 Front view of the laser cut kerf and key hole in 3 mm stainless steel utilising an oxygen assist gas at a laser power of 1300 watts

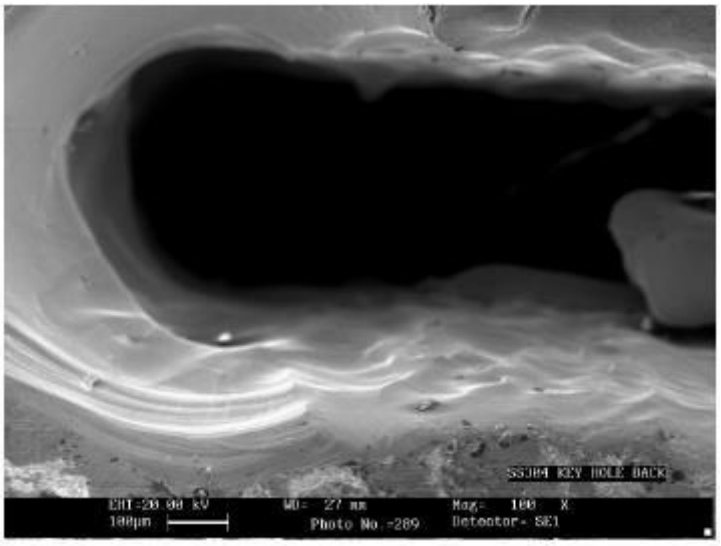

Figure 6.3 Bottom view of the laser cut kerf and key hole in 3 mm stainless steel utilising Nitrogen as an assist gas

Cutting speed (mm/min)	4500	5000	5500	6000
Kerf width (mm)	0.23	0.22	0.2	0.19

Table 6.1 kerf width versus cutting speed for stainless steel 2mm (SS304) Oxygen gas pressure is set at 5 bars, and the laser power is set to 1400 watts

Cutting speed (mm/min)	1000	2000	2500	3000	3500
Kerf width (mm)	1.0	0.79	0.66	0.59	0.55

Table 6.2 Kerf width against cutting speed for stainless steel 5mm (SS304) Oxygen gas pressure is equal to 4 bar, and the laser power is 2000 watts

Laser power (watts)	1200	1300	1400	1600	1700
Kerf width (mm)	0.2	0.22	0.225	0.24	0.27

Table 6.3 Kerf Width acquired while cutting stainless steel (SS-304) at various laser powers, oxygen gas pressure equal to 5 bar, and work piece 3mm thickness

Tables 6.1, 6.2, and 6.3 illustrate the relationship between kerf width and cutting speed and laser power. The width of the kerf achieved when cutting SS304 is between 0.2 and 0.27mm. However, it is noticed that the kerf width decreases as the cutting speed increases. Additionally, it was discovered that thekerf width is dependent on the assist gas pressure and increases with gas pressure until it reaches an ideal value. Table 6.4 illustrates the relationship between kerf and assist gas pressure. When reactive gas is used for cutting, it is discovered that the kerf breadth drops significantly with increasing gas pressure [B J Ranganath et al 2005]. A typical cut width of 0.19 mm to 1.0 mm for workpiece thicknesses ranging from 2 mm to 5mm at various cutting parameters

demonstrates that the laser cut kerf is modest, allowing for close nesting of parts after processing and minimising material waste.

Gas Pressure (bar)	1.0	2.0	3.0	4.0	5.0
Kerf width (mm)	0.565	0.53	0.56	0.55	0.54

Table 6.4 kerf width obtained when cutting stainless steel (SS-304) at various oxygen gas pressures, cutting speed of 1500mm/min, laser power of 2000watts, work piece thickness of 5mm

6.2 STUDIES ON TAPER:

During laser cutting of the material, it is noted that the diameter of the Key hole at the exit end of the cut is smaller than the diameter at the entrance end, resulting in a taper in the cut surface. This is demonstrated in the SEM photograph of an alloy steel key hole in figure 6.4. The taper created in the kerf when stainless steel-304 is cut with a CO2 laser is observed to vary with laser power, as illustrated in table 6.5.

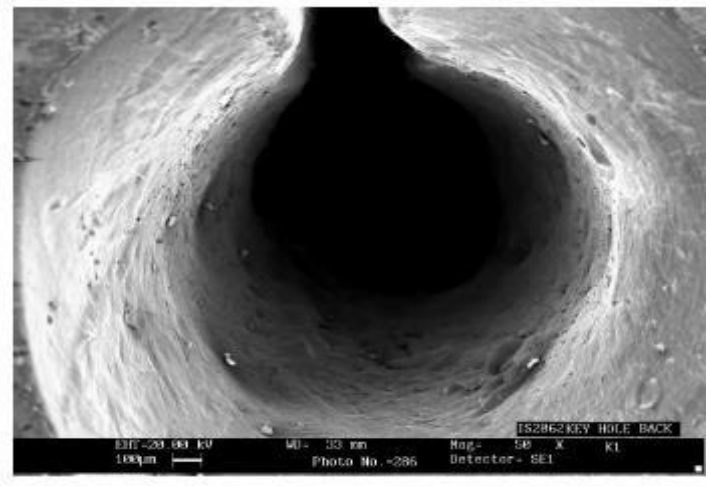

Figure 6.4 SEM image of a laser-cut hole demonstrating the alloy steel taper

Material	Laser power Watts	Taper per cm	taper	Angle in degrees
Stainless steel 304	1200	0.1 mm	1 :100	0.57
	1300	0.07 mm	1 : 150	0.38
	1400	0.05 mm	1 : 200	0.287
	1600	0.042 mm	1 : 150	0.38
	1700	0.04mm	1 :200	0.287

Table 6.5 Taper formed by laser cutting stainless steel 304

It was discovered that it decreases with input power, as illustrated in figure 6.5. Figure 6.5a depicts a taper model. While the taper created is minor (between 0.04 and 0.1mm per cm), it may have an effect on the component assembly following processing.

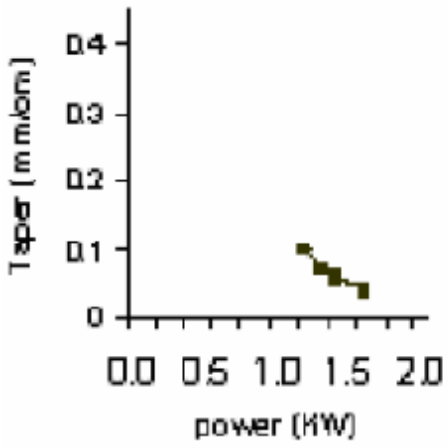

Figure 6.5: Keyhole taper with laser power

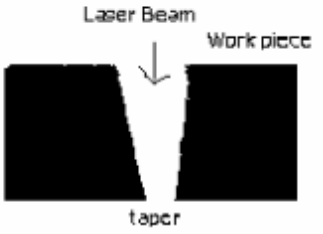

Fig 6.5a: Model of Keyhole taper

6.3 RATE OF MATERIAL REMOVAL:

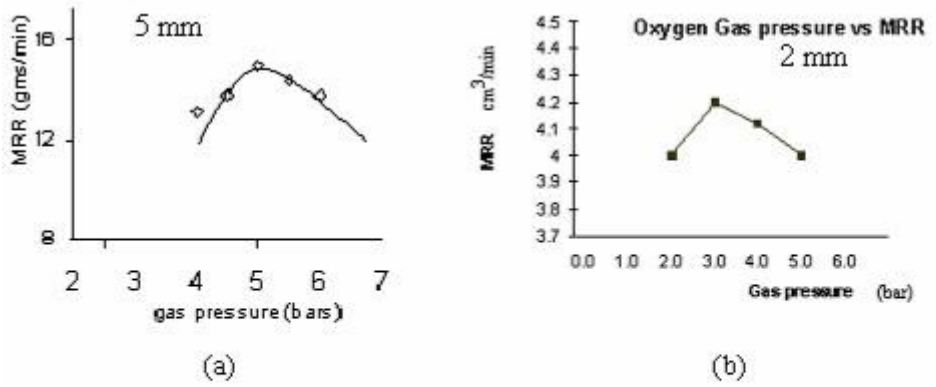

Figure6.6: MRR VS assist gas pressure in cutting Stainless steel -304. (a)5 mm thickness(b) 2 mm thickness . Laser power =1400 W Cutting speed = 4000mm/min.

The pace of material removal is critical in industrial manufacturing. MRR is affected by machining factors such as cutting speed, laser power, sample thickness, assist gas pressure, and focusing location in laser machining. Figure 6.6 illustrates the relationship between MRR and oxygen assist gas pressure. It demonstrates that MRR reaches a maximum value for a certain assist gas pressure value (fig6.6a) when the sample thickness is 5mm. The same pattern is found when a sample with a thickness of 2 mm is treated for various gas pressure values, as illustrated in figure 6.6b. Figure 6.7 illustrates the dependency of MRR on laser processing factors. When all other processing parameters are held constant, the MRR increases with laser power (figure 6.7a) and likewise with cutting speed (figure 6.7b).

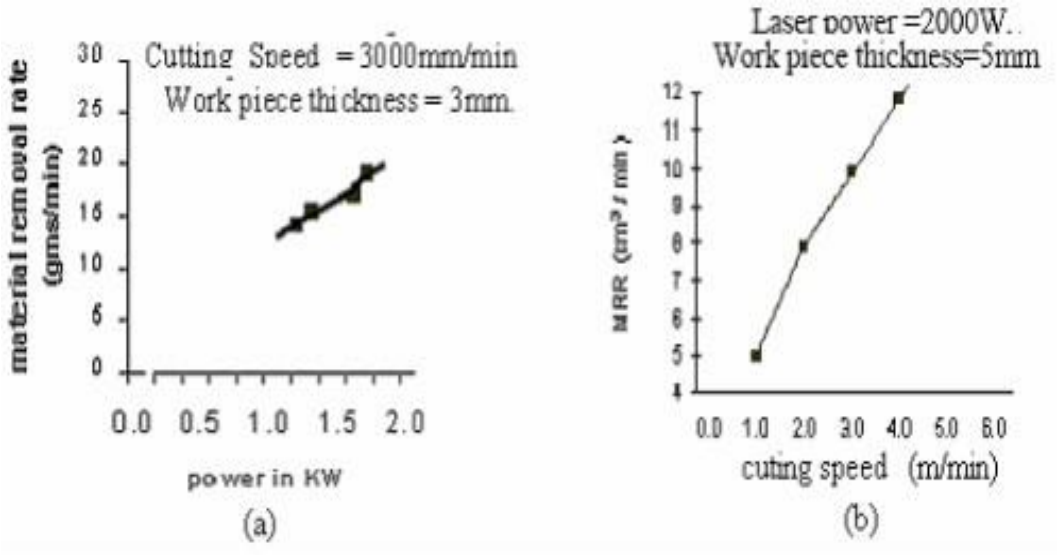

Figure 6.7: Variation of MRR with laser processing variables
a) CO_2 Laser power Vs MRR b) CO_2 Laser Cutting speed vs MRR

As shown in table 6.6, the results of this experimental work demonstrate some correlation with the previously published work of Powell et al [2000]. The discrepancies between the experimental and previously published values could be explained by changes in the cutting parameters. As shown in Table 6.6, material removal rates are essentially identical for thicknesses up to 3mm but dramatically increase for thicknesses more than 5mm. This could be explained by the enhanced energy availability caused by the chemical reaction between oxygen jet and iron, which results in the release of energy. The chemicalreaction that results in the release of energy is

$$xFe + y\ O \rightarrow Fe_xO_y + heat$$

Sl No		Thickness mm	Cutting speed m/min	Laser power Watts	Kerf width mm	Material removal rate mm^3/sec	Gas pressure bar
1	J Powel et al [2000]	5	1.53	800	0.35	44.60	8.0
	Present Experiment	5	1.5	2000	0.54	67.5	5.1
2	J Powel et al [2000]	3.25	2.4	800	0.35	45.50	6.5
	Present Experiment	3.0	3.0	1700	0.27	40.5	6.0
3	J Powel et al [2000]	1.9	4.08	800	0.3	38.76	6.5
	Present Experiment	2.0	5.0	1500	0.249	41.50	5.0

Table 6.6 comparing the rates of material removal from stainless steel -304

6.4 CHARACTERISTICS OF THE SURFACE:

6.4.1 EXAMINATIONS OF SURFACE ROUGHNESS:

The surface roughness (Ra) of laser cut SS-304 specimens was determined using a scanning electron microscope and a surface profilometer. The findings of the surface roughness analysis are presented in table6.7. Surface roughness is seen to vary between 3 and 6 m depending on the machining conditions. Additionally, the influence of assist gas pressure on the surface roughness is negligible for a given set of cutting variables. In comparison, as illustrated in figure 6.8, the effect of laser power on cut surface roughness is significant.

Work-piece thickness (mm)	Laser power (watts)	Gas pressure (Bar)	Cutting speed (mm/min)	Surface roughness (r_a µm)
3	1200	6	3000	6.07
3	1300	6	3000	5.86
3	1400	6	3000	4.53
3	1600	6	3000	5.32
3	1700	6	3000	6.97
2	1400	5	4500	3.73
2	1400	5	5000	3.79
2	1400	5	5500	3.25
2	1400	5	6000	4.56
2	1400	5	6500	3.63
2	1400	4	4000	3.37
2	1400	4.5	4000	3.21
2	1400	5	4000	3.62
2	1400	5.5	4000	3.17
2	1400	6	4000	3.03

Table 6.7 Ra values of 304 grade stainless steel laser cut surface

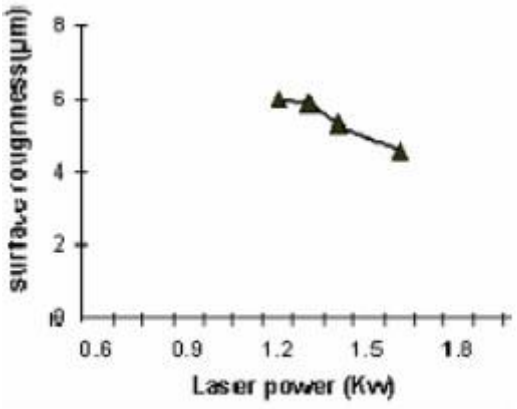

Figure 6.8: Laser Power vs surface finish

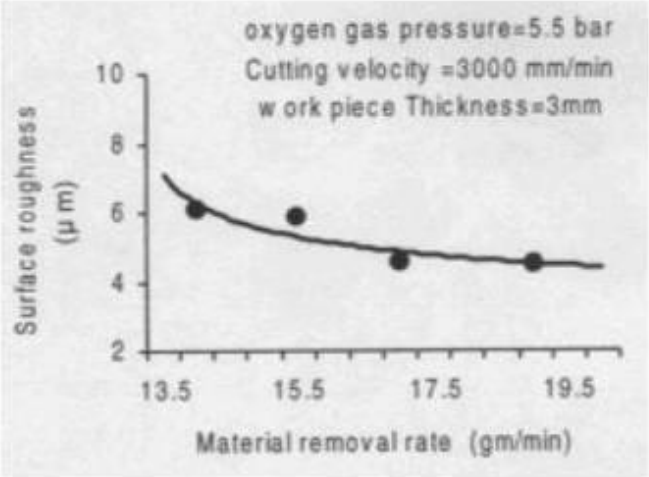

Figure 6.9: MRR vs Surface roughness for stainless steel -304

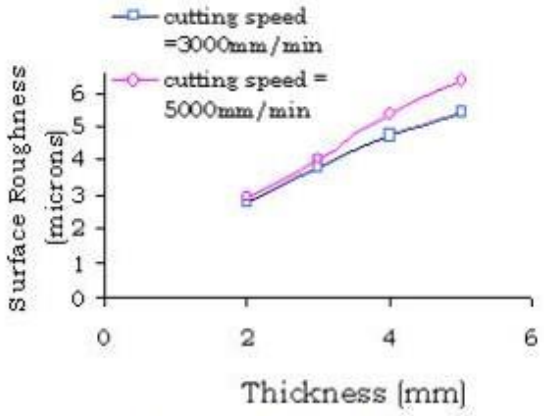

Figure 6.10: Variation of surface finish with cutting speed and work piece thickness

Additionally, the surface roughness of stainless steel-304 is dependent on the MRR. This relationship is seen in Figure 6.9. It is observed that the surface finish improves with increasing material removal rates. As illustrated in Figure 6.10, the surface smoothness degrades as the thickness of the work piece increases under the same cutting conditions. Increased cutting speed produces the same effect. Additionally, for a given cutting variable of 1400 watts laser power, 5 bar assist gas pressure, and 2mm work piece thickness, the surface smoothness of the laser cut surface decreases with increasing cutting speed, as illustrated in figure 6.11.

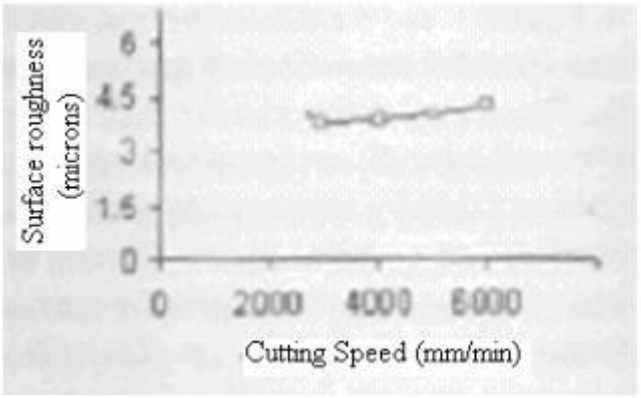

Figure 6.11 Surface variation Roughness as a function of cutting speed for a workpiece with a thickness of 2mm

6.4.2 SEM examinations of laser-cut surfaces:

6.4.2.1 Cracks at the laser cut surface:

It is noticed that the laser cut surface profiles vary depending on the cutting parameters used. When treated with a laser of 1600 watts at a speed of 3000mm/min and an oxygen support gas pressure of 6 bar, the cut surface of 3 mm stainless steel-304 exhibits cracks, as shown in the SEM photograph in figure 6.12. Even when the material is processed at a lower laser power of 1300 watts and at the same processing speed, the cracks continue, as illustrated in figure 6.13 by the SEM photograph.

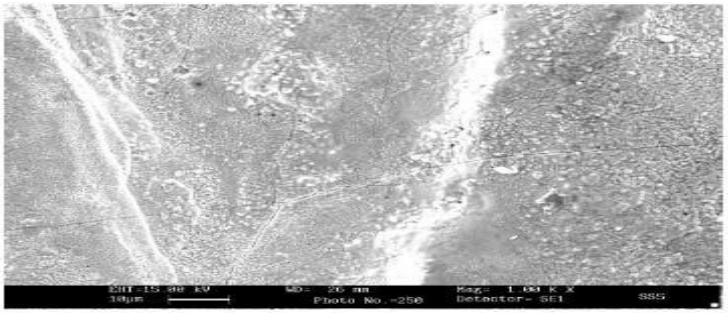

Figure 6.12 SEM micrograph of the sliced surface of ss304 after it has been treated with oxygen as an aid gas. Laser power is 1600 watts, gas pressure is 6 bar, and the cutting speed is 3000 millimetres per minute

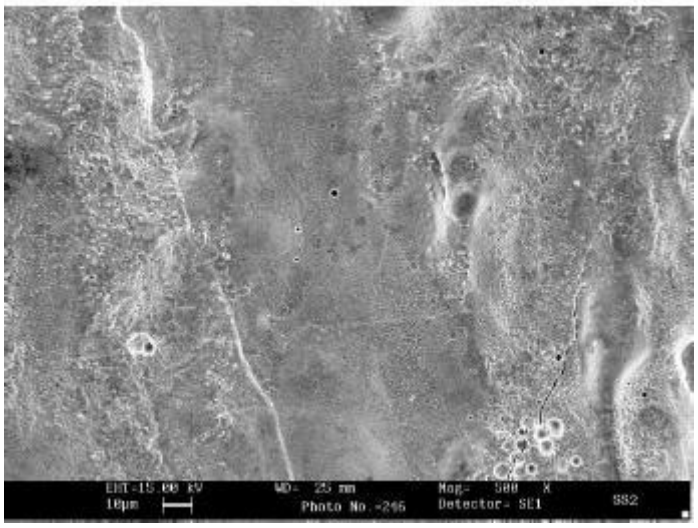

Figure 6.13 When treated with oxygen as an aid gas, a SEM micrograph reveals fissures in the cut surface of 3mm ss-304. Laser power is 1300 watts, gas pressure is 6 bar, and the cutting speed is 3000 millimetres per minute

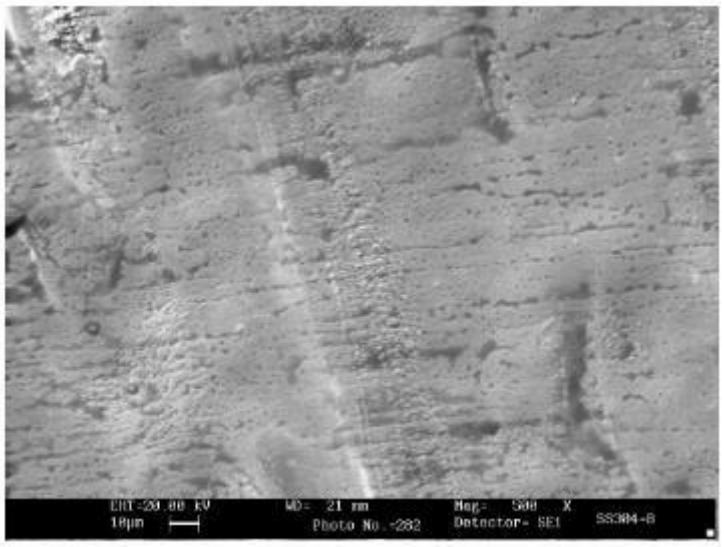

Figure 6.14 SEM micrograph of the cut surface of 3mm stainless steel after it has been treated with nitrogen as an assist gas. Laser power = 2700 watts, gas pressure = 14 bar, and cutting speed = 1500 millimetres per minute

However, as illustrated in figure 6.14, when the same material is processed with nitrogen assist gas at a laser power of 2700watts, the fissures on the cut surface appear to be nonexistent. However, cavities with a linear pattern are visible.

Although this also harms the cut surface, it is necessary to examine the absence of cracks under the aforementioned cutting conditions. When a laser with a power of 1600 watts processes alloy steel (IS2061) with a thickness of 5 mm at an operating pressure of 8 bar and a processing speed of 2750 mm/min, the cut surface damage is still more pronounced, even when nitrogen is employed as an assist gas, as illustrated in figure 6.15. These types of damage are frequently encountered as a result of thermal stresses generated during material processing, as documented in the literature (Ranganath B J 1999). Thus, by carefully selecting the processing settings as illustrated in Figure 6.16 and 6.17, the cracking of the cut surface can be minimised.

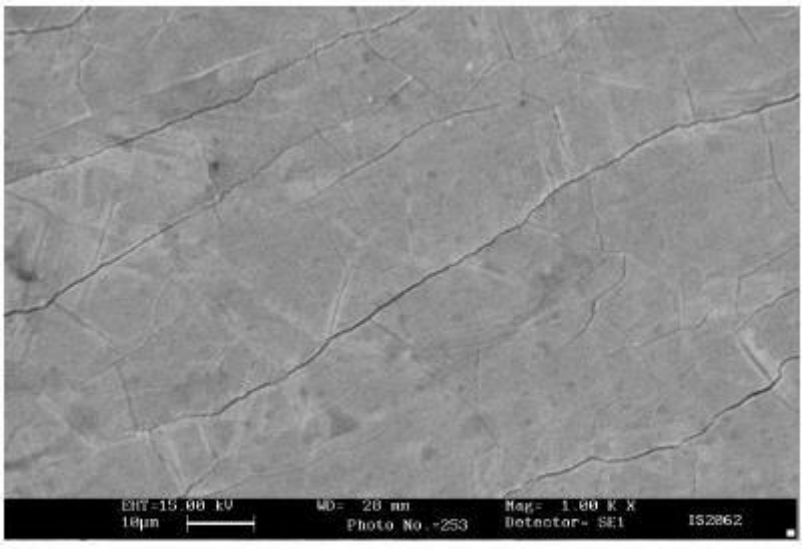

Figure 6.15 When alloy steel IS2062 is treated with nitrogen as an aid gas, SEM micrographs reveal fissures in the cut surface. 1600 watts laser power, 8 bar gas pressure, and a cutting speed of 2750 mm/min

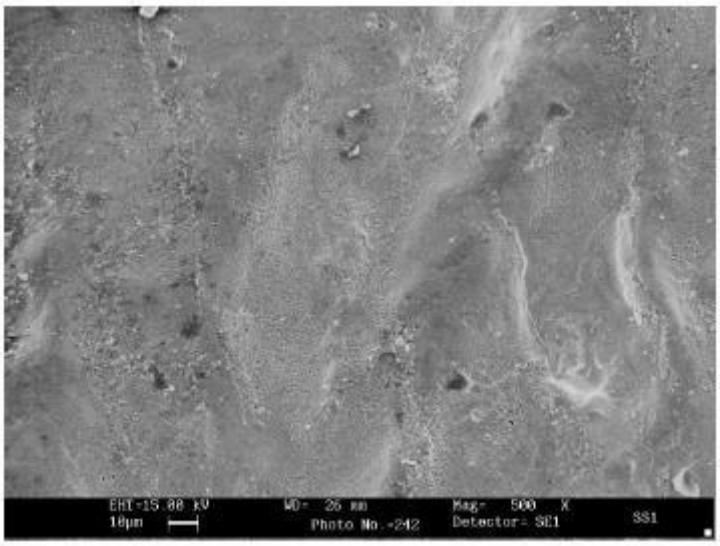

Figure 6.16 SEM micrograph shows the cut surface of SS304 after processing using oxygen as an aid gas. Laser power equals 1400 watts, gas pressure equals 6 bar, cutting speed equals 4000 mm/min, and workpiece thickness equals 2mm

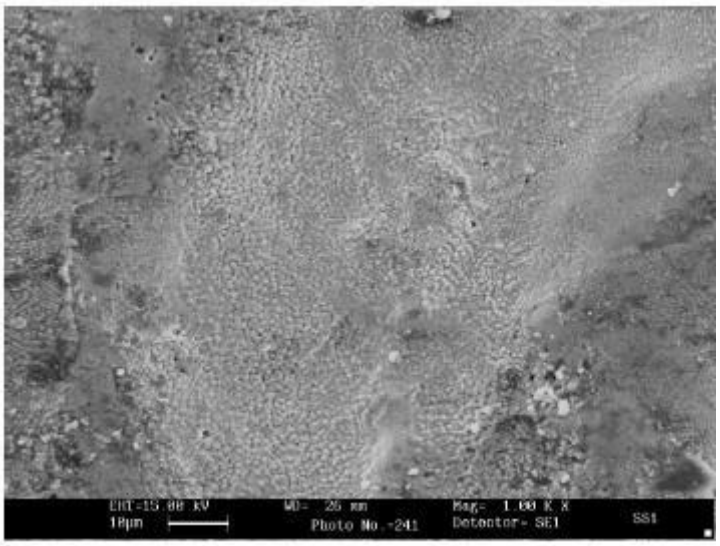

Figure 6.17 SEM micrograph of the cut surface of 3mm SS304 with a laser power of 1200 watts, a cutting speed of 3000mm/min, and a gas pressure of 6 bar.

6.4.2.2. IRREGULARITIES ON THE SURFACE—CREATION OF CRATERS/VALLEYS:

The surface imperfections of laser cut stainless steel surfaces vary significantly due to the variety of brands and grades available commercially. The variation should be attributed to the material's various metallurgical additives and phases. The imperfections on the surface are mostly caused by melting and resolidification during thermal processing. The surface topography of laser cut stainless steel -304 after various processing factors is illustrated in figures 6.18 to 6.25. In figure 6.18, the SEM micrograph of a laser cut surface with oxygen support gas reveals bigger grains with peaks and valleys for stainless steel -304 of 3mm thickness.

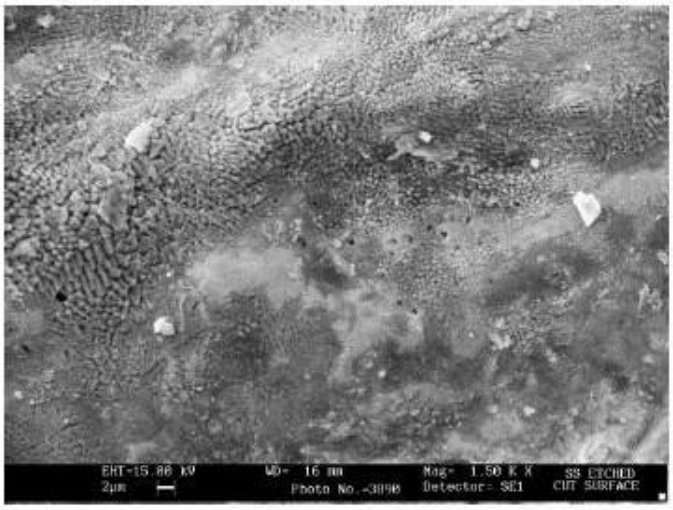

Figure 6.18: SEM photograph indicating grains and peaks and valleys for stainless steel -304 of 3mm thickness

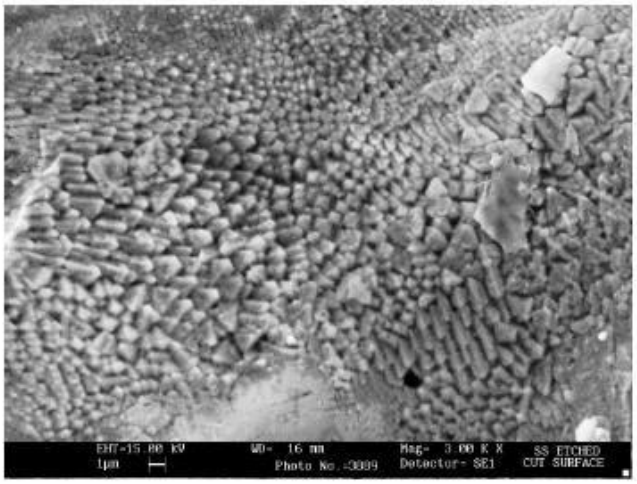

Figure 6.19: SEM Micrograph showing damage of the cut surface of 5mm stainless steel

The cut surface damage for the same material with a thickness of 5 mm is shown in figure 6.19. The surface topography of stainless steel 304 cut with various parameters, as illustrated in figures 6.20 to 6.25, demonstrates the solidification of fused material, including the creation of phase boundaries and orientation. There is evidence of assicular dispersion of fine grains, which is a common occurrence in high alloy stainless steel. Cavities of varying shapes and sizes are found as a result of the dispersion of distinct alloy phases inside the material's matrix.

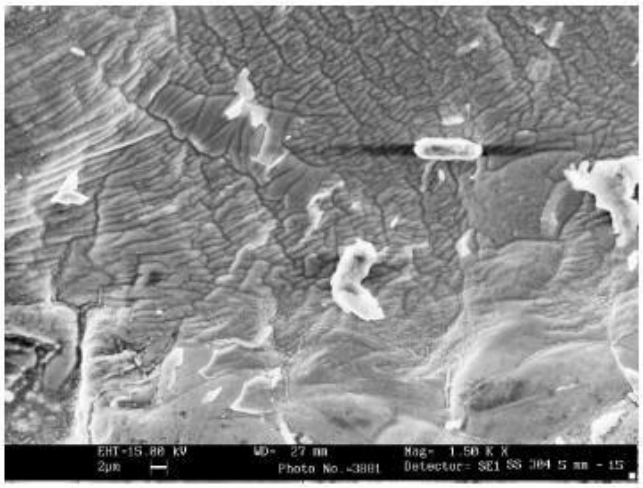

Figure 6.20: SEM Micrograph showing Surface topography of laser cut surface of 5mm stainless steel -304. Laser power = 2000watts, gas pressure =4 bar , cutting speed 1500mm/min , Assist gas used =oxygen

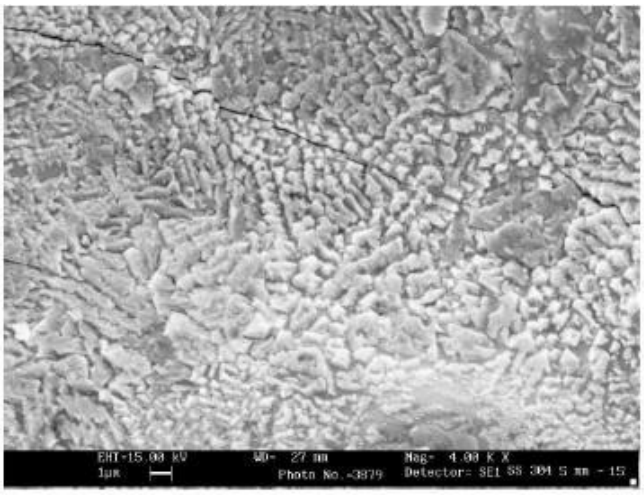

Figure 6.21 SEM Micrograph showing Enlarged view of Surface topography of laser cut surface of 5mm stainless steel -304,Laser power = 2000watts, gas pressure =4 bar , cutting speed 1500mm/min ,Assist gas used =oxygen

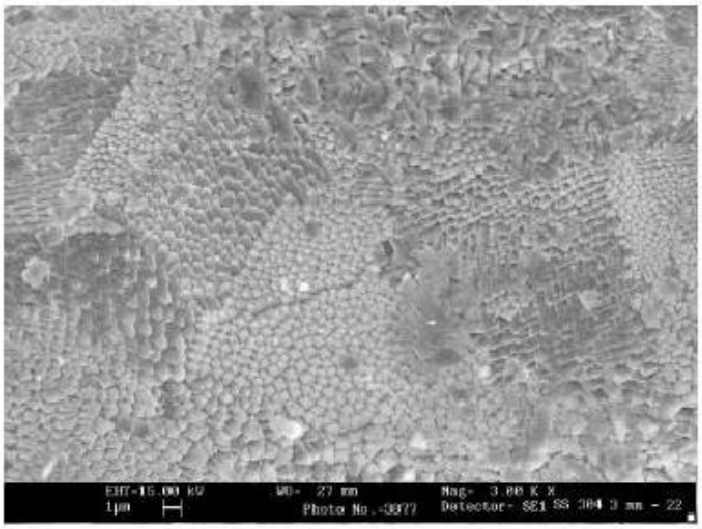

Figure 6.22: SEM Micrograph showing surface topography of CO_2laser cut surface of 3mm stainless steel -304. Laser power = 800watts, gas pressure 3.5 bar, cutting speed 2000 mm/min, Assist gas used =oxygen

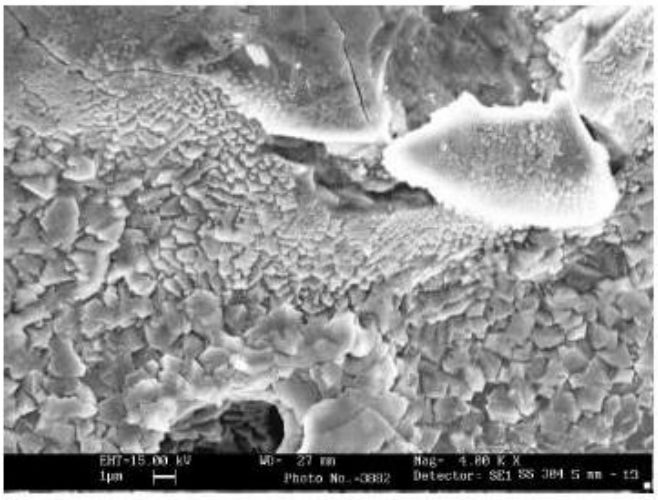

Figure 6.23: SEM Micrograph showing surface topography of CO_2 laser cut surface of 3mm stainless steel -304. Laser power = 2000watts, gas pressure 2 bar, cutting speed 1500 mm/min ,Assist gas used =oxygen

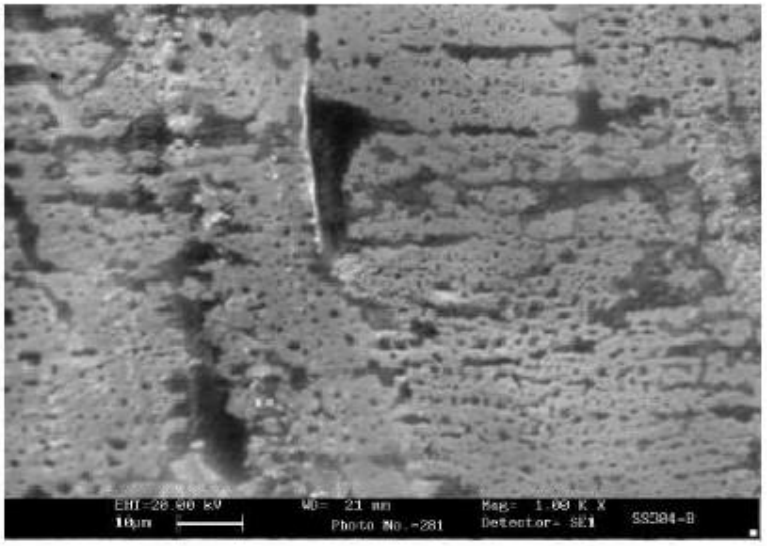

Figure 6.24: SEM Micrograph showing surface topography of CO_2laser cut surface of 3mm stainless steel -304.Laser power = 2700watts, gas pressure 14 bar, cutting speed 1500 mm/min ,Assist gas used =Nitrogen

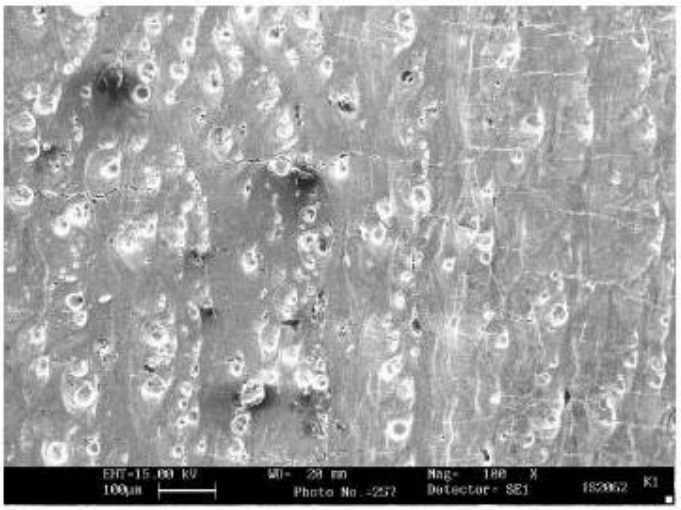

Figure 6.25: SEM Micrograph showing surface topography of CO_2laser cut surface of 12mm alloy steel IS2062. Laser power = 1650watts, gas pressure 14 bar, cutting speed 700 mm/min, Assist gas used =Nitrogen

Figure 6.25 depicts lateral cracks perpendicular to the path of the cut, together with dimples and valleys in the direction of the cut, demonstrating the material's ductile flow. This is corroborated by cracks formed as a result of thermal strains created during later cooling with the aid gas.

6.4.3 WHITE LAYER ON THE CUT SURFACE:

A study of the stainless steel-304 laser cut surface revealed the creation of a white coating on the cut surface. Figure 6.26 illustrates the creation of a white coating on the laser cut surface of stainless steel -304 [Ranganath B J and Viswanath G, 2006]. The term "white layer" refers to the fact that it appears white under a microscope even after etching. In steel thermal processing applications, a thin layer is generated that is resistant to etching and has adistinct composition. Typically, the white layer is made of 30% martensite and nearly 70% austenite, while the base material is formed of around 75% martensite and 25% austenite. The white layer is thought to be detrimental tothe performance of the part, affecting its tribological properties, corrosion resistance, and fatigue life. As a result, it is critical to analyse the production of the white coating and to decrease its thickness. The white layer's thickness is notuniform. The white coating has a determined thickness of around 50 m.

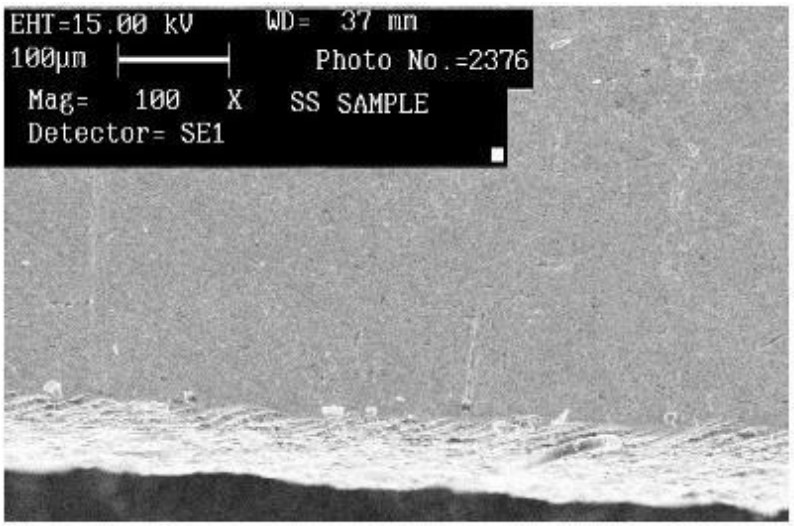

Figure 6.26: SEM micrograph of white layer in CO_2 laser cut surface of Stainless Steel-304

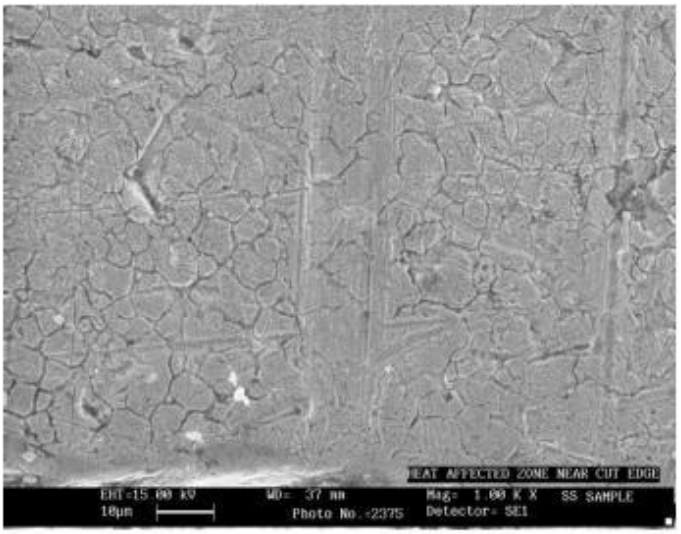

Figure 6.27: SEM micrograph of white layer in CO_2 laser cut surface of Stainless Steel-304 Enlarged view.

The most reliable laboratory method for detecting white layer is to use a microscope to examine a cross section of the completed work item. To visualise this structure under a microscope, the sliced sample's surface is polished and etched using a solution of Ferric Chloride and Hydrochloric acid. (five grammes ferric chloride in one hundred millilitres water + fifty millilitres con HCl) and etched for one minute. In the base material, the etched surface grains are visible, but not in the white layer. This white layer has properties distinct from the underlying material, as illustrated in the enlarged view of the section in figure 6.27.

6.4.4 EDXA STUDIES:

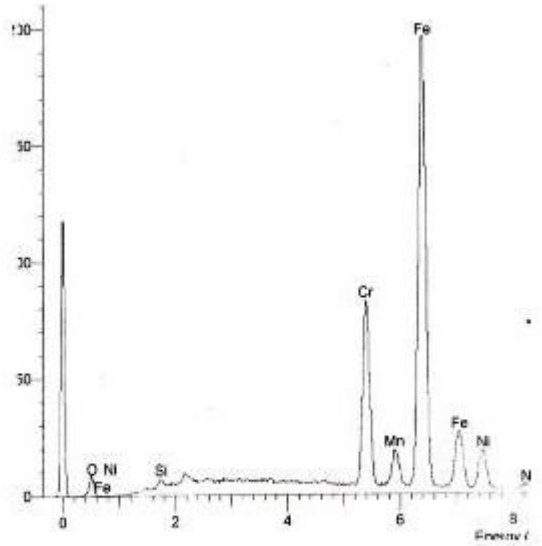

Figure 6.28: EDXA image of Base material stainless Steel -304

Fig 6.28 6.29 and 6.30 illustrate the EDX images of the base material and the laser cut surface, respectively. Iron and oxygen are being replenished, whereas chromium, nickel, silicon, manganese, and aluminum are being depleted. The increase in oxygen concentration is likely due to the use of oxygen assist gas to remove particles from the cut kerf.

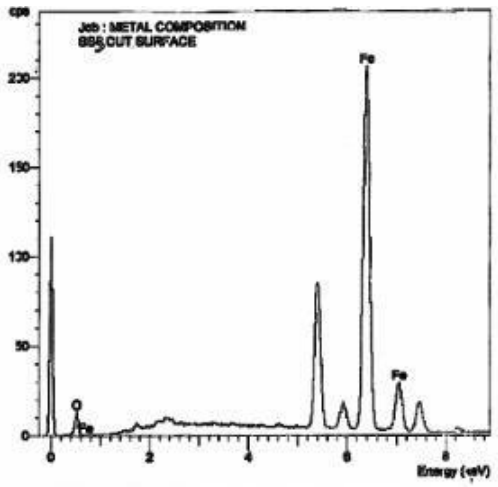

Figure6.29:EDXA image of CO_2 laser Cut surface of SS-304 material with oxygen cutting

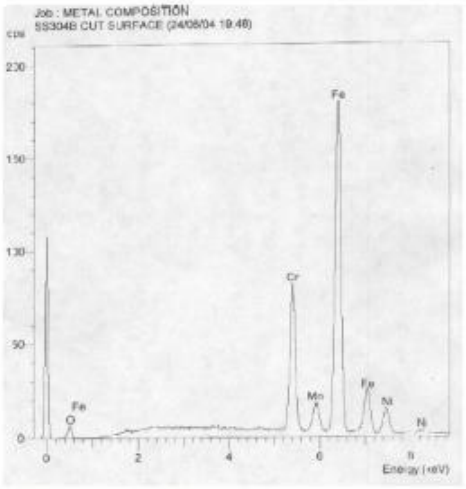

Figure 6.30: EDXA image of CO_2 laser Cut surface of SS-304 material with Nitrogen as assist gas.

The elemental makeup of stainless steel prior to and following laser cutting is shown in Table 6.8. It is possible to notice a change in the composition of the sliced surface. There is a depletion of Chromium, Nickel, Manganese, Aluminum, and Silicon, as well as a pickup of Iron.

Element	Composition of the base material (%)	Composition of the Laser cut surface (%)
Cr	18.03	17.59
Ni	9.79	9.09
Mn	1.74	1.22
Si	0.43	0.39
Al	0.13	0.11
Fe	69.89	71.60

Table 6.8 EDX examination of stainless steel 304 and its CO_2 laser cut surface reveals the elemental makeup in percentages

6.5 STUDIES ON MICROSTRUCTURE AND GRAIN SIZE:

Microstructure analysis of laser cut stainless steel -304 is performed using a Leco -500 microscope. This is important for determining the grain distribution and the heat impacted zone during laser cutting. The microstructure of the cut material perpendicular to the direction of the cut is shown in Figure 6.31. The granules are unaffected by the laser beam's heat source. The sliced microstructure reveals a uniform distribution of granules. The stainless-steel sample exhibits an austenite structure with no carbide precipitation along the grain boundaries. This demonstrates that there is no heat flux at the depth of the cut surface, despite the high heat intensity of the laser source. Fig 6.32 illustrates the microstructure of the SS304 surface distant from the laser cut surface.

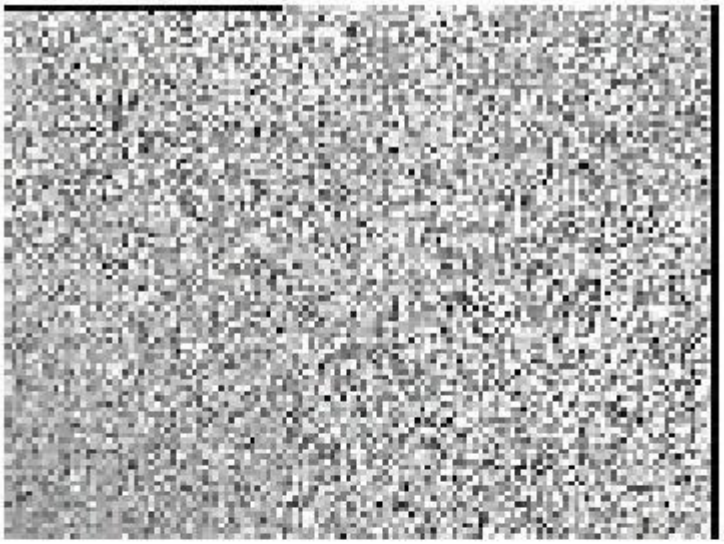

Figure6.31: Microstructure of CO_2 laser cut stainless steel- 304

Figure6.32: Enlarged view of Microstructure of CO_2 laser cut Stainless steel- 304

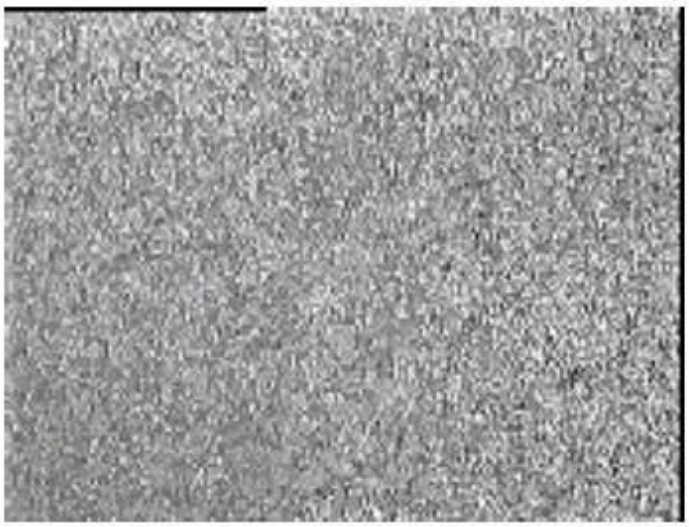

Figure6.33: Microstructure of the surface away from CO_2 laser cut surface of stainless steel -304

Figure6.34: Enlarged view of Microstructure of the surface away from CO_2 laser cut surface of stainless steel -304

In both positions, grain size analysis is performed, and the grain sizes determined in both areas conform to ASTM no. 8. Figure 6.35 illustrates the microstructure of a laser etched surface of stainless steel 304 etched with a 75- watt Nd: YAG laser. It is possible to see a torn surface with serrations. This is because the separated molten material ductile fails as a result of laser

impingement followed by material removal. The presence of a finely dispersed structure with well-distributed phases indicates that the metallurgical transformation will be less damaged.

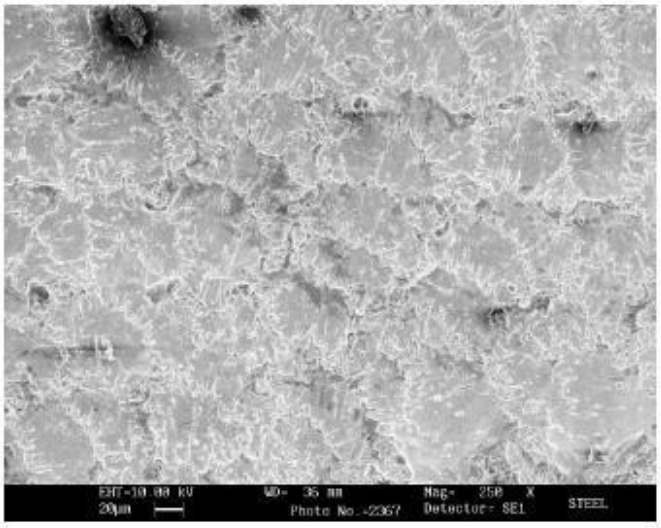

Figure 6.35: SEM photograph of microstructure of Nd: YAG laser etched surface of stainless steel 304.

6.6 STUDIES ON HEAT-AFFECTED ZONES:

The scanning electron microscope is used to investigate the heat affected zone during laser cutting of stainless steel -304. In figure 6.36, a micrograph of the laser cut surface illustrating the heat affected zone of a stainless-steel sample of 5 mm thickness cut at a speed of 2000mm/min using a 1200watt laser isdisplayed. The heat impacted zone is observed to extend to a substantial depthat the bottom of the cut surface, despite its tiny size in comparison to the samplethickness. Excessive heating on the cut surface followed by quenching as aresult of the assist gas obstructing heat conduction and concentrating thermal stress is attributable to the observed damage to the depth. Metallurgically, the material is unaffected by the depth of the material below the cut surface.

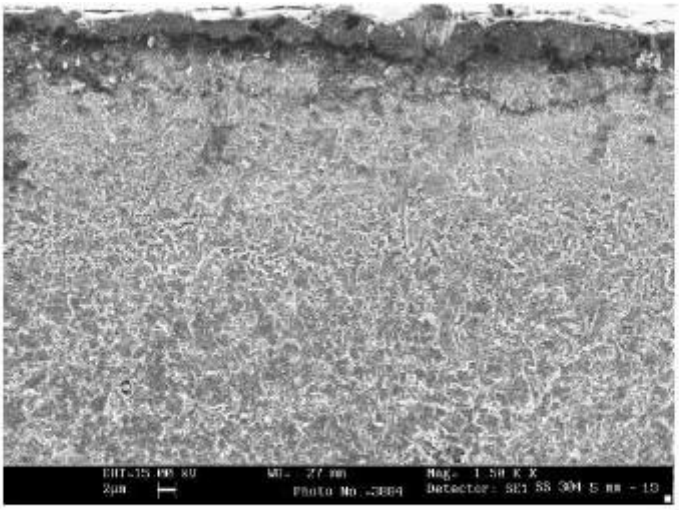

Figure 6.36: SEM photograph showing heat affected zone of CO_2 laser cut surface of stainless steel

6.7 LASER ETCHING OF METALS:

The Nd: YAG laser etched surface of stainless steel 304 is shown in Figure 6.37. It is possible to witness the control of the depth of cut achieved through laser machining and the presence of mattey surfaces caused by material removal at localised areas via laser evaporation. The material is removed by a very shallow cut, and the substance is evaporated locally. With specifically controlled scanning of the laser beam, the depth of cut can be adjusted by the number of pulses, etching speed, pulse duration, and laser power. As illustrated in Figure 6.38, the amount of material removed during etching is depending on the etching settings. Figure 6.39 illustrates an enlarged view of the etched surface in figure 6.37.

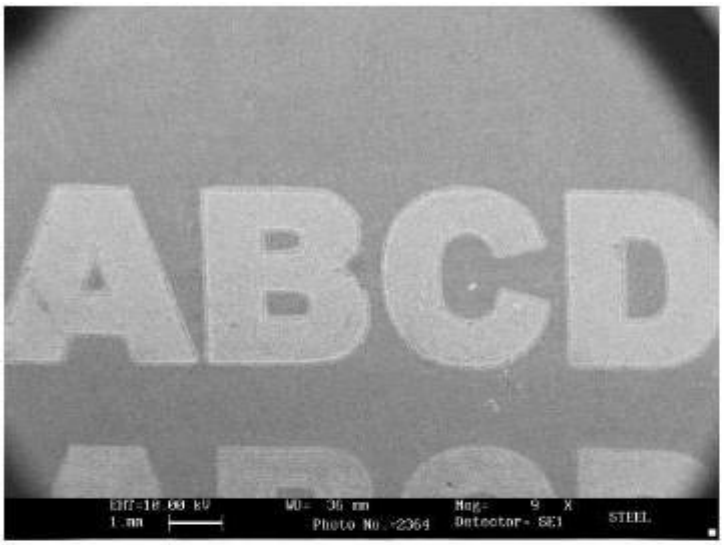

Figure 6.37: SEM photo of Etching of Steel by Nd:YAG laser beam : laser power =52 watts, etching speed =12 mm/sec. frequency =10khz, pulse length =300microsec

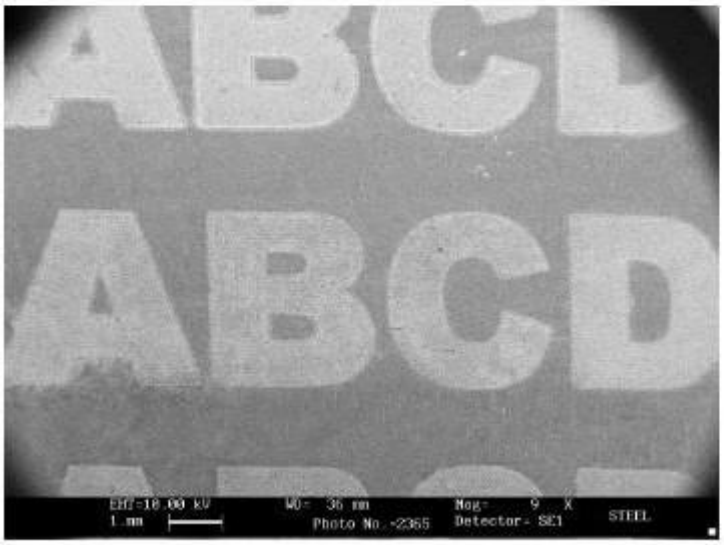

Figure 6.38: SEM photo of Etching of Stainless Steel by Nd:YAG laser beam laser power =75 watts, etching speed =100 mm/sec. frequency =3khz, pulse length =2microsec (II line)

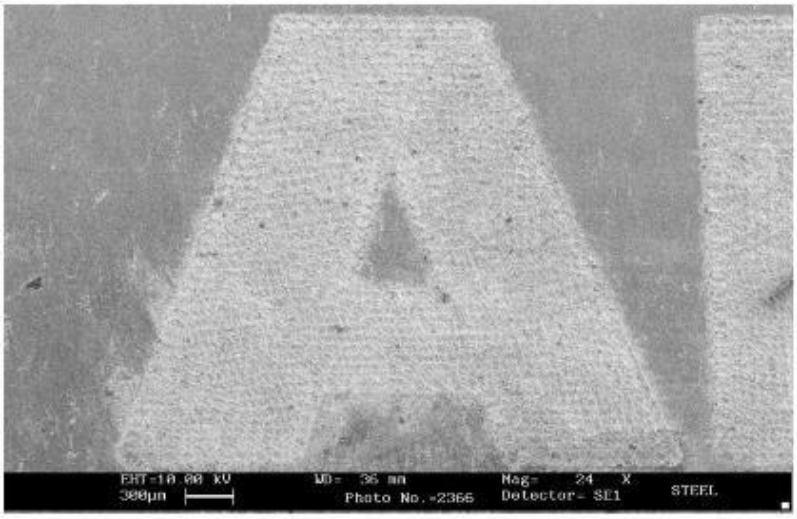

Figure 6.39: Enlarged view of SEM photo of Etching of steel by Nd:YAG laser beam . laser power =52 watts, etching speed =12 mm/sec. frequency =10khz, pulse length =300microsec.

CHAPTER 7

PROCESS MODELING

To simulate the laser cutting process of metals, two material removal mechanisms, meting and ablation, must be modelled along with the appropriate interface of vapour liquid. This requires knowledge of the metals' thermophysical properties, and the process will be more difficult. As a result, a basic and straightforward model of the material removal process is required. This trend has resulted in the development of models based on neural networks and multiple regression analysis to investigate the effect of process parameters on material removal rate and kerf width. A neural network model is constructed to investigate the effect of process factors on the surface quality of the laser cut surface. To investigate the temperature distribution during the cutting process and to construct a model using the Finite element method.

7.1 BASICS OF NEURAL NETWORK ANALYSIS:

Artificial neural networks (ANNs) are computer programmes inspired by biology that imitate the way the human brain processes information. ANNs learn (or are trained) through experience, not through programming. An ANN iscomposed of hundreds of individual units called artificial neurons or processing elements (PE), which are connected by coefficients (weights) to form the neural structure. The neural structure is organised in layers. The strength of neural calculations is derived from the network of neurons. Each PE consists of a set ofweighted inputs, a transfer function, and a single output. A neural network's behaviour is dictated by its neurons' transfer functions, the learning rule, and thearchitecture itself. Weights are the programmable parameters, and a neural network is thus a parameterized system. The summed weighted sum of the inputs constitutes the neuron's activity. The activation signal is transferred through the transfer function, which results in a single neuron output. Non- linearity is introduced into the network through the transfer function. The inter-

unit connections are optimised during training until the prediction error is minimised and the network obtains the specified degree of accuracy. Once trained and tested, the network can be given new input data to predict the output. In terms of model formulation, artificial neural networks require no prior knowledge of the data source, but they frequently require huge training sets due to the enormous number of weights that must be estimated. Additionally, ANNs can be used to solve problems using both experimental and bibliographical data. In a word, a neural network can be thought of as a black box capable of predicting a pattern in response to the recognition of a given input pattern. Once trained, the neural network can detect similarities in fresh input patterns, resulting in a projected pattern. In reality, ANNs are particularly beneficial for mapping problems that are tolerant of some errors but cannot be solved simply using hard and fast rules. ANN is a promising modelling technique, particularly for data sets with non-linear correlations, which areregularly found in modern engineering applications such as carbon dioxide lasermaterial processing.

The learning process is a critical feature of Neural Networks. A Neural Network's learning process can be compared to moulding a sheet of metal to represent the output (range) of the function being mapped. The training set (domain) represents the energy necessary to bend the sheet of metal into preset shapes. However, the metal will resist such reshaping by its very nature. As a result, the network will seek a low-energy configuration (i.e., a flat/unwrinkled shape) that satisfies the restrictions (training data). There are three fundamental methods of learning: supervised learning, unsupervised learning, and graded learning.

The nature of the data and the application's performance objective will dictate the type of learning method to be utilised. When the intended level of output is unknown, graded learning should be employed. If each training example

contains the intended output, a supervised learning approach should be utilised. When no explicit goals are known but some characteristic of the data set needs to be extracted, unsupervised learning will be applied. Both the inputs and outputs are delivered during supervised training. After processing the inputs, thenetwork compares the resultant outputs to the desired outputs. The system then calculates errors, causing it to modify the weights that regulate the network.This process is repeated while the weights are constantly adjusted. Unsupervised training provides the network with inputs but not with the expected outputs. After that, the system must pick which features to utilise to organise the input data.

7.2 PREDICTION OF KERF WIDTH USING A NEURAL NETWORK MODEL:

Figure 7.1 depicts the neural network that was employed in this work to represent laser-assisted material processing. The four input nodes correspond to the process parameters, which include the laser power, the assist gas pressure, the cutting speed, and the material thickness to be processed. The output layer, which consists of a single node, corresponds to the kerfwidth of the laser cut. The input and output nodes are mapped via a hidden layer composed of four nodes that assists the input layer in processing the data received. The output layer communicates the processed data to the user. Figure 7.2 illustrates the weights and biases of the various nodes that comprise the neural network.

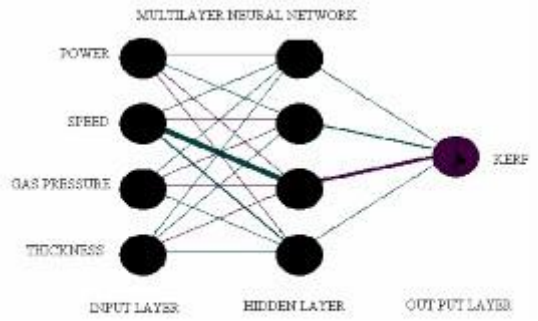

Figure7.1: Multilayer Neural network Model with 4-4-1 architecture.

EasyNN - [network]

File Edit View Zoom Action Window Options Help

```
Node 0      Input: power
      Input: 0.0000    Activation: 0.0000    Bias: 0.0000    Error: 0.0000
Node 1      Input: velocity
      Input: 0.0000    Activation: 0.0000    Bias: 0.0000    Error: 0.0000
Node 2      Input: pressure
      Input: 0.0000    Activation: 0.0000    Bias: 0.0000    Error: 0.0000
Node 3      Input: thickness
      Input: 0.0000    Activation: 0.0000    Bias: 0.0000    Error: 0.0000
Node 4      Hidden:
      Net input: 0.0000    Activation: 0.0000    Bias: -0.4196    Error: 0.0000
      Weight 0 from node 0: -0.268548                Weight 1 from node 1: 0.084857
      Weight 2 from node 2: 0.287225                 Weight 3 from node 3: 0.175222
Node 5      Hidden:
      Net input: 0.0000    Activation: 0.0000    Bias: -0.1800    Error: 0.0000
      Weight 4 from node 0: -0.322138                Weight 5 from node 1: 0.214286
      Weight 6 from node 2: 0.338557                 Weight 7 from node 3: -0.334803
Node 6      Hidden:
      Net input: 0.0000    Activation: 0.0000    Bias: 0.1531    Error: 0.0000
      Weight 8 from node 0: 0.387234                 Weight 9 from node 1: 0.214255
      Weight 10 from node 2: -0.043474               Weight 11 from node 3: -0.048326
Node 7      Hidden:
      Net input: 0.0000    Activation: 0.0000    Bias: -0.3905    Error: 0.0000
      Weight 12 from node 0: 0.123890                Weight 13 from node 1: 0.163228
      Weight 14 from node 2: -0.209037               Weight 15 from node 3: -0.070421
Node 8      Output: kerf
      Net input: 0.0000    Activation: 0.0000    Bias: -0.4595    Error: 0.0000
      Weight 16 from node 4: 0.170370                Weight 17 from node 5: -0.188223
      Weight 18 from node 6: 0.295770                Weight 19 from node 7: -0.379482
```

Figure 7.2: weights of the different nodes forming the neural network model for kerf of laser cut stainless steel -304

7.2.1 ALGORITHM FOR BACK PROPAGATION:

The back-propagation algorithm is used to train the multilayer Perceptron network. It is a gradient algorithm that iteratively reduces the mean square error between the desired and actual output. The output is calculated using a nonlinear sigmoid logistic function. [2001, Yegnanarayana B]

$$Y = f(x) = \frac{1}{1+e^{-x}} \text{--------7.1}$$

All weights and node offsets are set to random values when computing the output and error. The continuous input values u_1, u_2, u_3, and u_4 are supplied, together with the desired output values d_1, d_2, d_3, and d_4.....d_n.

The weighted total of the input to the j^{th} hidden layer node plus the bias input is

$$X_j = \sum w_{ij} u_j + \theta_j \text{----------7.2}$$

The outputs y_1, y_2 , y_3, y_4 . . y_n are calculated Using the sigmoid nonlinearity transfer function f(x) . Error term for the p^{th} pattern is calculated using the equation

$$E_p = \frac{1}{2}\sum (d_{pj} - y_{pj})^2 \text{ ----------7..3}$$

d_{pj} is the j^{th} component of desired output vector, y_{pj} is the calculated output of the j^{th} neuron in the output layer. Error for all patterns is

$$E = \sum_{p=1}^{n} E_p \text{------7.4}$$

For the out put layer error δ_{pj} in each node is calculated using

$$\delta_{pj} = y_{pj}(1 - y_{pj})(d_{pj} - y_{pj}) \text{ ------7.5}$$

Further, if α is the momentum factor and η, learning rate then weights between layers are updated using the equation

$$w_{ij}(m+1) = w_{ij}(m) + \eta \delta_{pj}\ y_{pj} + \alpha[w_{ij}(m) - w_{ij}(m-1)] \text{ --------7.6}$$

Weights are updated for each training set until the error objective is met. After training the network, it is possible to estimate the output values using the untrained data.

7.2.2 METHOD OF NETWORK LEARNING:

The neural network is trained using a supervised learning technique called back propagation. This strategy provided the network a collection of input and output data from the cutting tests. Initialize the network with random weights and bias. The learning rate is set to 0.5, the momentum factor is set to 0.8, and the error objective is set to 0.005.

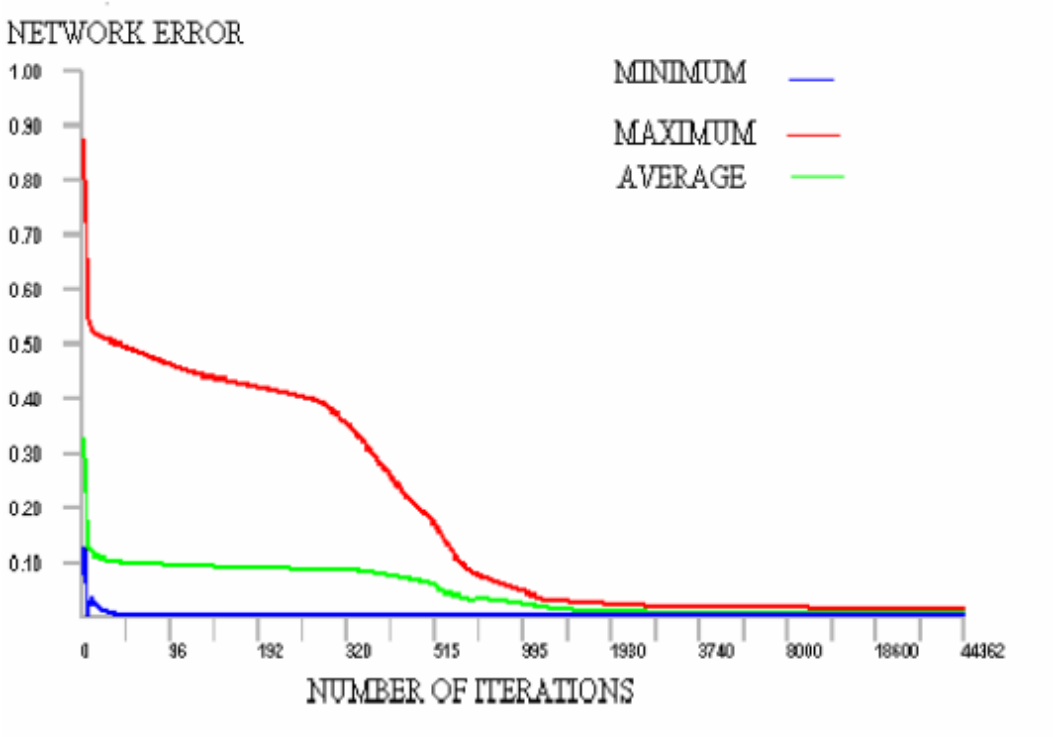

Figure 7.3: Graph showing the error during training of the network

During training, the neural network is continually presented with input data. Each presentation compares the neural network's output to the desired output and computes an error. This error is then given back to the neural network and used to alter the weights in such a way that the error lowers with each iteration and the neural model gets closer and closer to providing the output with the

specified error. The trained network attained an average error of 0.005 after 44362 iterations. Figure 7.3 depicts a graph of the network error during training.The trained network is validated against untrained data. We trained neuralnetworks using a variety of different architectures using the same input data.The network with the MLP 4-4-1 profile was found to be suitable for matching the experimental results.

7.3 THE NEURAL NETWORK MODEL'S RESULTS FOR KERF WIDTH:

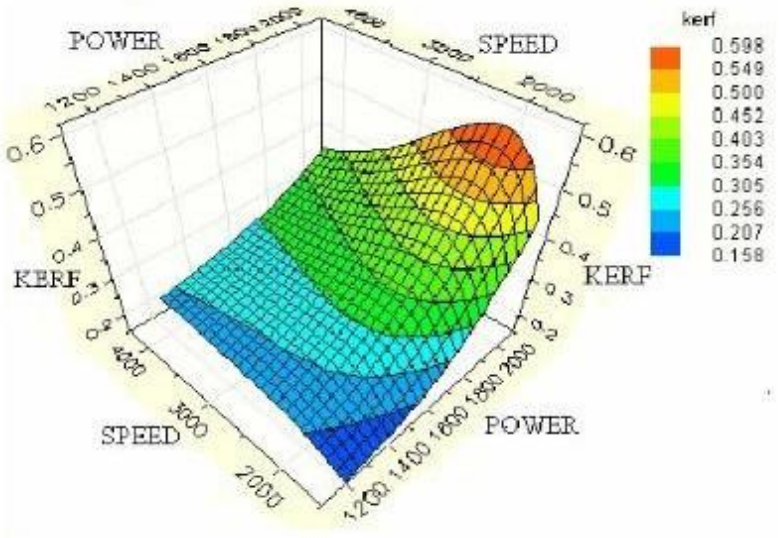

Figure 7.4: Response surface for kerfwidth with respect to cutting speed and laser power.

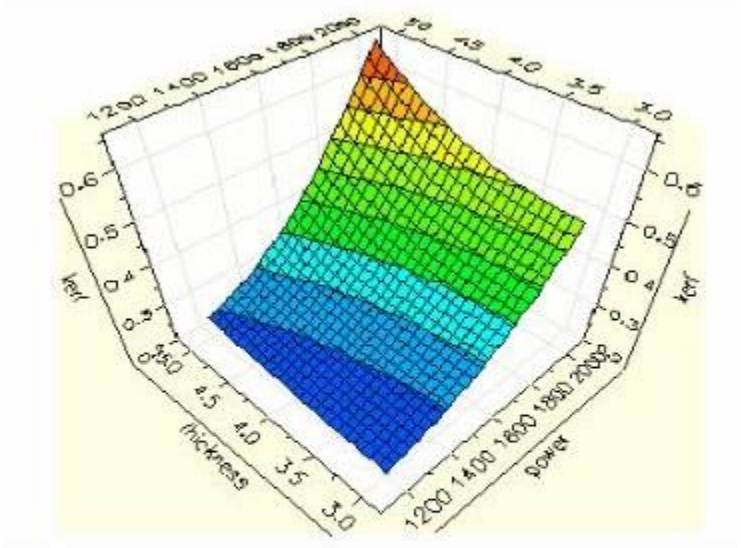

Figure 7.5: Response surface for kerfwidth with respect to work piece thickness and laser power.

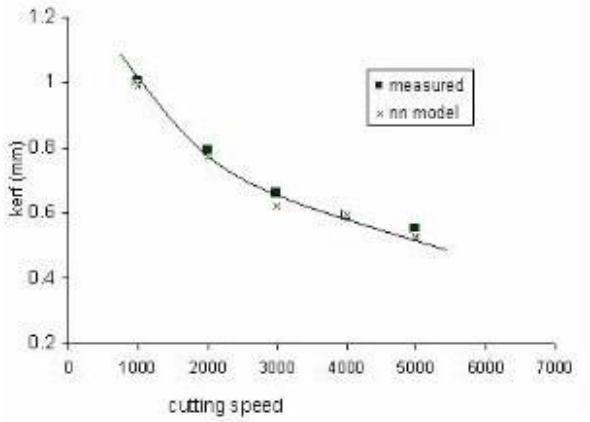

Figure 7.6 : Variation of kerf width with cutting speed for 304 grade 5mm thick stainless steel , assist gas pressure= 6 bar, Laser power=2kw Cutting speed = 1500 mm/min

The fluctuation in kerfwidth with cutting speed in laser machining is illustrated in Figure 7.6. The image depicts the effect of gas pressure on the kerf width in comparison to experimental results and ANN modelling. 7.7.

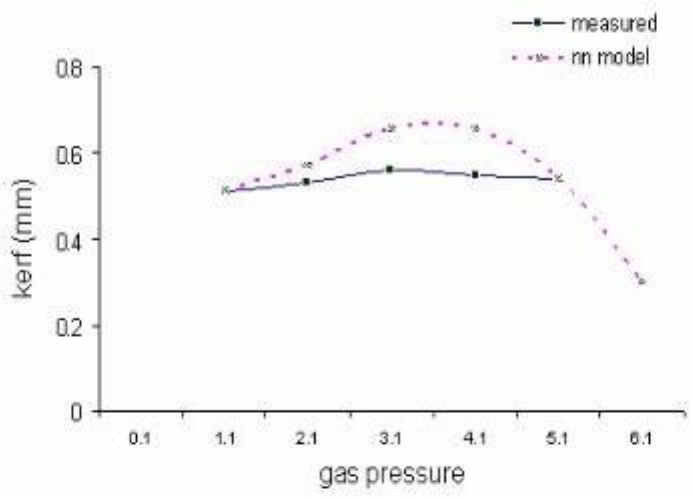

Figure 7.7 : Variation of kerf width with assist gas pressure for 304 grade 5mm thick stainless steel, Laser power= 2kwatts

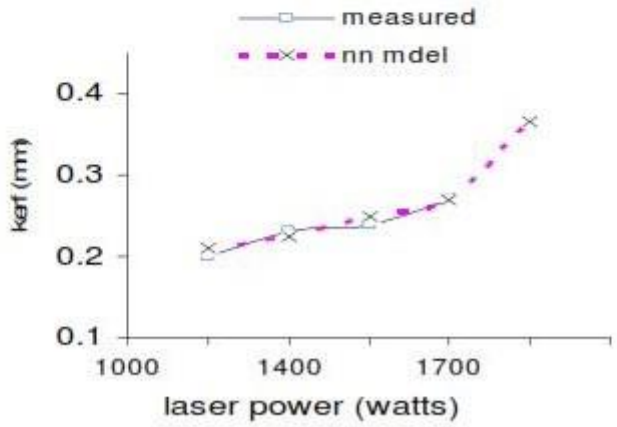

Figure 7.8: Variation of kerfwidth with laser power for304 grade 3mm thick stainless steel, Assist gas pressure =6bar (oxygen), Cutting speed= 3000mm/min

The effect of laser power on the generated kerf width in laser machining is illustrated in Figure 7.8. As the laser power increases, the kerf width increases, affecting the material removal rate and production rate. As can be seen from the above illustration, neural network modelling is advantageous for studying the behaviour of laser machining with its variables such as cutting speed, material

thickness, and production rate. This can be interfaced with the machine's computer control system to automate the process and ensure the best machining conditions for the most economical and optimal configuration, both dimensionally and metallurgically, according to our needs.

7.4 BASICS OF MULTIPLE REGRESSIONS:

Regression Analysis is a statistical technique that uses a series of data points to generate a line or curve with a known function. Minimize the average of all the distances between each point and the curve. The application of regression analysis is advantageous in the field of laser-assisted material processing due to the economics of testing and the presence of many processing factors. The purpose of regression analysis is to produce estimates of unknown parameters that demonstrate the effect of changing one of the independent variables on the values taken by the dependent variable. The most frequent type of regression is linear regression, which involves drawing a straight line through the data points. This type of regression is referred to as "Linear" or "First Order" regression. Due to the fact that not all data is best represented by a straight line, higher degrees of regression are used. Several types of regression analysis are possible, including the following:

I order : $Y = CX+D$

II order : $Y = BX^2+ CX +D$

III order: $Y = AX^3+BX^2+ CX +D$

Constants The letters A, B, C, and D are referred to as the "Regression Coefficients."

The third order coefficient is denoted by A, while the second order coefficient is denoted by B.

The first order coefficient is denoted by C, while the zeroth order coefficient is denoted by D.

7.5 KERFWIDTH REGRESSION MODEL:

Multiple regressions can be used to determine the independent variables' relative predictive importance. Through the use of hierarchical regression, the dependent variable's variance can be explained by one or a group of additional independent variables. The least squares technique is the most often used methodology for estimating regression models. The fundamental concept behind is to minimise the sum of square residuals. Under certain assumptions, the result of the minimal sum squared error criteria is impartial, consistent, and efficient.

Eighteen sets of data were gathered during laser cutting trials, with each set having values for five parameters. Using the other Processing factors such as cutting speed, gas pressure, laser power, and sample thickness, the first twelve sets of data were utilised to construct a statistical model for the kerf width. The remaining data sets were utilised to validate the model's output. Table7.1 contains further information. A statistical model for the kerf width is built utilising data from material processing trials and the processing parameters cutting speed, gas pressure, laser power, and sample thickness.

Using experimental data, we determined the influence of kerf width on each process parameter. Several user-defined regression models were created to match the experimental data using that dependence as the initial reference. A regression model was chosen for additional research that produced the desired results within a reasonable margin of error. The model specification that has been chosen is

Kerf = (A/(1+exp(X2)))+(B*X4)+(C*X4**2) +(D*X2*X3) +(E*X1*X3**2)

+(F*X1**2*X4)+(G*X1*X3*X4)

X1 =Laser power, X2 =Gas pressure, X3 =Cutting speed, X4 =Sample thickness.

The constants A, B, C, D, E, F, and G are to be assessed using the experimental data.

Table7.1: Data from CO_2laser cutting test

Serial number	Laser power X_1 Watts	Assist gas pressure X_2 Bar	Cutting speed X_3 mm/min	Sample thickness X_4 mm	Measured Kerf width mm
1	1200	6	3000	3	0.2
2	1300	6	3000	3	0.22
3	1400	6	3000	3	0.23
4	1600	6	3000	3	0.24
5	1700	6	3000	3	0.27
6	2000	1.1	1500	5	0.51
7	2000	2.1	1500	5	0.53
8	2000	3.1	1500	5	0.56
9	2000	4.1	1500	5	0.55
10	2000	5.1	1500	5	0.54
11	2000	4.1	1000	5	1.00
12	2000	4.1	4000	5	0.59
13	1900	4.1	3000	3	0.32
14	1900	3.1	3000	3	0.36
15	1900	5.1	3000	3	0.34
16	2000	2.1	4000	5	0.63
17	2000	3.1	4000	5	0.61
18	2000	5.1	5000	5	0.42

7.5.1 REGRESSION RESULTS:

A summary of the current regression model's regression findings is provided.

Number of iterations performed =11, Iteration limit chosen =200

Standard Deviation of the estimate = 0.00920531

Correlation coefficient (R^2) = 0.9992967

Adjusted Correlation Coefficient (adj R ^2) = 0.9984528

Analysis of Variance: a) F = 1184, b) P(F) = 0.00

The R-square value of 0.998 obtained from the regression results suggests that the model accounts for nearly all variability associated with the model's variables.

Table 7.2 : 't' and P(t) values of parameters of the proposed regression model

PARAMETERS	t	P(t)
A	-.274059E+01	0.041
B	-.568376E+01	0.002
C	0.145191E+02	0.000
D	-.137730E+01	0.227
E	0.407652E+02	0.000
F	0.766687E+01	0.001
G	-.372518E+02	0.000

Table 7.3: Comparison of experimental and regression model results for kerfwidth in laser cutting SS -304 steel.

Experimental value of kerf [mm]	Kerfwidth from regression model [mm]
0.20	0.2055
0.22	0.2144
0.23	0.2248
0.24	0.2501
0.27	0.2649
0.51	0.5070
0.53	0.5403
0.56	0.5507
0.55	0.5442
0.54	0.5425
1.00	0.9999
0.59	0.5901

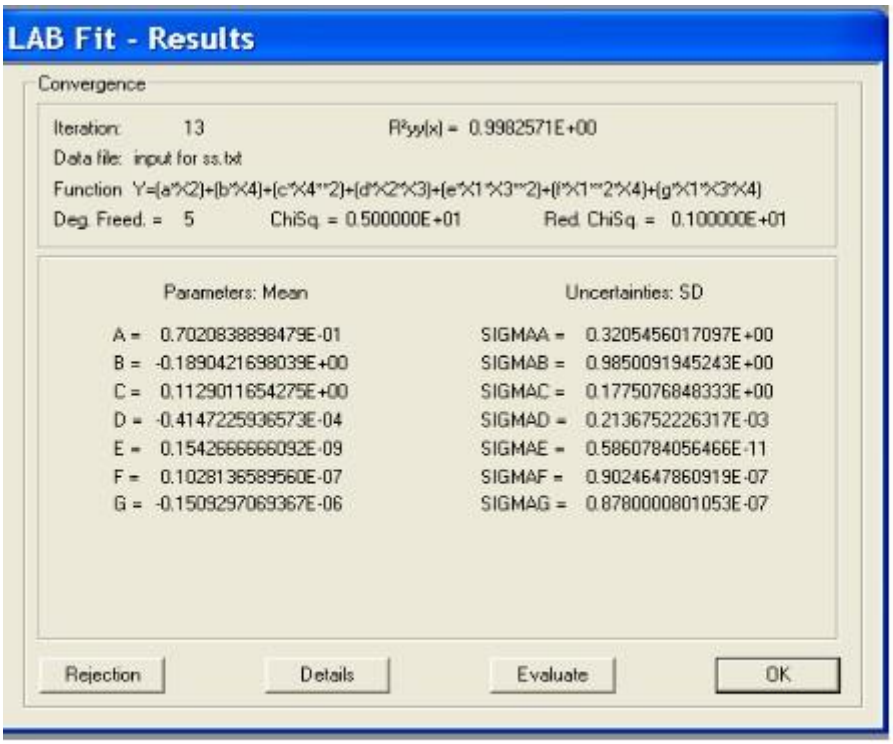

Figure 7.9: Results of evaluation of constants of Regression model for Kerf analysis.

7.6 DISCUSSION OF RESULTS OF THE MODEL:

7.6.1 THE EFFECT OF CUTTING SPEED ON THE WIDTH OF THE KERF:

The fluctuation in kerfwidth with cutting speed in laser material processing is illustrated in Figure 7.10 with a constant laser power of 2000W and an oxygen support gas pressure of 5 bar. It is observed that for a given power and gas pressure, a minimum kerf cutting speed exists. At cutting speeds below or above the threshold, the kerf increases for all thicknesses. Additionally, the minimum kerf at threshold cutting velocity increases as the work piece thickness increases.

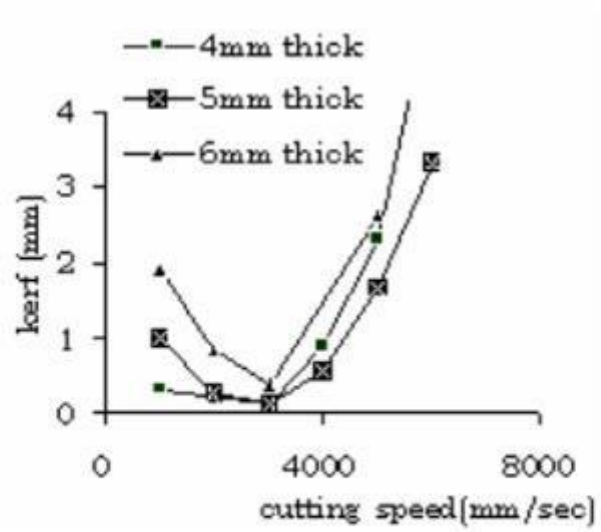

Figure 7.10: Variation of kerf with cutting speed, Laser power =2000watts, assist gas pressure =5 bar.

7.6.2 EFFECT OF GAS PRESSURE ON KERFWIDTH:

Figure 7.11 illustrates the effect of gas pressure on the laser cut kerf for various work piece thicknesses. It is noted that for a given pressure, kerf exhibits a weak maxima.

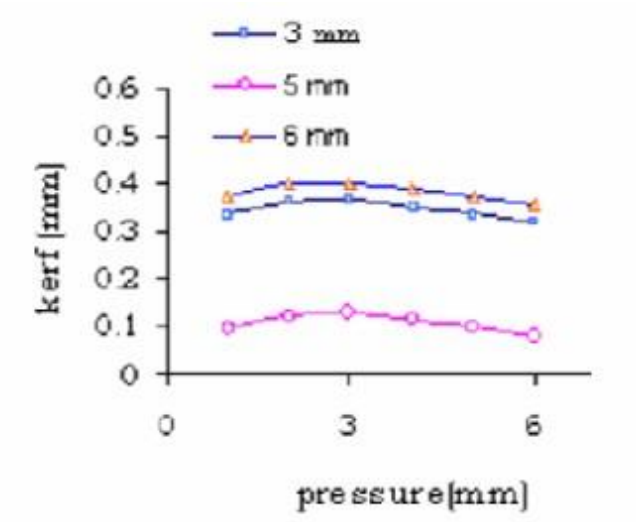

Figure 7.11: Variation of kerfwidth with assist gas pressure. Cutting speed =3000mm/min, Laser power = 2000w, work piece thickness = 3mm.

7.6.3 EFFECT OF THICKNESS ON KERF:

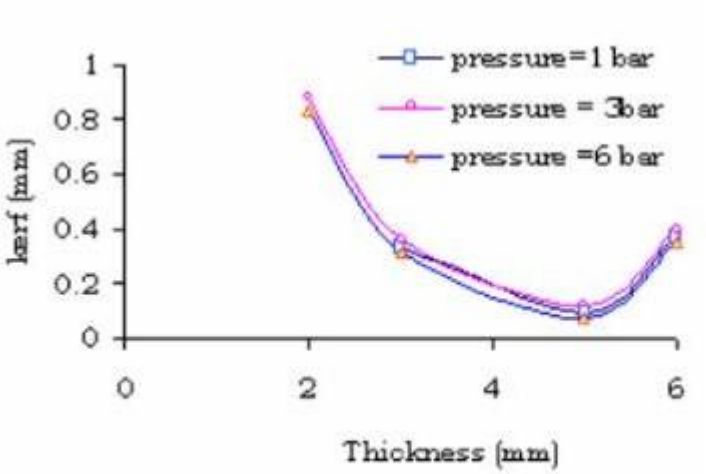

Figure 7.12: Variation of kerf with work piece thickness, laser power=2000watts Cutting speed =3000mm/min

Figure 7.12 illustrates the influence of thickness on the kerf cut by laser at various pressures. The smallest kerf possible for a given power and cuttingspeed is attained.

7.6.4 THE EFFECT OF LASER POWER ON THE WIDTH OF THE KERF:

Figure 7.13 illustrates the fluctuation in kerf width with laser power at various cutting speeds for a given thickness. It is noticed that the kerf width rises with laser power for a given sample at a given gas pressure. Additionally, it increases when the cutting speed at a given power increases. The kerf width grows when the cutting speed is increased. At lower cutting speeds, this gain is negligible. With increasing speed, the variance in kerf width becomes noticeable.

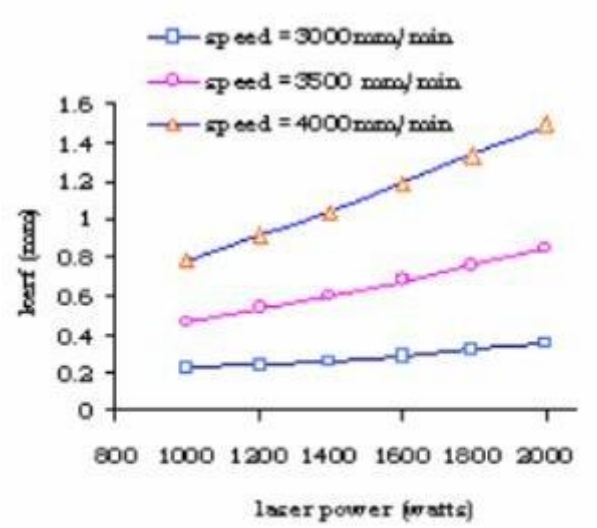

Figure 7.13 : Variation of kerf with laser power, gas pressure = 4 bar , work piece thickness = 3mm.

7.7 MODEL OF A NEURAL NETWORK FOR SURFACE ROUGHNESS:

Figure7.14 illustrates the neural network used in this study to simulate the surface roughness of a CO 2 laser cut stainless steel -304 surface. The network is designed in a 4-7-1 fashion. The four input nodes correlate to the process parameters, which include the laser power, assist gas pressure, cutting speed, and material thickness to be treated. The output layer, which consists of a singlenode, correlates to the roughness of the Laser cut surface. The input and output nodes are connected by a hidden layer composed of eight nodes that assists the input layer in processing the data it receives. The output layer communicates the processed data to the user. The many parameters used in the network modelling method are depicted in Figure 7.15.

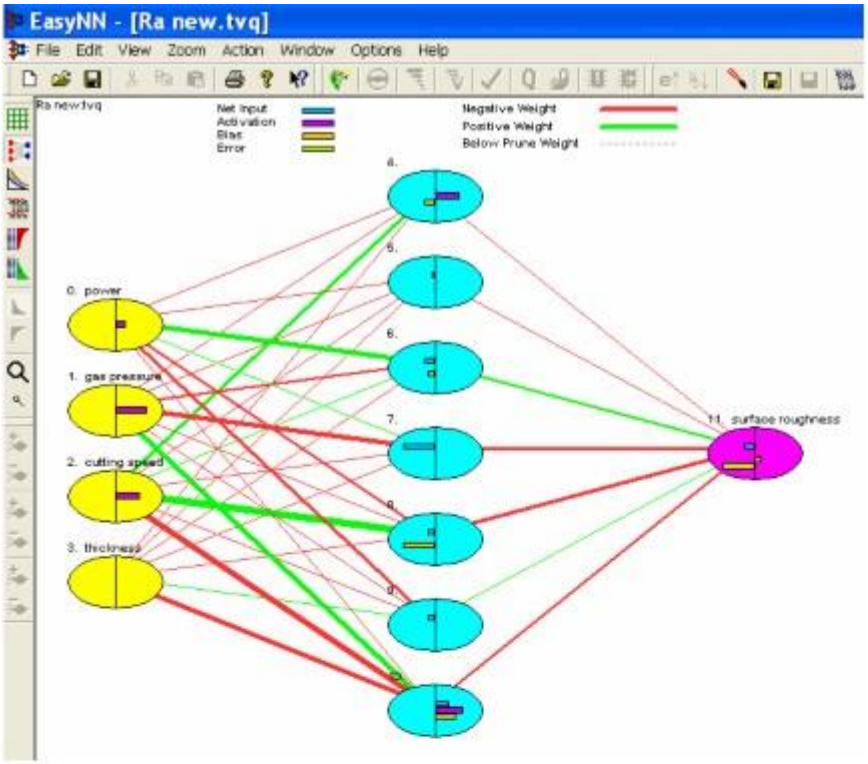

Figure7.14: Multilayer Neural network Model with 4-7-1 architecture for optimising surface roughness of laser cut surface of SS-304.

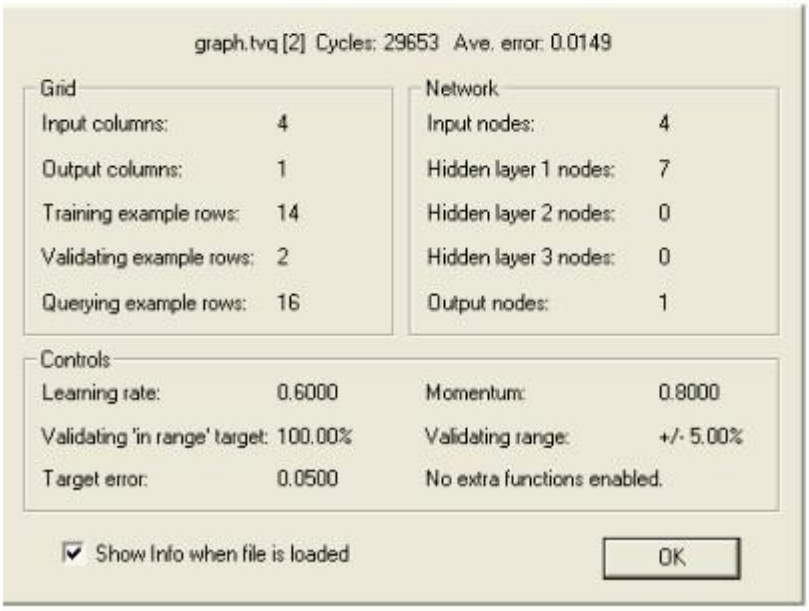

Figure 7.15: Information of Multilayer Neural network Model with 4-7-1 architecture for optimising surface roughness.

Figure 7.16: Weights of Multilayer Neural network Model with 4-7-1architecture to optimise surface roughness in cutting stainless steel by CO_2 laser.

Sixteen experimental values were utilised to model the process, fourteen were used to train the network and the remaining four were used to validate the results. The weights of the various layers are depicted in Figure 7.16. The error

target was set to 0.05 utilising a 0.6 learning rate and a 0.8 momentum rate. The network was trained using the back propagation algorithm using the experimental data. After 29653 iterations, the error objective was attained.

7.8 RESULTS OF THE NN MODEL FOR SURFACE ROUGHNESS OF STAINLESS-STEEL CUT BY CO_2 LASER:

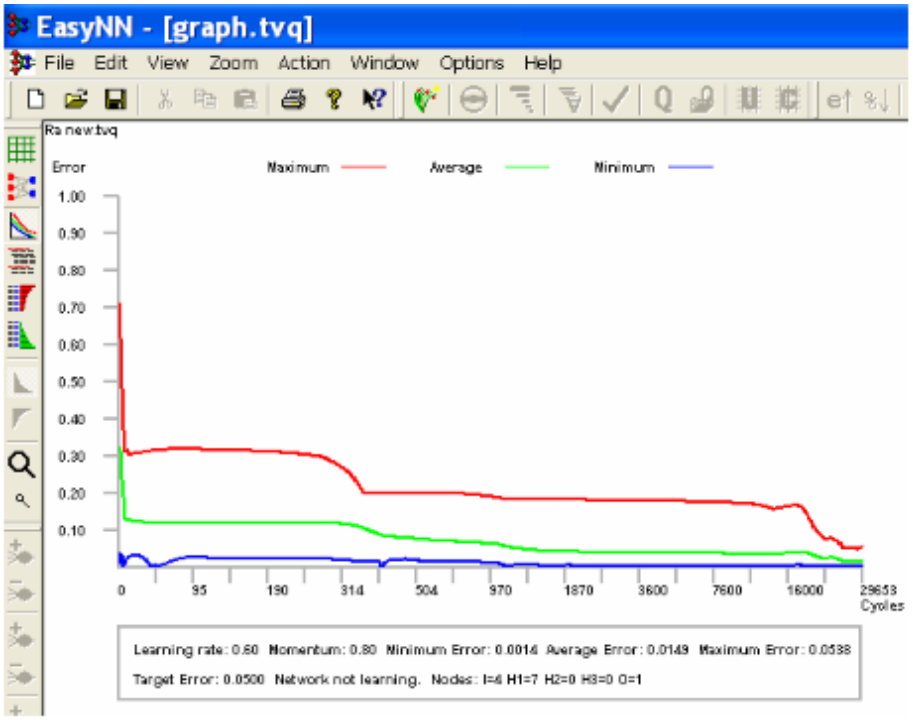

Figure 7.17: graph of network error during training of Multilayer Neural network Model with 4-7-1 architecture.

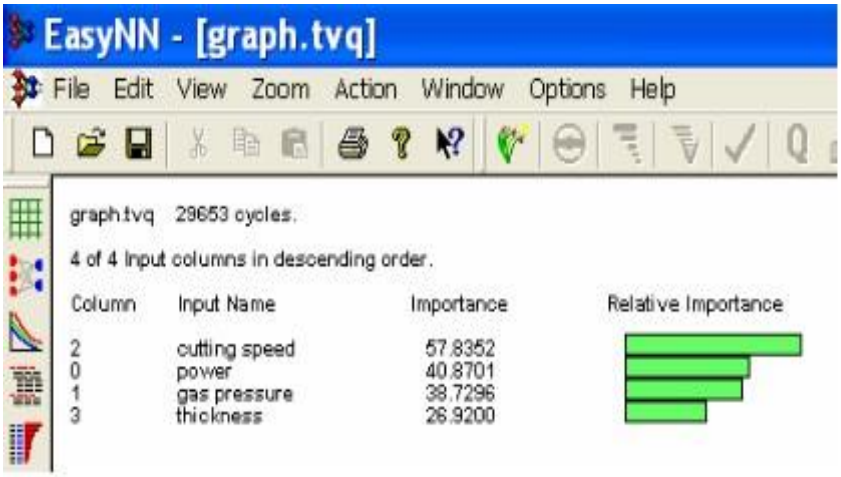

Figure 7.18: Relative importance of process parameters in Neural network Model with 4-7-1 architecture.

The neural network model designed to forecast and optimise the cutting parameters produced good results for the surface roughness of CO_2 laser cut stainless steel -304 within the specified error limits. Cutting speed is determined to be more important than the other cutting parameters in terms of optimising the surface roughness. Figure 7.18 illustrates the relative relevance of all the cutting parameters utilised in the current model. Figure 7.19 illustrates theresults of the neural network model for surface roughness. T denotes the test data in the results. Q denotes the network's output in response to a querysubmitted with the trained network. The predicted values for the surface roughness of the CO_2 laser cut surface of stainless steel agree with the measuredvalues.

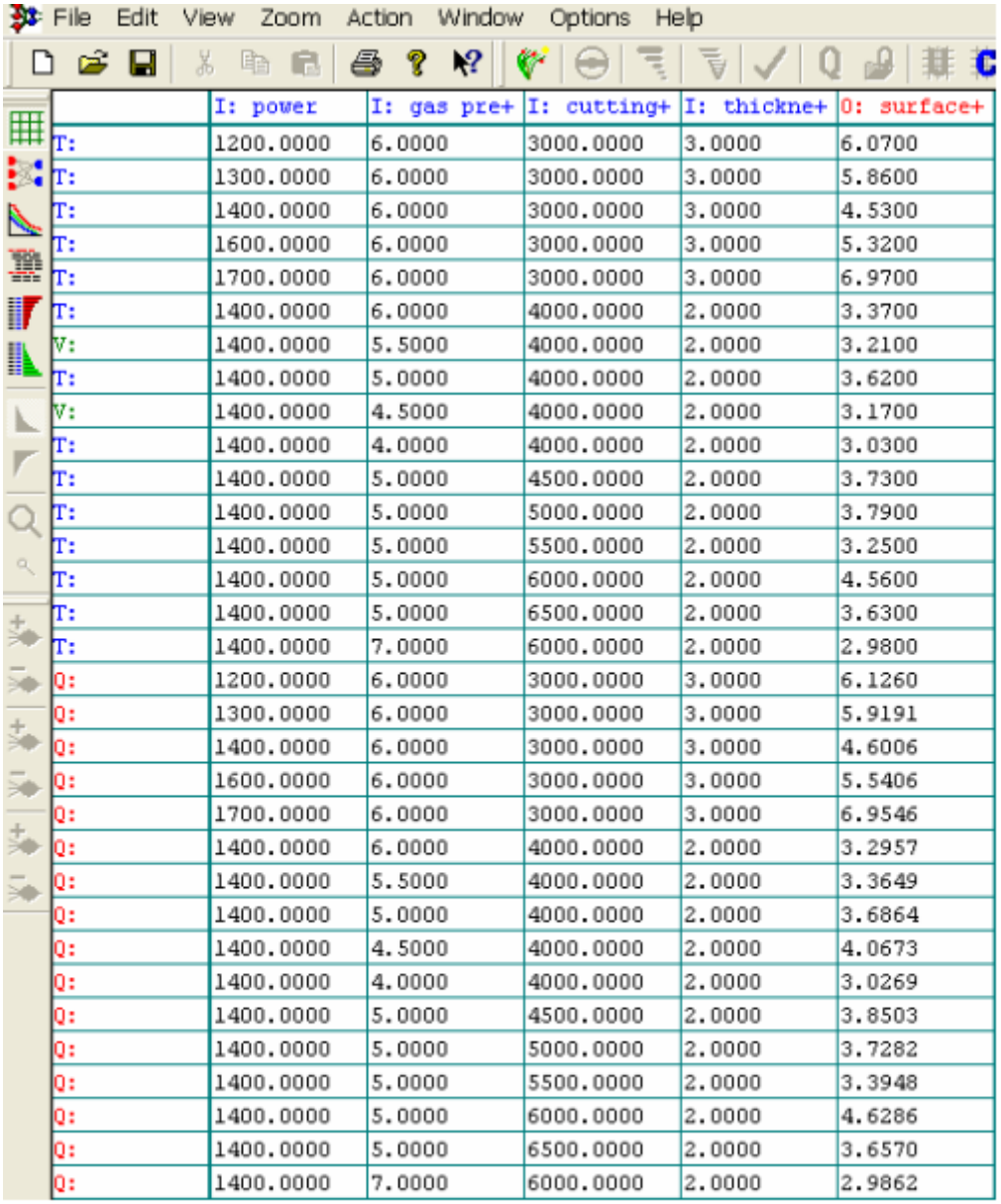

	I: power	I: gas pre+	I: cutting+	I: thickne+	0: surface+
T:	1200.0000	6.0000	3000.0000	3.0000	6.0700
T:	1300.0000	6.0000	3000.0000	3.0000	5.8600
T:	1400.0000	6.0000	3000.0000	3.0000	4.5300
T:	1600.0000	6.0000	3000.0000	3.0000	5.3200
T:	1700.0000	6.0000	3000.0000	3.0000	6.9700
T:	1400.0000	6.0000	4000.0000	2.0000	3.3700
V:	1400.0000	5.5000	4000.0000	2.0000	3.2100
T:	1400.0000	5.0000	4000.0000	2.0000	3.6200
V:	1400.0000	4.5000	4000.0000	2.0000	3.1700
T:	1400.0000	4.0000	4000.0000	2.0000	3.0300
T:	1400.0000	5.0000	4500.0000	2.0000	3.7300
T:	1400.0000	5.0000	5000.0000	2.0000	3.7900
T:	1400.0000	5.0000	5500.0000	2.0000	3.2500
T:	1400.0000	5.0000	6000.0000	2.0000	4.5600
T:	1400.0000	5.0000	6500.0000	2.0000	3.6300
T:	1400.0000	7.0000	6000.0000	2.0000	2.9800
Q:	1200.0000	6.0000	3000.0000	3.0000	6.1260
Q:	1300.0000	6.0000	3000.0000	3.0000	5.9191
Q:	1400.0000	6.0000	3000.0000	3.0000	4.6006
Q:	1600.0000	6.0000	3000.0000	3.0000	5.5406
Q:	1700.0000	6.0000	3000.0000	3.0000	6.9546
Q:	1400.0000	6.0000	4000.0000	2.0000	3.2957
Q:	1400.0000	5.5000	4000.0000	2.0000	3.3649
Q:	1400.0000	5.0000	4000.0000	2.0000	3.6864
Q:	1400.0000	4.5000	4000.0000	2.0000	4.0673
Q:	1400.0000	4.0000	4000.0000	2.0000	3.0269
Q:	1400.0000	5.0000	4500.0000	2.0000	3.8503
Q:	1400.0000	5.0000	5000.0000	2.0000	3.7282
Q:	1400.0000	5.0000	5500.0000	2.0000	3.3948
Q:	1400.0000	5.0000	6000.0000	2.0000	4.6286
Q:	1400.0000	5.0000	6500.0000	2.0000	3.6570
Q:	1400.0000	7.0000	6000.0000	2.0000	2.9862

Figure 7.19: Results of the neural network Model for surface roughness in cutting of stainless steel by CO_2 laser. T represents the test data. Q is the network output when a query is made with the trained network.

7.9 FEM MODEL TO STUDY TEMPERATURE DISTRIBUTION DURING LASER CUTTING OF STAINLESS STEEL:

Typically, in laser material processing, the laser beam warms and melts, and occasionally evaporates, the workpiece in a limited region defined primarily by the focal spot. This heat is absorbed largely by the material's surface. With increasing specific heat and density, the temperature reached for a given heat input per unit volume drops. Thus, the temperature achieved on the work piece's

surface and interior along the processed track is mostly determined by the processing speed, the work piece's thermal characteristics, and its thickness. Obviously, the maximum temperature is attained when the laser strikes the work piece, and it decreases continually in the lateral direction in a co-ordinate system that moves in lockstep with the beam's position relative to the work piece. The laser beam strikes previously unheated regions in the direction of relative movement between beam and work piece, resulting in significant heat conduction and the appearance of a substantial temperature differential in the depth of cut. Temperature distribution inside the material is critical, as it determines the microstructure of the work piece, the heat affected zone, and the processing quality.

The temperature distribution within the work piece material can be estimated analytically or numerically. Rosenthal D [1946] offered the first analyticalmodel for the idea of a moving heat source. However, due to the material's temperature-dependent thermophysical properties, the uncertainty in the percentage absorption of the laser beam power by the work piece, and other physical conditions affecting the laser beam material interaction, calculating the temperature distribution is complicated. To some extent, these issues are overcome by using numerical computing methods such as the finite element method (FEM) rather than analytical methods. However, the published results on utilising the finite element method to examine the temperature distribution during the cutting of stainless steel -304 with a laser beam are quite limited.

7.9.1 MODELLING USING FEM:

The finite element model for laser cutting stainless steel-304 is produced using commercial ANSYS software and is based on the thermal and mechanical boundary conditions encountered during cutting. After that, the model is applied to the cut material, stainless steel, by specifying its physical parameters such as Young's modulus, thermal conductivity, specific heat capacity, and density. Following that, the material is separated into smaller nodes and elements

(Tetrahedron) in order to do finite element analysis on it. The mesh is composed of twenty noded brick elements. Figure7.20 depicts the analysis's solid modelling.

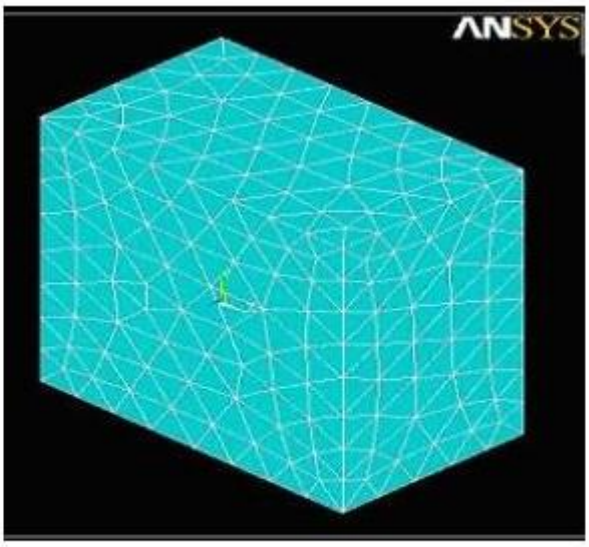

Figure7.20: 3-Dimensional Model of work piece meshed with Thermal solid 20 noded Brick element

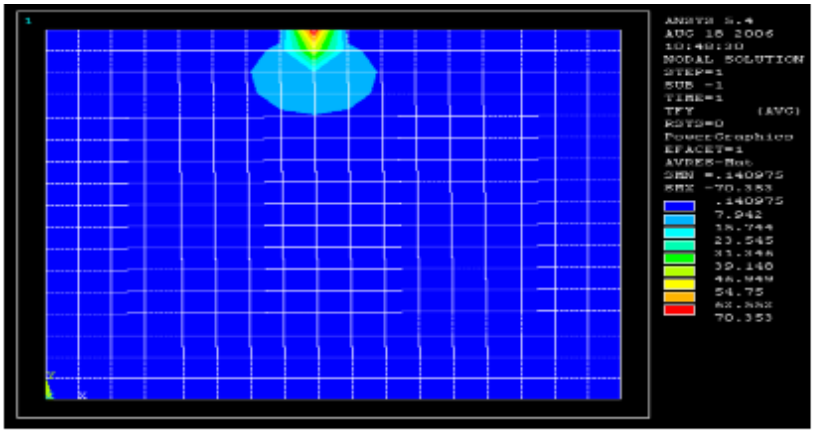

Figure7.21: Temperature distribution along the laser beam direction (nodal solution) in cutting stainless steel by CO_2 laser

By applying a heat flux equal to 1600 watts of laser power to the solid model, the required working conditions for laser cutting stainless steel are generated. The solution illustrates the temperature distributions along the X and Y axes at various nodes. The output of the finite element model indicates that the majorityof heat is absorbed at the surface where the beam strikes the material. The nodal

solution analysis for the temperature distribution along the Laser beam direction is shown in Figure 7.21. Figure 7.22 illustrates the temperature distribution perpendicular to the beam direction during the nodal solution analysis.

Additionally, the elemental solution for the temperature distribution coincides with the nodal solution's results. The temperature distribution of the elements solution in the transverse direction to the laser beam is depicted in Figure 7.23. The temperature distribution's form extends further into the material's depth than it does in the horizontal direction. By changing the laser beam power, the depth of the temperature gradient can be successfully adjusted. This will maintain control of the heat-affected zone and any subsequent deterioration caused by thermal effects and strains.

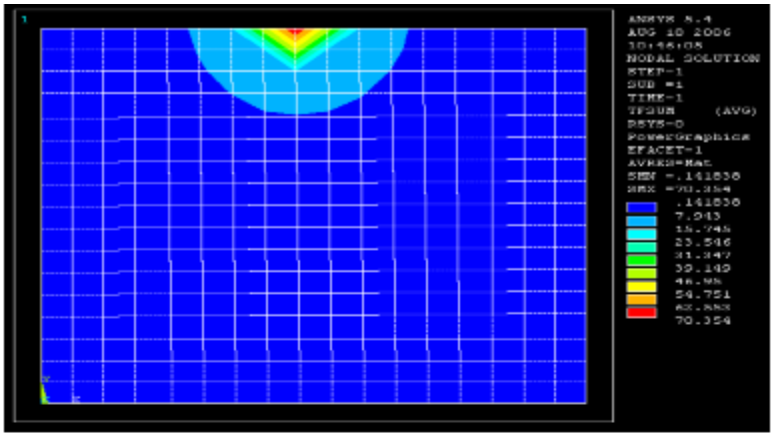

Figure7.22: Temperature distribution perpendicular to the laser beam direction (nodal solution) in cutting stainless steel by CO_2 laser

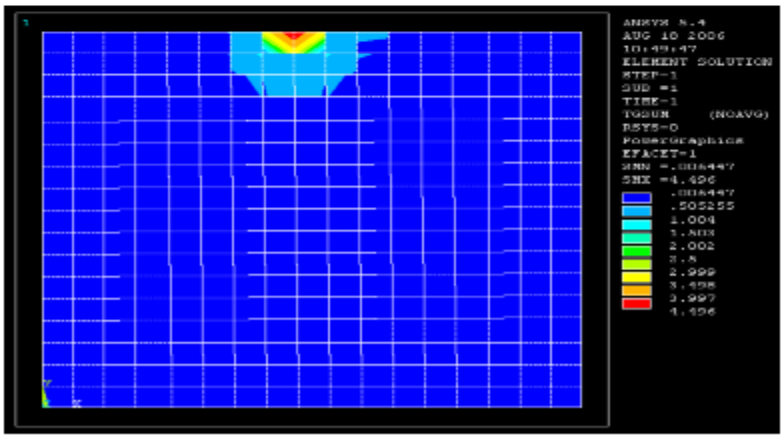

Figure7.23: Temperature distribution along perpendicular direction to the laser beam direction. (Elemental solution) in cutting stainless steel by CO_2 laser

As a result of these temperature distribution techniques, it is clear that the heat impacted zone is constrained and extremely small while cutting stainless steel with a CO_2 laser. This is consistent with the experimental results from metallurgical and scanning electron microscopy (SEM) research presented in the early chapters of laser cutting stainless steel-304.

CHAPTER 8

CONCLUSION

This thesis concludes by summarizing the major findings from the experimental work, modeling studies, and future research.

8.1 THE PRIMARY RESULTS OF EXPERIMENTS WITH CO_2 LASER CUTTING: `

The kerf is discovered to be dependent on various cutting parameters when stainless steel-304 is laser cut. This has an effect on the material removal rate, which is determined by the laser cutting settings.

Material removal rates are almost identical for thicknesses up to around 3mm but dramatically increase for thicknesses of 5mm and more. This is because of the increased energy availability caused by the chemical reaction between oxygen jet and iron, which results in the release of energy.

The experimental results on the kerf and material removal rates of SS-304 are consistent with previously published work by Powell et al [2000] at a lower laser power. The kerf width grows as the laser power increases, but reduces as the cutting speed increases.

It demonstrates that MRR has an optimal value for a given assist gas pressure. It grows in proportion to the laser's power.

The taper created in the kerf of stainless steel-304 laser cutting is found to vary with laser power. It is discovered that it decreases as input power increases.

The surface finish is shown to be reliant on a variety of cutting parameters and MRR. It is preferable to have a greater MRR.

Additionally, the influence of assist gas pressure on the surface roughness is negligible for a given set of cutting variables.

Thermal cracks are seen on the laser cut surface when oxygen is used as an assist gas. If nitrogen is utilised as an aid gas for the same cutting circumstances, cracks will be minimised.

On the laser cut surface, a white coating is visible. The layer is approximately 50 metres thick. The cutting circumstances dictate the layer thickness.

On the cut surface, material composition changes due to the absorption ofcertain elements such as iron and the loss of others such as chromium, nickel, manganese, and silicon, affecting the material and surface qualities.

The microstructure of cut material exhibits a regular distribution of grains. Although the heat affected zone is tiny in laser cutting, the damage beneath the surface caused by the heat affected zone at the outer cut surface is obvious.

Due to the thermal nature of laser cutting, damage caused by thermal strains will occur along the structures. To minimise these impacts, it is vital to carefullyselect the right machining settings for the material being machined.

8.2.1 STUDIES ON LASER ETCHING WITH A Nd: YAG LASER:

- Etching creates a matted surface on the work piece as a result of material removal on a localised scale using laser pecking with a regulated depth of cut.
- The structure of the mattey surface can be regulated to the required level by laser machining conditions that influence the depth of cut.

8.3 STUDIES IN MODELING:

- On the basis of experimental data, two neural network models have been created. The model is capable of forecasting the surface roughness of the laser cut surface, the kerf width and hence the material removal rate, as

well as other process parameters that can be used to optimise the cutting process.

- There is a minimum cutting speed required to get the smallest kerf width while maintaining all other cutting parameters constant.
- To forecast Kerf width, an analytical regression model was constructed. The model is useful for predicting the values of cutting parameters used in CO_2 laser cutting.
- A FEM model has been created that predicts that when stainless steel is cut with a CO_2 laser, the temperature distribution is constrained to a narrow region both along the cut line and in the transverse direction ofthe cut. This is backed by experimental data and electromagnetic theory predictions for light propagation in conducting materials.

8.4 THE WORK'S IMPORTANCE:

While laser material removal applications are not a one-size-fits-all solution for all machining needs, they do offer significant advantages over alternative approaches in certain situations.

The laser cutting process has been optimised using neural network modelling to meet the user's individual needs. To automate the system, the neural network model must be interfaced with the laser cutting equipment.

Economic factors such as input cost, processing time, and cut quality can all be optimised to maximise machine use.

The findings of this thesis contribute to the improvement of process planning decisions for laser machining of 304 grade stainless steel in order to maximise its manufacturing applications. This will benefit manufacturing's economics by increasing productivity and capacity utilisation.

8.5 OPPORTUNITIES FOR FUTURE WORK:

- Due to the widespread usage of heat-treated samples in a variety of high-tech industrial applications, it is desirable to investigate the effect of process parameters on heat treated samples at various temperatures.
- A study of the effect of process factors on annealed and cold rolled samples of several grades of stainless steel that are frequently utilised in the nuclear sector.
- The study can be expanded to investigate the influence of other laser types, assist gases, and laser strength.
- A thorough examination of the white layer may uncover opportunities to optimise the process and thereby regulate the cut surface characteristics.

REFERENCES:

[1] Akcan. S, Shah S, Moylan S P, Chhabra P N, Chandrasekhar S, Yang H T Y (2002) Metallurgical and Material transactions A vol 33A,1245.

[2] Baruah G D (2000) Essentials of laser and non-linear optics: Pragathi Prakashan, Meerut (India).

[3] BasemF. Yousef, George. Knopf , EvgueniV, Bordatchev , SuwasK. Nikumb (2003) NN modeling of MR process during laser machining The Intl. Journal of Advanced Manufacturing Technology, Vol 22, no 1-2, pp 41-53.

[4] ruinsma, PLWM[1991] Laser cutting of steel and stainless steel Roestvast Staal (Netherlands). Vol. 7, pp. 50-55.

[5] Cohen M I, (1972) Material processing- in Laser Handbook vol II, Recchi F T and Schulz-Dubois E O (Ed.) North-Holland.

[6] Cusanelli, G; Hessler-Wyser, A; Board, F; Demellayer, R; Perez, R; Flukiger, R (2004) Microstructure at the submicron scale of the white layer produced by EDM technique Journal of Materials Processing Technology. Vol. 149, no. 1-3, pp. 289-295.

[7] Chen S L (1998) analysis and modeling of Reactive three-dimensional high power CO2 laser cutting, Proc of I Mech E part B Journal of Engg manufacture, Vol 212, no2, pp113-128.

[8] David L carrol and James A Rothenflue (1997) Experimental study of cutting thick aluminum and steel with a chemical oxygen-iodine laser using an N2 or O2 gas assist ., Proc of SPIE vol 3092,pp758-763.

[9] David Smith (2000), Gas-assisted laser cutting Industrial laser solutions for manufacturing, Dec 2000.

[10] Dutta Majumdar J and I manna (2003) Sadhana vol 28, parts 3&4 , pp495-562.

[11] Duan J Man H C and Yue T M (2001) Modeling of laser fusion cutting process: I Mathematical modeling of the cut kerf geometry for laser fusion cutting of thick materials, J Phys D: Appl Phys, 34,2127-2134.

[12] Farooq K and A Kar,(2000) Thermal and Dimensional Characteristics of Vapour

plasma Plume and layer deposition in laser aided rapid manufacturing, High Temp Material Processes,4,161-199.

[13] Grabowski A. Nowak M. and leziona (2006)J.Journal of Achievements in Materials and Manufacturing Engineering, Volume 17 Issue 1-2 pp61-64.

[14] Gerald Davis, (Dec 2001) Laser cutting Techniques, The Fabricator.

[15] Gabzdyl, J.T.; Morgan, D.A., (1992) "Assist gases for laser cutting of steels," ICALEO Oct 25-29 1992 pp. 443-447.

[16] Griffiths, B J, (1987) Mechanisms of White Layer Generation Concerning Machining and Deformation Processes, J. Tribology (Trans. ASME). Vol. 109, no. 3, pp. 525-530.

[17] George Chryssolouris, (1997), Laser Machining theory and practice, Springer-Verlag New York, USA.

[18] Horikawa, Hideyuki; Fushimi, Takashi; Takasaki, Takuya; Yamaguchi, Shigeru, (1999) "Flow characterization in a laser-cut kerf," CLEO/PACIFIC (Rim '99) vol 2, pp. 358-359.

[19] Hsu, M.J.; Molian, P.A., (1995) "Off-axial, gas-jet-assisted, laser cutting of 6.35-mm thick stainless steel," Journal of Engineering for Industry, Transactions of the ASME vo117 no2, pp. 272-276.

[20] Freund HP and Antonsen Jr T M [1996] principles of Free electron lasers 2nd edition Chapman& Hall, London.